DOCTORAL THESIS

Performance of Lower-Carbon Concretes After High-Temperature Exposure

Marcin Sundin

Building Materials

LULEÅ UNIVERSITY OF TECHNOLOGY

Performance of Lower-Carbon Concretes After High-Temperature Exposure

Marcin Sundin

Supervision:
Andrzej Cwirzen, John L. Provis, Hans Hedlund, Karel Dvorak

DOCTORAL THESIS

Performance of Lower-Carbon Concretes After High-Temperature Exposure

Marcin Sundin

Building Materials

Department of Civil, Environmental and Natural Resources Engineering
Luleå University of Technology
SE-97187 Luleå
Sweden

2025

Front Page: Image from the thermal camera during large-scale testing.

Printed by Luleå University of Technology
URN: urn:nbn:se:ltu:diva-114425
ISBN: 978-91-8048-881-5 (print)
ISBN: 978-91-8048-882-2 (electronic)
OAI: oai:DiVA.org:ltu-114425
DiVA, id: diva2:1991920

Luleå 2025

Academic Thesis

For the Degree of Doctor of Philosophy (Ph.D.) in Building Materials, which is due permission of the Technical Faculty at Luleå University of Technology will be publicly defended in:

Room E632, Luleå University of Technology
Thursday, October 23th, 2025, 10:30

Opponent Examiner:

Prof. **Jeanette Orlowsky**, TU Dortmund University, Germany

Examining committee:

Prof. **Izabela Hager**, Cracow University of Technology, Poland
Prof. **Erik Schlangen**, Delft University of Technology, The Netherlands
Assoc. Prof. **Eleftherios Anastasiou**, Aristotle University of Thessaloniki, Greece

Principal Supervisor:

Prof. **Andrzej Cwirzen**, Luleå University of Technology, Sweden

Assistant Supervisors:

Adj. Prof. **Hans Hedlund**, Luleå University of Technology, Sweden
Dr. **John Provis**, Paul Scherrer Institut PSI, Switzerland.
Assoc. Prof. **Karel Dvorak**, Brno University of Technology, The Czech Republic

Chairman:

Dr. **Magdalena Rajczakowska,** Luleå University of Technology, Sweden

"There is a crack in everything, that's how the light gets in."

Leonard Cohen

"Dripping water hollows out stone, not through force but through persistence."

Ovid

Acknowledgments

This thesis was conducted within the Building Materials group at the Department of Civil, Environmental and Natural Resources Engineering, Luleå University of Technology. The project and research were funded by the Development Fund of the Swedish Construction Industry (Svenska Byggbranschens Utvecklingsfond, SBUF).

Professor Andrzej Cwirzen provided me with this opportunity and served as my main supervisor during these four years. He supported me with advice and gave me the freedom to explore different parts of academic work. This helped me grow both professionally and personally. I am thankful for his trust, support, and knowledge, and for being a kind person who always saw the human side of me.

My gratitude also goes to my assistant supervisors: Hans Hedlund, John L. Provis, and Karel Dvořák. Thank you for your help, guidance, and kind words along the way.

I wouldn't be here without my dear colleagues, with whom I shared so many moments, both the joyful and exciting ones filled with compassion, and those marked by sadness, doubt, and frustration.

A special place in my heart belongs to Ilda Tole and Magdalena Rajczakowska, who helped me, guided me, and made me laugh countless times. Their academic paths and scientific determination have often been a source of admiration and a great example to follow.

Carina Hannu has been the superhero of my time at this university. She helped me adapt to both the Swedish and local systems, untangled many of my mistakes, and always found good solutions to my problems. The fact that she wears a beautiful and legendary perfume by Guerlain makes it even more special to honour her here.

A big thank you to my mother-in-law, Margareta Sundin, for giving me the idea that pursuing a PhD in Sweden was even possible. And to my mum, Jolanta Zyzak, who raised me and taught me a strong work ethic and to treat people equally. Last not least, to my dear husband, Patrik, for his support and belief in me, whether I thought I could do it or not. He has always stood by my side.

It wouldn't be fair not to thank all the staff at LTU for providing countless litres of coffee and cakes, office supplies, cheerful "Hej, hej!" greetings, and for keeping my office clean. These small gestures were often little sparks of joy on foggy days.

August 2025, Luleå,

Marcin Sundin.

Summary

This research was initiated in response to the urgent need to reduce CO_2 emissions, the ongoing green transition within the building materials sector, and the persistent gap in both knowledge and practice regarding the performance of environmentally friendly concretes under high-temperature exposure.

The study investigates the behaviour of concrete and paste mixtures incorporating ground granulated blast furnace slag (GGBFS) and calcium sulfoaluminate (CSA) cement following one hour of exposure to elevated temperatures. Mechanical testing, chemical analysis, including real-time monitoring during heating, and microstructural observations were used to evaluate thermal damage and to understand the materials' response under those conditions. Various binder types, fillers, fibres, and admixtures were examined to assess their influence and to identify both strengths and limitations.

The results demonstrated a beneficial effect of GGBFS in systems based on Portland cement, particularly in enhancing residual strength and thermal stability. In CSA-based systems, the inclusion of eggshell powder (ESP) was found to contribute positively to post-fire performance. On the other hand, certain admixtures caused unexpected disturbances at high temperatures, suggesting the need for careful compatibility testing and awareness of mix constituents when designing thermally resistant concretes.

The experimental programs were designed as an initial step toward broader exploration and formed a key component of an ongoing research effort. The findings are intended to support and complement existing studies in both academia and industry, with the goal of improving the fire resistance and overall durability of sustainable concrete materials.

Key words:
Concrete, low carbon, fire, GGBFS, CSA, slag, high temperature.

Table of content

List of figures

List of tables

Notations

Symbol	Description	Unit
T	temperature	°C
T0	ambient temperature	°C
t	time	min
wi	Number of pixels showing cracks or pores	-
A	Image length	pixels
B	Image width	pixels
MII_i	Integrity index	-
Cp	Specific Heat Capacity	J/(kg·K)
Λ	Thermal Conductivity	W/m·K

Abbreviation	Description
ACC	Accelerator
AE	Air entrainer
AST	Adiabatic Surface Temperature
CEF	Fire Testing Centre
CFD	Computational Fluid Dynamics
CSA	Calcium sulfoaluminate cement
CTE	Coefficients of thermal expansion
C–S–H	Calcium Silicate Hydrate
EDX	Energy-dispersive X-ray spectroscopy
ESP	Eggshell powder
FA	Fly ash
FEM	Finite Element Methods
FSI	Field Structure Interface
GGBFS	Ground granulated blast furnace slag
HPC	High performance concrete
ITB	Building Research Institute
ITZ	Interfacial Transition Zone
LSP	Limestone powder
LTU	Luleå University of Technology
MSB	Swedish Civil Contingencies Agency
PC	Portland cement
PP	Polypropylene
RISE	Research Institutes of Sweden
SCM	Supplementary cementitious material
SEM	Scanning electron microscopy
UHPC	Ultra-high-performance concrete
w/b	Water to binder mass ratio
XRD	X-ray diffraction

Chapter 1

1. Introduction

Recent reports from the Intergovernmental Panel on Climate Change (IPCC) highlight the necessity to reduce carbon dioxide and other greenhouse gas emissions. In response, the United Nations Sustainable Development Goal 12 (SDG 12) promotes and pushes the sustainable use of raw materials and encourages the transition toward more environmentally responsible and aware industrial practices. These changes are essential for both human well-being and the stability of the global ecosystem.

One promising solution in the construction sector is the partial replacement of Portland cement with industrial waste and by-products such as ground granulated blast furnace slag (GGBFS), fly ash, mine tailings, or rice husk ash. These alternative materials have the potential to reduce the carbon footprint of concrete and, when integrated with appropriate technology, design strategies, and execution methods, can also enhance the material's performance. Concretes incorporating such components are commonly referred to as greener concrete or low-carbon concrete, since the CO_2 attributions of those waste materials are usually lower than cement.

Fire safety is a crucial, but often overlooked, aspect of sustainable structural design. Due to its complexity and the relatively low frequency of fire incidents, it is usually underrepresented in research. According to fire statistics from Nordic countries gathered by the Swedish Civil Contingencies Agency (MSB) [1], the number of building fire events consistently ranges between 6,000 and 7,000 per year (2016–2021). Most of these involve “other buildings,” followed by apartment blocks and houses, which are mostly constructed of wood.

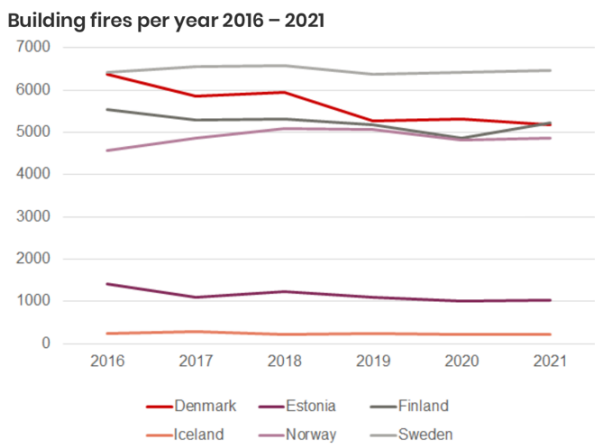

Figure 1 Building fires statistics per year 2016-2021 [1]

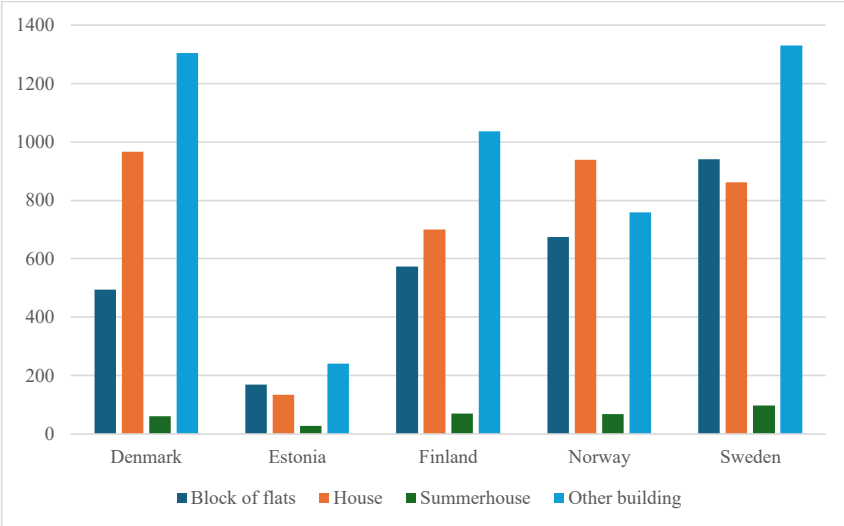

Figure 2 Building fire statistics by category in Nordic countries [1]

It is well known that regular concrete is the second most used material in the world, after water. Traditional concrete production relies mainly on Portland cement, which is responsible for 8–10% of global human-made carbon dioxide emissions. In 2023, the world CO_2 bill for cement production reached 48,366,293,000 t [2].

As a result, there is growing interest in developing new materials and technologies to reduce the carbon footprint of concrete. One possible, well-established, solution is to use industrial waste and by-products to replace part of Portland cement in concrete. These materials can help reduce carbon emissions and, when combined with proper technology, design, and execution, may also improve concrete performance.

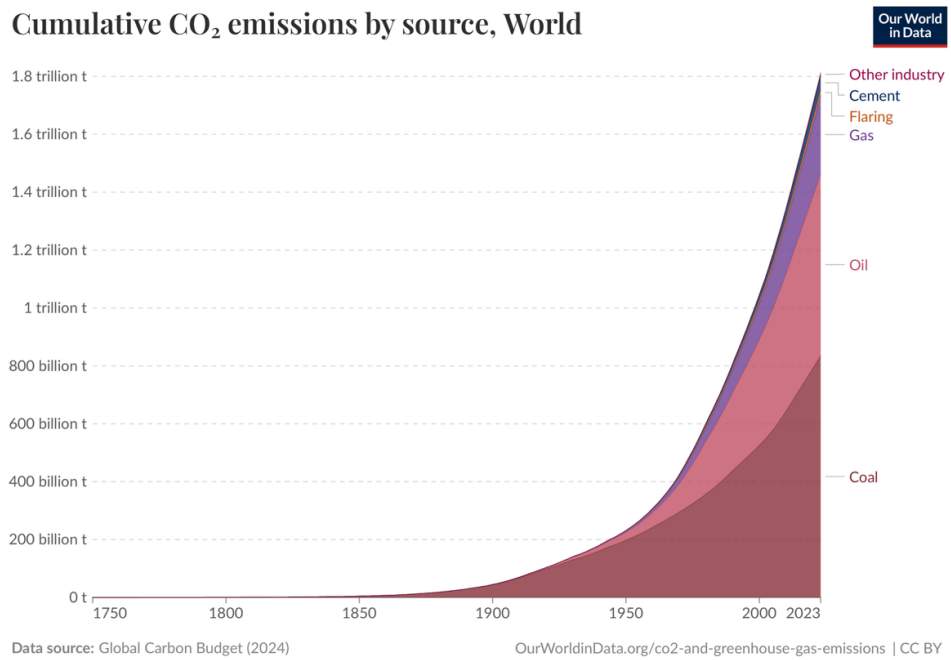

Figure 3 Cumulative CO_2 emission by source [2]

It is important to acknowledge that fire hazards can be decisive for structural integrity. Fires are also known to cause significant deterioration, particularly at structural joints, which is very often impossible to simulate or model.

Although traditional concrete has been studied for many years and is widely recognized for its fire and temperature resistance, some phenomena, such as spalling, are still not fully understood. This is largely due to the variable nature of fire events in real-life conditions. In the case of greener concretes, the issue is further complicated by the inconsistent chemical and physical properties of industrial waste materials, which vary depending on their source. As a result, there is a need to deepen our understanding of how such variations influence behaviour under high-temperature exposure. Authorised and fully standardised fire tests may only be carried out by accredited research institutes such as RISE (Sweden), CEF (France), or ITB (Poland). Since this research is conducted in the LTU building materials laboratory, it serves only as a small contribution to the broader and more complex field of fire research. Nevertheless, the more research is carried out, the more accurate the data and models become, ultimately helping to provide clearer guidelines and deeper understanding.

Aim and objectives

This study aims to investigate, test, analyse, and collect data on the performance of low-carbon concrete after exposure to high temperatures. The concrete mixes under examination incorporate ground granulated blast furnace slag (GGBFS) with different types of Portland cements, calcium sulfoaluminate (CSA) cement, various fillers, and selected concrete additives.
The hypothesis of this research is as follows: "The incorporation of industrial by-products and low-carbon cements into concrete contributes to improved performance following high-temperature exposure".
The purpose of this research is to investigate the behaviour of these binder combinations after exposure to elevated temperatures under controlled laboratory conditions.

Research objectives are as follows:

- To design concrete mixes incorporating GGBFS, CSA cement, various fillers, and selected concrete additives aimed at reducing the overall carbon footprint.
- To expose these concrete mixes to elevated temperatures under controlled laboratory conditions, simulating fire scenarios.
- To evaluate the mechanical performance of the mixes before and after high-temperature exposure.
- To assess changes in physical and chemical properties.
- To analyse the microstructural and chemical changes occurring in the binder matrix due to high-temperature conditions.
- To compare the post-exposure performance of lower-carbon mixes with that of conventional Portland cement-based concrete.
- To identify the synergistic effects, if any, of combining different types of cement with GGBFS admixtures, a filler is used to improve fire resilience.

This research aims to create a base of knowledge and collect experimental data. This could help improve existing technologies and products already available on the market. The goal is to support the use of alternative materials in making concrete mixes with a lower carbon footprint. These mixes should be able to resist fire, offer better safety during fire events, and help buildings and structures last longer. In the long run, the project hopes to make these solutions more popular and easier to use in real construction work, contributing to more sustainable and safer building practices.

Scientific approach

This study begun with a literature review to understand the current knowledge and recent progress in the field of fire-exposed eco-concretes. The goal was to see what has already been done, identify gaps in the research, and choose suitable methods and laboratory setups. This review helped shape the main research questions and guided the direction of the project.

The first practical step was to select a simple but reliable muffle furnace that could provide the right thermal conditions to simulate fire conditions. At the same time, concrete mixes were designed using industrial by-products, with the goal of avoiding the use of chemical admixtures. Early tests showed that admixtures could affect how the concrete behaves under high temperatures, so they were designated to be a part of a separate part of the research plan. The number of test variables was carefully limited: only the temperature conditions were changed during testing, while the water-to-binder (w/b) ratio remained the same for all mixtures.

The materials used: aggregates, sand, fillers, cement, and ground granulated blast furnace slag (GGBFS), are all available on the Swedish market. This choice was made to ensure that the results would be useful and relevant for local companies and stakeholders. For testing and analysis, standard and well-known methods were used. These included compressive strength testing, X-ray diffraction (XRD), scanning electron microscopy (SEM), and energy-dispersive X-ray spectroscopy (EDX). These tools made it possible to study the changes in the concrete's structure and composition after high-temperature exposure.

In summary, the scientific approach in this PhD project was based on practical choices, clear limits, and a focus on real-world application. The aim was to carry out solid, focused research with results that can be useful both in science and in practice.

Research questions

1. How does the partial replacement of cement with GGBFS influence the thermal resistance of concrete in fire exposure? (**Paper A, Paper B**)
2. What microstructural and chemical changes occur in cement-GGBFS blends during high-temperature exposure? (**Paper C**)
3. What are the limiting factors affecting the high-temperature performance of CSA cements compared to PC and GGGFS-based binders? (**Paper D**)
4. What are the factors influencing the high-temperature performance of concretes? (**Paper B, Paper C, Paper D, Paper E**)

Limitations

The main goal of this study was to assess the performance of selected lower-carbon concrete mixes when exposed to high-temperature. The aim was to observe changes on micro and macro levels. Due to the complexity of thermal testing, each part of the process had to be carefully controlled. This included choosing the right type of muffle furnace, selecting a suitable sample size, placing the samples evenly inside the chamber with the same distance from the heating elements and between samples, setting accurate heating and cooling rates, and handling the samples properly after testing to limit rehydration caused by humidity in the air.

Due to the sensitivity of these steps, it is difficult to directly compare results with those from other studies. Even small differences, such as the specific furnace model used, can lead to noticeable differences in outcomes, even if the temperature range and heating program are the same. Other factors like airflow inside the furnace, the size of the chamber, and how heat spreads can affect how the material behaves. These differences can influence how much the concrete degrades, how much strength it retains, and what changes occur in the microstructure. For this reason, it is important to be careful when comparing results from different studies and to always consider these differences in equipment and procedures.

Due to time constraints, the mix ingredients and temperature thresholds were kept the same throughout the study. Even small changes in mix design would have significantly increased the number of required tests.

Another limitation of this study was the fact that concrete samples could only be tested after they had fully cooled down to room temperature.

Chapter overview

This thesis is divided into five chapters and appended research papers.

Chapter 1 gives an overview of the project, including its goals and limitations. Formulates research questions and explains the scientific approach

Chapter 2 contains a summary of the literature review focusing on concrete materials exposed to high temperatures.

Chapter 3 describes the materials selected for the study and the testing methods used to assess their performance.

Chapter 4 presents the results and is divided into four main sections: Portland cement – Ground granulated blast furnace slag blends, Calcium sulfoaluminate cement, Large-scale Testing, and Unexpected findings.

Chapter 5 provides a discussion of the key results and presents the main conclusions drawn from the work.

List of appended publications

Paper A

Title: Eco-Concrete in High Temperatures. *Materials 2023, 16(12), 4212*

Authors: M. Sundin, H. Hedlund, A. Cwirzen
Findings: Concrete made with industrial waste materials like fly ash, GGBFS, rice husk, and mine tailings can offer improved fire resistance and maintain compressive strength up to 700 °C. Strength gains are often linked to matrix densification and sintering. Above 700 °C, strength declines due to thermal degradation and moisture loss. Eco-concrete tends to exhibit less spalling and cracking than PC. Some fiber-reinforced mixes showed no deterioration and even signs of self-healing. Cooling conditions, especially rapid cooling, significantly affect post-fire performance.

Paper B

Title: Physical Changes and Performance at High Temperatures of Cement-Slag Blended Concretes, *Accepted for publication in Fire and Materials, 2025.*

Authors: M. Sundin, M. Rajczakowska, J.L. Provis, H. Hedlund, A. Cwirzen

Findings: This study evaluated three cements combined with varying amounts of GGBFS, exposed to 400 °C and 800 °C for 1 hour. Most mixes lost strength at higher temperatures, but at 400 °C, many showed either strength improvement or retention within experimental limits. Blends with a 50:50 PC/slag ratio performed best, showing minimal mass loss, improved compressive strength, and low water absorption. While 800 °C negatively affected all mixes, slag content alone did not fully determine thermal performance. PC 52.5-based mixes showed the highest thermal stability. Increased slag content led to deeper red-brown coloration but no clear trend in crack formation. SEM analysis at 400 °C revealed no cracks in mixes containing 50 wt.% of GGBFS, though dehydration and porosity increased. At 800 °C, matrix disruption and gel separation occurred, with denser microcracking in slag-rich mixes, though aggregates stayed intact. The results suggest that elevated temperatures boost slag reactivity and hydration, but excessive slag content may reduce matrix stability under heat.

Paper C

Title: Evolution at elevated temperatures of cement pastes blended with ground granulated blast furnace slag (GGBFS). *Submitted for publication.*

Authors: M.Sundin, M. Rajczakowska, K. Dvorak, A.Jancikova, H. Hedlund, A.Cwirzen

Findings: The study shows that cement types (CEM 32.5, 42.5, 52.5), along with GGBFS and quartz powder, influence concrete's thermal stability. Quartz generally increases porosity and triggers earlier phase transformations. Samples without quartz were more stable at intermediate temperatures, while quartz-containing ones showed phase changes and porosity increases between 400 °C and 800 °C. These effects stabilized at 1200 °C. Quartz also undergoes alpha-to-beta transformation, enhancing thermal compatibility. Melilite formed after high-temperature exposure, especially in CEM 32.5 mixes without quartz, likely due to higher

alumina and silica content and the influence of fly ash. Melilite's thermal stability properties improve performance under heat. Although quartz-induced porosity and decomposition of calcite and portlandite can reduce strength, the formation of stable phases like åkermanite and C_3A may counteract these effects. Optimizing quartz content can help balance thermal performance and cost efficiency, especially when early thermal resistance is not a priority.

Paper D

Title: Effects of eggshell and limestone on CSA cement-based system exposed to high temperatures. *Submitted for publication.*

Authors: M. Sundin, S. Ruiz Martínez, K. Dvorak, M. Szelag, H. Hedlund, A.Cwirzen

Findings: This study found that replacing part of CSA cement with eggshell powder improves thermal stability compared to limestone-modified and unmodified mixes. While CSA and CSA–limestone blends failed at 800 °C, eggshell-modified mixes retained integrity and compressive strength. This is linked to improved pore structure, which allowed moisture release and reduces internal pressure. SEM and EDX revealed dense, needle-like crystalline phases in high-temperature samples with high calcium and sulfur content. Though resembling ettringite, these thermally stable phases likely belong to sulfate- or aluminate-based compounds. The findings highlight eggshell powder's potential to enhance performance while promoting sustainability. Future research should optimize dosage and fineness, study long-term durability, and investigate the crystalline phases in greater detail. Combining eggshell with other waste materials may further improve thermal performance and reduce the carbon footprint.

Paper E

Title: Effects of admixtures on cement-slag concrete at elevated temperatures, *Conference Proceedings, Conference on durability of infrastructures, 22-28 March 2025, Mendrisio, Switzerland. Accepted for publication in Springer Nature, 2025.*

Authors: M. Sundin, J. Provis, H. Hedlund, A. Cwirzen

Findings: Commercial admixtures significantly affect concrete's thermal behaviour. Air-entraining agents improved thermal stability, while accelerators caused instability, vivid discoloration, and explosive spalling, even at recommended dosages. Superplasticizers increased mass loss, indicating heat sensitivity. Strength gains were observed at 400 °C, but performance dropped at 800 °C, especially in mixes with accelerator addition. These results highlight the need for caution in admixture selection. High accelerator content poses serious safety risks, especially in non-professional concrete production, where quality control may be limited.

Chapter 2

2. Literature review

2.1. Fire

Fire is one of the most destructive phenomena affecting buildings and infrastructure made of concrete [3]. Beyond its immediate threat to human life and property, fire imposes significant challenges on the structural integrity of construction materials. Understanding fire as a physical process, as well as its interaction with materials like concrete, is essential in designing structures that are not only robust but also resilient and safe. This chapter provides an overview of fire behaviour, its effects on concrete, and the relevance of fire science in the context of sustainable, high-performance concretes.

Fire is a chemical reaction called combustion that occurs between a fuel and an oxidizer, typically involving the rapid oxidation of materials and the release of heat, light, and various combustion products [4]. The process requires three elements: fuel (wood, plastic, fabric, etc.), oxygen (air) and heat (ignition source).

When these elements are in the right proportions and conditions, fire ignites and can propagate rapidly, depending on environmental and material factors.

2.1.1. Fire event stages

Fires in buildings typically develop through five key stages [5], [6]. Ignition is the initial phase, where a material is heated until it combusts. In the growth stage, the fire spreads, igniting nearby materials and increasing in intensity. Pre-flashover leads to the fully developed fire, the hottest and most destructive phase (flashover), where all combustible materials in the compartment are actively burning (post-flashover). In the decay stage, the fire begins to subside as it runs out of fuel or oxygen. Each stage affects materials differently, especially those designed to resist high temperatures or maintain structural stability. After these stages comes the exhausting phase**,** where the fire is fully extinguished, either naturally through total decay or with human intervention such as fire extinguishers (powder, foam, water) or fire suppression systems (both passive and active). During this period, materials and structures often suffer the greatest damage due to water pressure, rapid temperature changes, and mechanical stresses. The structure may also become significantly weakened, which can jeopardize its overall stability [7].

2.1.2. Fire and Building Safety

Building fire design must include several key considerations to ensure structural performance and occupant safety. Fire resistance refers to the ability of structural elements such as walls and slabs to maintain their load-bearing capacity and integrity during exposure to high temperatures [8]. Fire divisions involve the use of fire-resistant barriers to prevent the spread of flames and smoke between different sections of a building. An effective evacuation strategy ensures that all users can exit the structure safely within a limited timeframe before conditions become life-threatening. Fire suppression systems, including sprinklers and passive fire protection coatings, are used to slow or control the development of fire. These fire safety aspects are integrated into national and international fire codes and testing standards. They

provide guidelines for the design, assessment, and performance classification of buildings under fire conditions. Fire safety is particularly important in the design and evaluation of building materials. In the context of concrete structures, understanding how materials respond to elevated temperatures is essential for keeping structural stability, protecting human life, and determining post-fire lifespan. Standardized fire curves are used to simulate fire event exposure [6]. These curves represent the evolution of temperature over time and are commonly applied in experimental studies and regulatory testing to assess material behaviour and structural performance under realistic fire scenarios.

2.1.3. Definition and Purpose of Fire Curves

A fire curve, or time–temperature curve, is a graphical representation that describes how temperature increases during a fire as a function of time. These curves are essential to take into consideration during:

- Designing fire-resistant structures,
- Establishing testing protocols for fire resistance,
- Calibrating thermal and structural models,
- Understanding material degradation mechanisms under elevated temperatures.

Standard fire curves are defined by various national and international standards (e.g., ISO 834, ASTM E119, EN 1363-1), and each curve is developed to represent specific fire scenarios.

2.1.4. Types of Fire Curves

- *Standard Fire Curve (ISO 834 / EN 1363-1) [9], [10]*

The most popular curve in regulatory fire testing, represents a fully developed compartment fire and it is defined as:

$$T=T0+345\cdot log_{10}(8t+1)$$

Where:
T- *temperature [°C],*
T0 - *ambient temperature (usually 20°C),*
t -*time [min].*

This curve does not include the cooling phase and is primarily used to test fire resistance ratings (e.g., R30, R60, R90). R-values stands for fire resistance in minutes (e.g., R30 = 30 min, R60 = 60 min).

- *Hydrocarbon Fire Curve (HC) [9], [10]*

It represents fuel-based fires, particularly in petrochemical or tunnel environments, where the HC curve reaches higher temperatures faster:

$$T=1080(1-0.325e^{-0.167t}-0.675e^{-2.5t})$$

Where:
T- *temperature [°C],*
t -*time [min].*

The hydrocarbon curve is recommended for applications where fire intensity is higher and more immediate, such as vehicle fires in confined spaces.

- *RABT-ZTV Tunnel Fire Curve [9], [10]*

This curve is used in tunnel fire testing in Germany. It has a steep rise (up to 1200°C in 5 minutes), a constant high-temperature plateau, with a following controlled cooling phase.

- *Real Fire Curves (Parametric Fires) [9], [10]*

These parametric fire curves are more complex, considering more factors. They are based on actual fire loads, ventilation conditions, and set-ups, and compartment geometry. These are used in performance-based design, with a cooling phase that significantly impacts the thermal shock and residual capacity of materials.

2.1.5. Complexity and challenges of fire modelling

Fire modelling in concrete structures is a complex and multifactorial process that presents significant challenges due to the wide range of variables involved. Each component of the concrete mix influences how the material will respond to fire exposure, with interactions varying depending on the specific conditions of the fire scenario. The binder type, whether cement-based [11], [12], geopolymer [13], [14], [15], or another materials combination [16] influences the thermal stability of concrete. High-performance binders [17] can delay degradation, while weaker binders [18] may compromise the material's fire resistance.

Additionally, the water-to-binder (w/b) ratio plays a critical role in determining the porosity and density of the concrete [19], [20]. Lower water-to-binder (w/b) ratios generally produce a denser microstructure, whereas higher ratios result in increased porosity. For optimal fire performance, the microstructure should be sufficiently dense to ensure strong bonding but also maintain enough porosity to facilitate the evacuation of gases released during thermal or chemical processes.

The aggregates, whether natural, artificial, or recycled, also influence fire performance [21], [22]. Limestone aggregates have different thermal conductivities compared to granite or basalt aggregates, impacting the speed at which heat is transferred through the concrete. Even the size, volume, and type of aggregates [21] affect the concrete's ability to resist cracking under thermal stress. Smaller aggregates may compact better and reduce crack formation under fire exposure, while larger aggregates can lead to increased vulnerability due to uneven heating and expansion.

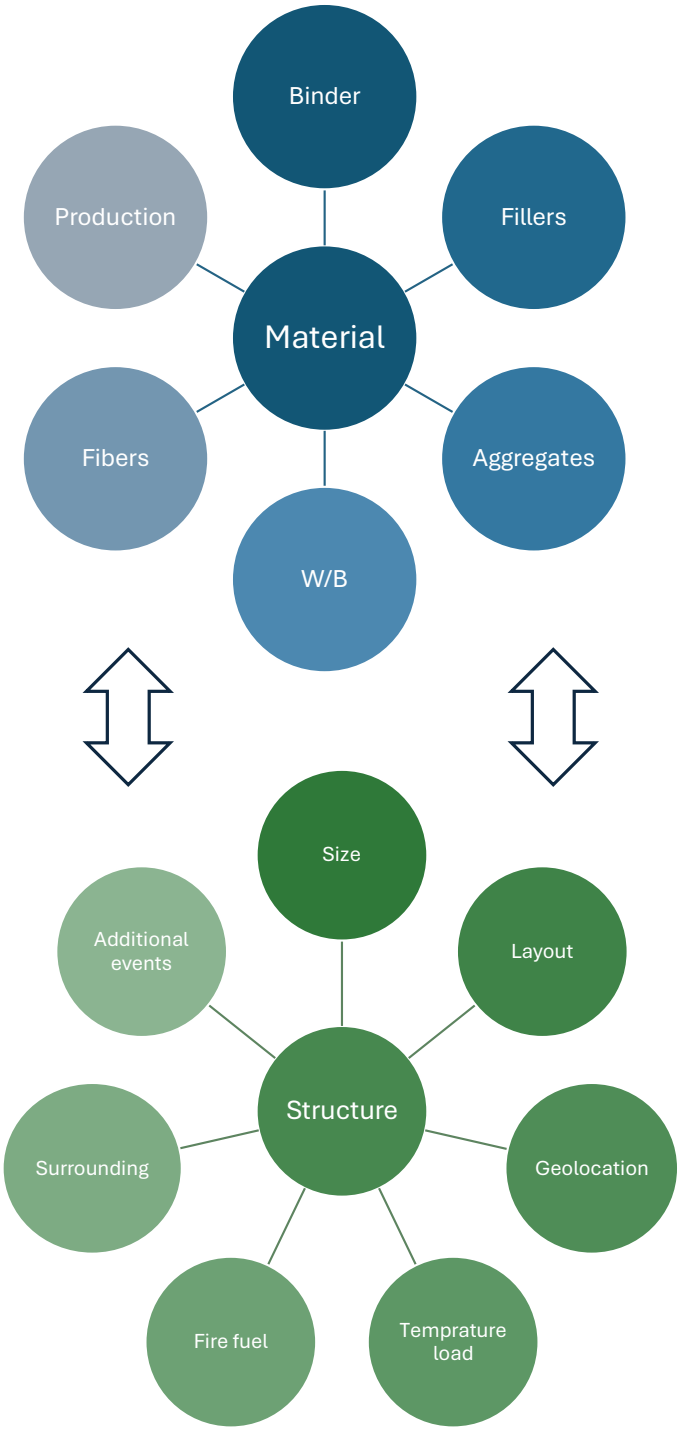

Figure 4 Suggestion of factors to be taken into consideration for fire modelling.

Admixtures added to enhance workability, durability, or set times can also affect fire performance *[Paper E]*. Retarders or accelerators might alter the thermal properties of the mix, while air-entraining agents can improve freeze-thaw resistance [23] but may reduce fire resistance *[Paper E]*. The presence of steel reinforcement [24], [25] or synthetic fibres [26], [27], [28] further complicates the situation. Steel rebars lose strength at high temperatures, which can lead to potential structural collapse. Synthetic fibres like polypropylene [29] may melt under fire exposure, leaving voids in the concrete matrix, which is beneficial in this context. The type, quantity, and distribution of fibres used are therefore crucial factors in determining fire resistance.

The mixing process itself is very influential. Poor mixing can result in an uneven distribution of components [30], [31], leading to areas with different fire resistance ranges. For instance, dry powder clumps in the mix can create weak points, which are more susceptible to rapid thermal degradation. On the other hand, a well-mixed concrete is uniform and helps to distribute heat more evenly and improves fire performance.

The countless materials, mix combinations, and compositions create countless cases to study, address, and assess to provide reliable and precise data that can be used in real life.

Fire scenarios also significantly influence the performance of concrete, as the severity, duration, and nature of the fire directly affect how the material reacts [32], [33], [34]. A scenario involving rapidly rising temperatures will impact concrete differently than a slower-burning, lower-temperature fire. In this context, the literature distinguishes between two primary fire types [35]: compartment fires, where the fire remains confined to a specific area, and traveling fires, where the flames move across various parts of a structure. Each scenario imposes different thermal and mechanical stresses on concrete elements. The unpredictability of fire origin, spread patterns, and intensity further complicates the modelling process, making accurate fire performance predictions particularly challenging.

The building design and size of the construction itself play a key role. Bisby et al. [36] published a comprehensive review regarding this aspect. A large, open-plan building may allow fire to spread quickly, while a smaller, compartmentalized structure might slow the spread of flames and protect certain areas. In multi-story buildings, fire can travel quickly via stairwells, shafts, and ventilation systems. The building's design and content inside (fire fuel load [37], [38], [39], [40]), along with fire protection systems like sprinklers and fire barriers, must be accounted for in fire modelling in a context of concrete structural elements. Geographical location, seasons, and weather anomalies further complicate fire modelling for concrete [41], [42]. Coastal areas with high humidity can cause concrete to absorb moisture [43], [44], which might reduce its fire resistance due to steam expansion. In arid regions [45], concrete may dry out more quickly, becoming more brittle and prone to cracking. Seasonal changes, such as freezing and thawing cycles in colder climates [46], [47], can create microcracks that weaken concrete, making it more vulnerable to thermal stress during a fire.
The higher potential for explosions during fire events gives another layer of complexity [48]. Explosions can cause rapid temperature fluctuations, shockwaves, and pressure changes that may overwhelm concrete's ability to withstand fire. Technical explosions, like those caused by gas leaks or electrical faults, create rapid bursts of energy that concrete might not be able to absorb effectively, leading to immediate damage.

In conclusion, fire performance modelling for concrete structures is influenced by a very complex spectrum of factors, including material properties, fire scenarios, human behaviour,

and geographical context. A deep understanding of these variables, combined with advanced simulation tools, is crucial to ensure that concrete structures meet safety and resilience standards under real-world fire conditions. Only with such comprehensive modelling, is it possible to reliably predict the performance of concrete structures when exposed to extreme fire scenarios. Khan et al. [49], in their comprehensive publication regarding fire models, described and grouped them into three primary groups, each varying in complexity and applicability to different fire scenarios:

- Category I: Idealized Uniform Fire Models include models that assume a uniform temperature across all structural components exposed to fire, without accounting for the dynamic nature of fire behaviour or heat transfer. These models, such as the ISO**,** ASTM**,** and Hydrocarbon fire curves, provide a simple approximation of fire effects in situations where the fire is fully developed, but they do not reflect the complexities of real-world fire scenarios.
    - Category IB includes models that apply a steady-state maximum temperature over a specified period, commonly used for ventilation-controlled fires. These models, such as Kawagoe [50], Thomas et al. [51], Law [52], Babrauskas [53] assume that the fire reaches a maximum temperature and sustains it over time. However, they still do not fully account for the fire's growth or decay phases, limiting their application in dynamic fire situations.
    - Category IC represents a more refined approach by introducing time-variant temperatures to represent the fire's growth and decay phases. This category includes models like Eurocode 1 [54], Magnusson and Thelandersson [6], which provide a better approximation of how fire conditions evolve over time, but they still rely on simplified temperature curves derived from experimental data rather than modelling the actual fire dynamics.
- Category II: Non-Uniform Fire Models takes a more sophisticated approach by accounting for non-uniform temperature distributions, which are critical in scenarios involving localized or fuel-controlled fires and traveling fires. These models, such as Hasemi's [55], Rein's [56], and ETFM [57], [58], simulate fire behaviour in more complex environments like large open-plan spaces, tunnels, or industrial settings, where fire does not spread evenly. They offer a more accurate representation of fire dynamics in cases where fire behaviour varies across different parts of a building, allowing for a better prediction of temperature gradients and their effects on structural components. These models are more applicable in real-world scenarios, where fire growth is often irregular and heavily influenced by factors such as ventilation, fuel load, and the presence of combustible materials.
- Category III: Realistic Fire Models represents the most advanced and accurate fire models, using experimental data and detailed field models to define thermal boundaries and simulate convective and radiative heat transfer. These models, such as Field Structure Interface (FSI) [59] and Adiabatic Surface Temperature (AST) [60]**,** consider the actual physical behaviour of the fire and its interaction with structural elements, providing precise temperature gradients and heat fluxes. These models are way much more complex and need powerful computer set-ups and advanced simulation methods, but they provide the most accurate predictions of how fire affects a structure's safety and strength. Their detailed data input makes them particularly useful for critical applications, such as performance-based fire safety engineering for buildings or infrastructure. There are also hybrid models, like Computational Fluid Dynamics (CFD) [61], [62] with Finite Element Methods (FEM) [63], [64], [65] to address the simulation of interaction between fire and structure. CFD is used to model the gas phase

of the fire, including heat transfer, smoke movement, and fire dynamics, while FEM is used to analyse the structural response to the fire's heat and stresses. The combination of these models allows for a more integrated and realistic simulation of fire scenarios, as both the fire and structural responses are modelled simultaneously. This approach still faces challenges, particularly in terms of computational cost and the difficulty in achieving two-way coupling, where both fire and structural models interact in real-time. Most current simulations rely on one-way coupling [66], where fire data is used as input for structural analysis, but the future of fire modelling may move toward more sophisticated two-way coupled models [67], [68].

To support the development and application of such approaches, for example, the SFPE Handbooks of: Fire Protection Engineering [69], Fire Exposure to Structural Elements [70] and Engineering Standard Calculating Fire Exposures to Structures [71] compile in-depth reports on various modelling strategies and approaches for calculating the structural response to fire.

The increasing availability of computational resources and the growing potential of AI open new doors and opportunities for fire modelling. Still, fundamental data on the performance of different concrete mixtures under fire must be explored, gathered and clearly defined. This data serves as a crucial input for the development of reliable, next-generation fire models.

2.2. Fire and Concrete Materials

Concrete is commonly known as a fire-resistant material because it does not burn and has low thermal conductivity [72]. However, its behaviour during fire exposure is more complex and influenced by several factors [73], [74]. One key factor is the mix design, which significantly affects how concrete responds to high temperatures. The type of cement used is particularly important, as different cements have distinct chemical compositions and react differently when heated. For example, calcium sulfoaluminate (CSA) [18], [75] cement exhibits different fire performance compared to Portland cement (PC) [76], [77]. Even within Portland cement, various classes behave differently under elevated temperatures [Paper C]. Additionally, the water-to-cement ratio plays a crucial role, as it influences the concrete's porosity and density, both of which affect its thermal and mechanical performance during fire exposure[78].

When cement is mixed with water, a hydration reaction begins [79]. This reaction is what allows concrete to harden and gain strength. The main compounds in cement are tricalcium silicate (C_3S) and dicalcium silicate (C_2S). They react with water to form calcium silicate hydrate (C–S–H) and calcium hydroxide (portlandite, $Ca(OH)_2$).

C_3S + water → C–S–H + $Ca(OH)_2$
C_2S + water → C–S–H + $Ca(OH)_2$ (slower reaction)

The C–S–H gel is the main compound responsible for the concrete's strength and durability. Portlandite helps fill pores and contributes to the overall structure, but it is more sensitive to heat [76], [80]. However, when concrete is exposed to high temperatures, these hydrated products begin to decompose, *Table 1*.

Table 1 Temperature effects on PC based concrete matrix [81]

Temperature Range	Effects on Concrete
100–200°C	Evaporation of free water – minor strength reduction
200–400°C	Dehydration of C–S–H gel – initiation of microcracking
400–600°C	Decomposition of portlandite – substantial strength loss
600–800°C	Aggregate expansion, extensive internal damage
>800°C	Severe matrix degradation

In summary, cement-based concrete possesses fixed limitations when subjected to elevated temperatures. These include a loss of mechanical strength, thermal incompatibility among constituents, microstructural deterioration, and a decline in durability after fire exposure. These challenges highlight the need for alternative binder systems or supplementary materials capable of improving thermal resistance and post-fire recovery.

2.2.1. Cement blends with GGBFS concretes

Concrete incorporating supplementary cementitious materials (SCMs), such as ground granulated blast furnace slag (GGBFS), demonstrates enhanced performance at elevated temperatures [16], [82], [83], [84], [85]. This improvement comes from significant changes in the material's physical, chemical, and thermodynamic properties. The inclusion of GGBFS leads to a denser cementitious matrix with a more refined pore structure [86]. While Portland cement (PC) hydration typically results in a heterogeneous network of capillary pores (0.01–10 μm) and microcracks [87], the pozzolanic and latent hydraulic reactions associated with GGBFS reduce total porosity and shift the pore size distribution toward finer gel pores (<0.01 μm) [86]. These gel pores are more thermally stable. It improves the resistance to internal pressure buildup (spalling) and thermal degradation.

From a microstructural perspective, this densification reduces permeability and slows the migration of moisture and gases under heat [86]. It delays the onset of thermal damage. Thermodynamically, GGBFS-blended concretes also respond differently to heat compared to pure PC systems [88]. Their finer pore structure and higher content of amorphous phases [89] result in lower thermal conductivity, which limits heat transfer and reduces internal thermal gradients. It minimizes thermal stresses (cracking or spalling) by acting like an internal insulator. Although some scientists have observed, but only limited direct evidence has been reported, that concrete containing slag may release hydrogen sulfide (H_2S) upon heating, such a risk cannot be entirely dismissed. [90]. Particularly if sulfide-rich aggregates or slag phases undergo decomposition in reducing or moisture-rich conditions. H_2S is a known toxic gas, and its potential generation under high-temperature testing should be considered and appropriately monitored.

Table 2 Temperature effects on PC-GGBFS based concrete matrix [81]

Temperature	Phase decomposition
<200°C	Evaporation of free water, mass loss: potential improvement in mechanical properties due to temperature-induced gel formation
200-400°C	Strength gain: associated with gel formation and reduced porosity
400-800°C	Strength loss: caused by gel crystallization and reduced mechanical performance
>800°C	Formation of β-C_2S along with crystalline phases such as åkermanite, merwinite, and gehlenite [82]

GGBFS-blended binders typically have a higher specific heat capacity [91], allowing the material to absorb and store more thermal energy before undergoing a phases change. As a result, dehydration and decomposition reactions occur more gradually, as reflected in thermogravimetric analysis (TGA) [92], which shows a smoother and delayed mass loss curve for GGBFS concretes. This gradual thermal response contributes to improved thermal stability.

In terms of bulk density, GGBFS systems often exhibit slightly higher oven-dry densities due to improved particle packing and the pozzolanic infilling of voids, though this is influenced by the replacement ratio and curing conditions [83]. Under high-temperature exposure, GGBFS concrete typically shows reduced mass loss and improved dimensional stability, thereby lowering the risk of explosive spalling [93]. When exposed to temperatures up to approximately 600 °C, GGBFS-blended concretes tend to outperform PC systems in terms of fire resistance [85]. This is largely attributed to the consumption of calcium hydroxide through the latent hydraulic reaction between GGBFS and PC hydration products, forming additional calcium silicate hydrate (C–S–H) gel. Since portlandite decomposes between 450 and 550 °C [94], GGBFS concretes having less portlandite suffer less mass loss and microstructural disruption in this critical temperature range. At temperatures exceeding 700 °C, the integrity of GGBFS-based matrices can begin to deteriorate due to the thermal decomposition of C–S–H and the sintering of gel phases [83]. While the dense microstructure initially slows moisture transport and pore pressure accumulation, the reduced availability of free lime weakens the material's ability to buffer decomposition products. At these elevated temperatures, recrystallization processes during cooling down lead to the formation of a high-temperature phase such as melilite [95], åkermanite ($Ca_2MgSi_2O_7$), gehlenite, ($Ca_2Al(AlSiO_7)$), merwinite ($Ca_3MgSi_2O_8$), and other calcium–magnesium silicates [96]). These phases form through partial melting and solid-state reactions involving the slag's constituent oxides (Ca, Mg, Si, Al), *Table 3*.

Table 3 Mineral phases in slag-containing concrete and their behavior at elevated temperatures .

Mineral Phase	Chemical Formula	Formation Temperature (°C)	Effect on properties
Åkermanite [96]	$Ca_2MgSi_2O_7$	900–1200	Improves thermal stability and refractoriness, forms a more stable matrix but may induce microcracking if excessive
Gehlenite [82], [97]	$Ca_2Al(AlSiO_7)$	900–1000	Makes concrete hard but brittle and unable to regain strength
Merwinite [95]	$Ca_3MgSi_2O_8$	700–900	Enhances dimensional stability, contributes to high-temperature strength but can cause brittleness

The formation of these crystalline phases can enhance thermal and dimensional stability by creating a stronger matrix, but overdevelopment may introduce microcracks and reduce the overall binding capacity.

The interfacial transition zone (ITZ), typically more compact in GGBFS concretes at ambient conditions [98], may also suffer under thermal exposure. Thermal expansion mismatches and shrinkage-induced stresses can lead to localized debonding within the ITZ, contributing to deterioration in mechanical performance.

In summary, *Table 4*, the superior high-temperature performance of GGBFS concrete lies in its thermodynamically advantageous microstructure characterized by reduced porosity, finer pores that keep their size and distribution under heat exposure, lower thermal conductivity, and higher heat capacity. These properties synergistically enhance the material's resistance to

internal thermal stresses, delay degradation processes, and help preserve structural integrity under fire or prolonged high-temperature exposure.

Table 4 Comparison here is presented on the basis of concretes containing similar aggregates

Property	**PC Concrete**	**GGBS Concrete**
Total Porosity [99], [100]	Higher (includes more capillary pores and microcracks)	Lower (higher gel pore fraction)
Pore Size Distribution [99], [100]	Coarse pores (>0.1 µm)	Finer pores (<0.01 µm), more uniform
Bulk Density (20°C)	Typically 2200–2350 kg/m³	2250–2400 kg/m³
Thermal Conductivity (λ) [101]	1.2–2.0 W/m·K	Lower (0.7–1.5 W/m·K), varies with moisture and mix
Specific Heat Capacity (cp) [102]	~0.75–0.88 kJ/kg·K	~0.85–0.95 kJ/kg·K, better energy absorption
Thermal Expansion Coefficient [103], [104]	Increases at >400°C	More gradual, less volumetric instability
Dehydration & Mass Loss	Rapid between 100–600°C	Delayed [92]
Spalling Risk [82]	High due to vapor buildup and thermal shock	Lower due to fine pores and better internal moisture release

2.2.2. Calcium sulfoaluminate (CSA) concrete

Calcium sulfoaluminate (CSA) cement-based concretes show different thermal behaviour compared to traditional PC systems due to differences in hydration chemistry, mineralogical composition, and microstructure [18]. The primary hydration product in CSA cements is ettringite [105], [106], which forms quickly in the presence of calcium sulfate and reacts with ye'elimite (C_4A_3S). The main hydration reactions at ambient temperatures are:

- Ye'elimite hydration (with gypsum):
  $C_4A_3S + 2\ CSH_2 + 34\ H \rightarrow C_6AS_3H_{32}$ (ettringite)
- Secondary reactions (in low-sulfate conditions):
  $C_4A_3S + 18\ H \rightarrow C_4AH_{13} + AH_3$

These reactions produce a dense and crystalline matrix with a lower $Ca(OH)_2$ content and faster strength gain compared to PC [107]. Under thermal exposure the behaviour differs due to the decomposition of sulfate-bearing hydrates and the loss of crystalline water [108]. TGA of CSA concrete typically reveals multiple mass loss steps: 50–150 °C from evaporable and bound water; 200–300 °C due to decomposition of ettringite into monosulfate (AFm) and alumina gels; and 350–600 °C linked to further dehydration of monosulfate and C–A–H phases [109], [110]. CSA systems show minimal portlandite decomposition, as $Ca(OH)_2$ is not a primary hydration product. CSA concretes demonstrate moderate thermal conductivity and lower internal thermal stress due to their fine-grained pore structure and lower porosity [111], [112], [113]. The thermal stability of ettringite is relatively low, and its decomposition around 100°C [18] can lead to significant microcracking, particularly if not stabilized by additional pozzolans. This early change contributes to shrinkage and dimensional disability at higher temperatures. But when properly modified, CSA concretes display better volumetric stability and slower heat-induced mass loss than PC, due to their low calcium hydroxide and low calcium silicate content [114], [115]. The compressive strength of the samples tested immediately after heating was reduced to 7% at 100 °C, 42% at 200 °C, and 39% at 300 °C. When tested 30 minutes later, the strength losses were 12% at 100 °C, 45% at 200 °C, and 43% at 300 °C. At the testing temperatures of 200 and 300 °C, several internal cracks developed

during the heating phase prior to loading. As a result, the first straight part of the stress–strain curve became shorter, showing that the material could carry less load, according to the study of Tchekwagep et al. [116] The material also became more flexible at higher temperatures, which might be helpful if the structure cracks during a fire.

Table 5 Calcium sulfoaluminate (CSA) phase decomposition [108]

Temperature	Phase decomposition
<90°C	Ettringite dehydration and decomposition to monosulfate and calcium sulfate
>150°C	Partial monosulfate dehydration
200-230°C	Alumina trihydrate dehydroxylation
>450°C	Monosulfate dehydration

To summarize, CSA concrete displays unique high-temperature behaviour shaped by its ettringite-rich chemistry and low portlandite content. Although ettringite starts to break down at around 100 °C, which can cause problems, a well-designed system can still show less thermal cracking and lower mass loss. Adding supplementary cementitious materials (SCMs) can improve these properties and make the system more environmentally friendly and suitable for real-life use.

2.2.3. Aggregates

Aggregates influence the performance of concrete under high-temperature exposure, both physically and chemically [21]. Their mineralogy, size, and thermal compatibility with the cement matrix determine how the material responds to thermal stress. Siliceous aggregates, such as quartz-rich granite or sand, undergo a sharp allotropic transformation near 573 °C (from alpha to beta quartz) [117], [118], [119], resulting in sudden and anisotropic volume expansion. This induces extra stress which leads to microcracking and debonding at the interfacial transition zone (ITZ). The ITZ is a thin, microstructurally distinct region between the aggregate surface and the cement paste [120], [121], [122]. The ITZ is often the weakest link in the concrete matrix due to its higher initial porosity, lower density, and greater concentration of portlandite, making it particularly vulnerable and sensitive to thermal degradation.

One of the most critical factors influencing damage at high temperatures is the incompatibility of thermal expansion between aggregates and the surrounding cement matrix. Aggregates and paste typically have different coefficients of thermal expansion (CTE) [123]. Siliceous aggregates often exhibit a higher CTE than the cement paste, which leads to differential movement during heating [124]. This mismatch generates internal tensile stresses at the aggregate–paste interface, resulting in the initiation and propagation of microcracks. These stresses intensify with temperature changes, especially during rapid heating and cooling. It can compromise the bond within the ITZ. Calcareous aggregates such as limestone tend to have lower and more compatible thermal expansion behaviour [125]. It reduces stress development and preserves ITZ integrity to a greater extent. Also, limestone aggregates begin to chemically decompose into calcium oxide and carbon dioxide at around 900 °C, which introduces additional porosity and mass loss [125]. Xing et al. [126] reported that flint aggregates in their setup were prone to explosive spalling at 300 °C.

The thermal expansion mismatch leads to cracking around coarse aggregates more than spherical [127]. Round shapes better distribute and spread the expansion and evenly “press” the matrix around [122].

Aggregate size plays an additional role [128]. Larger aggregates contribute to more pronounced local stress concentrations (spalling) due to their lower surface area-to-volume ratio and accumulation of heat. This increases the severity of damage caused by thermal incompatibility. Smaller aggregates provide more uniform distribution of stress but enlarge the total ITZ surface [129], which can increase the extent of thermal degradation in the matrix. As temperature rises, dehydration of hydrates, microcracking, and sintering processes cause the porosity of the ITZ to increase, while its relative density decreases. This results in reduced mechanical interlock and a loss of stiffness and strength [119], [130]

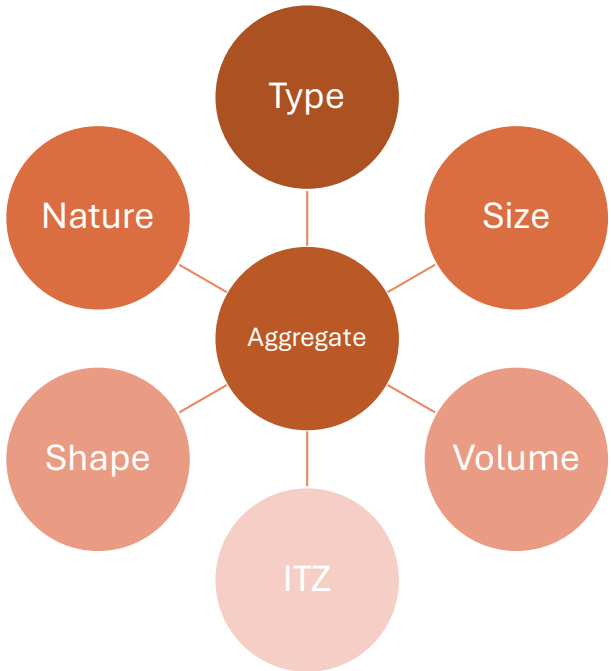

Figure 5 Aggregate-related factors influencing the fire resistance of concrete.

Using recycled materials in concrete raises new questions about how well they handle heat compared to natural materials. Recycled components like crushed concrete [131], [132], slag [133], [134], waste glass [135] or plastic [136] can help the environment by saving natural resources and cutting down on carbon emissions. Their behaviour when exposed to high temperatures has not been fully studied and understood. Usually, recycled aggregates absorb more water and have more pores, which can change how heat moves through the concrete. Some of these materials might also react or change when heated, which could weaken the concrete. So far, studies have not clearly shown that recycled materials perform better than natural ones in high temperatures. More research is needed to understand how they behave under heating.

In summary, since aggregates typically make 60-70 vol.% of concrete [137], and considering the variety in their origin, mineral composition, and size, it is crucial to carefully design aggregate mixes to minimize their potential to contribute to the deterioration of the concrete element exposed to higher temperatures.

2.2.4. Fiber

Presence of fibres in concrete is a proven way to improve its performance under high temperatures [138], [139], [140], *Table 6*. This includes better thermal stability, less cracking, and stronger mechanical properties during/after heating. All concretes can suffer serious damage when exposed to fire or heat. Trapped moisture inside the dense concrete turns into steam, creating high pressure [141]. This can cause internal cracks and even explosive spalling. Fibres help reduce these events by either holding cracks together [142], lowering temperature differences inside the concrete [143], or creating small channels or micro-chambers that release pressure when the fibres melt or break down[144]. Polypropylene (PP) fibres melt at around 160 to 170°C [29], [145]. When they melt, they leave behind tiny pathways or chambers that let steam spread and escape. This is a great mechanism to lower the risk of spalling. While PP fibres do not help to sustain the strength at high temperatures, they are important during the early stages of heating.

In contrast, steel fibres can retain their strength up to around 600°C [26]. They prevent cracks from growing and help the concrete stay strong after being heated. At temperatures above 600-700°C, depending on their thickness and material type, steel fibres may soften or rust. Basalt and carbon fibres can resist much higher temperatures. Basalt fibres stay stable up to about 800°C [146], [147].

Carbon fibres can keep working even beyond 1000°C (only when there is not oxygen present), which makes them useful in buildings that must resist fire [148], [149]. Unfortunately, these fibres are more costly and very often worsen the workability of fresh mix. Using a mix of different fibres can give the best results if the proportions are right. A combination of PP fibres (to prevent spalling) with steel fibres (to improve strength) could help concrete resist sudden temperature changes. However, it is important to choose the right type and amount of fibre, and to make sure they are evenly spread in the mix.

Table 6 Properties of selected fibers

Fibre Type	Melting/Decomposition Temp	Main Benefit	Limitations
Polypropylene	~160–170 °C	Reduces spalling, creates vapor channels	No post-fire strength contribution
Steel	Up to ~600–700 °C	Enhances residual strength, crack bridging	Oxidation and loss of ductility >700 °C
Basalt	Up to ~800 °C	High thermal stability, good bonding	Brittle, may reduce workability
Carbon	>1000 °C (no presence of oxygen)	Excellent thermal resistance, high strength	Costly, challenging dispersion

Adding fibres to concrete improves its thermal and mechanical properties and strengthens the interfacial transition zone (ITZ). During fire exposure, the ITZ is a critical zone where cracks can form because of uneven expansion, pressure from evaporating moisture, and shrinkage [147]. Fibres help to limit this damage. Steel fibres can bridge cracks in the ITZ and lower stress near aggregates. This prevents cracks from growing and supports the concrete regain strength after heating. Fibres also reduce shrinkage and keep the concrete to remain intact when thermal stress is developed [150].

In conclusion, the presence of fibres in concrete has many advantages in fire scenarios. They delay fire damage of the ITZ, limit cracking, and improve long-term durability. Choosing the right type and number of fibres and ensuring their uniform distribution are the keys to create fibre-reinforced concrete that performs well under high temperatures.

2.3. Fire testing

2.3.1. Setup and Sample Size

Although standard fire testing protocols [9] such as ISO 834 and ASTM E119 provide frameworks and instructions for testing and assessing the behaviour of construction materials at elevated temperatures, researchers frequently adapt these protocols to match laboratory capabilities, project-specific objectives, financial constraints, or material and time limitations. Those modifications typically involve adjusting the specimen size to fit available equipment or material limitations, using different types of furnaces such as muffle furnaces, radiant panels, or gas burners, changing support conditions, insulation methods, and thermocouple placements, as well as modifying heating durations and post-fire cooling procedures [36]. The thermal gradient, which is defined by the number and placement of heating elements, also plays a crucial role [151]. Using single-sided versus uniform heating can significantly influence the behavior of the sample .
These parameters often need to be adapted on a case-by-case basis. It is important to notice that, even small changes in the setup might lead to significant differences in thermal degradation patterns, mechanical performance, and post-fire recovery characteristics. As a result, comparability between studies becomes limited unless these adaptations are explicitly reported and critically analysed.

Sample size plays a key role in determining heat transfer dynamics during fire exposure [152]. Smaller specimens, such as cubes ranging from 50 to 100 mm [153], [154], [155], tend to allow faster and more uniform heat penetration. While these sizes ease repeatability and testing, they may overlook microcracking, dehydration, spalling and chemical phase transformations. Due to their limited mass and confinement, smaller samples do not accurately reflect the thermal changes or boundary conditions of real structural elements. They rarely reproduce explosive spalling, pore pressure buildup, or differential thermal strain. Moreover, the lower confinement in small samples allows moisture to escape more freely, altering the development of pressure-induced damage.

Larger specimens, including cylinders or prisms exceeding 150 mm [156], [157], [158], [159], [160], show slower and more uneven heat penetration. This better represents the thermal gradients observed in real-life structural components. However, the associated variability can mask or delay visible signs of damage, making it more challenging to isolate the fire resistance properties of the material itself. Mechanically, larger samples are more representative of actual structures, yet they are subject to scale-dependent stress distributions and cracking patterns. This creates a methodological dilemma: while smaller samples offer experimental control and simplicity, they may misrepresent real behaviour. Larger samples enhance realism but complicate repeatability and increase testing complexity.

2.3.2. Heating Source and Sample Orientation

The type of heating system and the orientation of the sample strongly influence test results. Furnaces that operate through radiant heat [161], convective airflow[162], microwave heating source [163], or direct flame exposure [164] generate distinct thermal environments. Similarly, the orientation of the specimen (horizontal [165] or vertical [27]) affects heat distribution and the mechanical restraints imposed during testing. These variables, in turn, influence the occurrence of spalling and the pattern of crack propagation. Because these configurations are seldom standardized, comparing results across different studies becomes challenging unless testing conditions are clearly documented and analytically addressed.

Instrumentation placement also varies. Thermocouples [166], strain gauges [159], and acoustic emission sensors [158] are positioned differently depending on the research objective and available equipment. Some studies focus on measuring surface temperatures [157], while others embed sensors deep within the specimen to monitor internal heat flow [167]. This lack of consistency leads to fragmented datasets, which hinders cross-study integration and slows the advancement of a unified understanding of fire-damaged materials.

2.3.3. Cooling Phase and Post-Fire Conditioning

The handling of specimens after fire exposure also varies significantly across studies [154], [168], [169]. Some researchers conduct mechanical testing immediately after heating to capture the peak state of thermal damage [170]. Others allow specimens to cool naturally [171] or under controlled conditions before testing [172]. The selected cooling regime strongly affects residual strength, crack development, and chemical recovery processes, including the rehydration of calcium silicate hydrate (C-S-H) and carbonation of lime-based residues [169], [173], [174], [175], [176].

Even when thermal exposure parameters are similar, differences in post-fire protocols can result in conflicting interpretations of material durability. These inconsistencies make it difficult to draw conclusions or establish reliable performance data.

2.4. Spalling

Spalling is the breaking, flaking, or explosive detachment of surface layers of concrete, usually caused by extreme heat exposure (fire events) [177]. It can occur suddenly and violently, throwing chunks of concrete and exposing inner layers, including steel reinforcement, which may lead to loss of structural integrity. A higher water content usually means more pores in the concrete, which can hold more moisture [178]. During a fire, this moisture turns to steam and can create internal pressure, increasing the risk of spalling [179]. The released water vapor increases the pore pressure, which can result in spalling, especially if the water is trapped inside. Spalling in concrete exposed to high temperatures is a complex phenomenon involving chemical [180], physical [181], and mechanical [182] processes that result in the breaking off or detachment of surface layers, *Figure 6*.

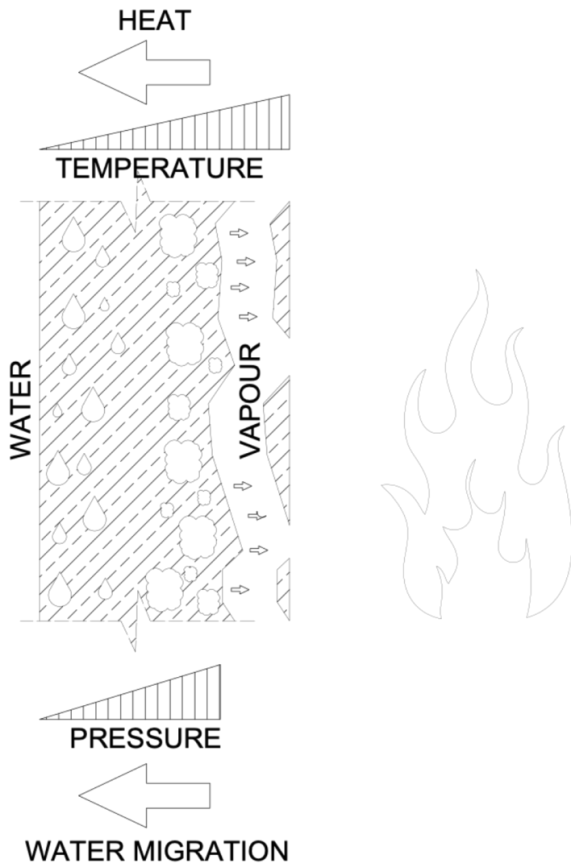

Figure 6 Simplified scheme of spalling in a concrete element

Chemically, spalling is closely linked to the dehydration and decomposition of cement hydration products such as calcium silicate hydrate (C–S–H) and portlandite ($Ca(OH)_2$). They begin to break down between 400 and 600 °C [180]. This degradation reduces the binding capacity of the cement matrix, making it more brittle and prone to cracking. Physically, one of the primary causes of spalling is the rapid vaporization of pore water and chemically bound water. When concrete is rapidly heated, water trapped in small capillaries and pores turns into steam and increases internal pore pressure [181]. If the vapor pressure exceeds the tensile strength of the concrete, microcracks can form and propagate, leading to explosive spalling. This effect is particularly severe in (too) dense, low-permeability concretes (e.g. UHPC [147], [183]) where moisture cannot escape freely. The research on normal strength concrete (NSC) showed that it is less vulnerable to spalling compared to high-strength concrete (HSC) or ultra-high-performance concrete (UHPC) [184]. The influence of moisture content should not be overlooked. Research indicates that in traditional, lower-density concrete, the likelihood of spalling is relatively low when the moisture content stays under 3–4 wt.% [185]. Several hypotheses explain the spalling mechanism [177]. The vapor pressure hypothesis suggests that trapped steam pressure in the pore system builds up faster than it can dissipate, causing internal stresses that fracture the concrete surface. The thermal gradient hypothesis emphasizes that

temperature differences between the heated surface and the cooler interior induce differential thermal expansion, generating tensile stresses, especially at the interfacial transition zone (ITZ) between aggregates and cement paste, which is often the weakest region. There have been reports claiming that aggregate type and size can also induce this phenomenon [128], [184], [186]. The chemical degradation hypothesis focuses on the loss of structural integrity from dehydration reactions and the transformation of hydration products into more brittle mineral phases at high temperatures [187].

Blended cements, although increasingly popular due to CO_2 reduction goals, are also susceptible to spalling [188], but in many cases those deterioration events are minimised. As reported by Burak in [189], replacing PC with 10–20 wt.% of GGBFS lowers the surface temperature of concrete. It reduces internal thermal gradients and the risk of spalling. Similarly, Kumar et al.[190] noted enhanced fire resistance with ultra-fine slag replacing PC. Concrete with 30–70% ground granulated blast furnace slag (GGBFS) was tested [191]. Only the 50% and 70% GGBFS mixes exhibited spalling at 600 and 800 °C. However, a follow-up study [192] found that all mixes, including the 0% slag reference, spalled at 800 °C, though pure PC concrete showed the least damage. Comparable edge spalling was observed in PC, PC-FA, and PC-BF binder combination concretes at the same temperatures but under a slower heating rate of 1 K/min [193]. In contrast, Ghazy et al. [194] found spalling only in PC-FA concrete after exposure to 800 °C at a faster rate (30 K/min). Concrete mixes incorporating pure PC, 20% volcanic ash (VA), 20% fly ash (FA), a combination of 20% VA with 10% furnace arc slag (FAS), and 20% FA with 10% FAS as partial cement replacements were evaluated [195]. After exposure to 800 °C, noticeable surface spalling was observed in both the PC reference mix and the mix containing 20% VA combined with 10% FAS. Additionally, blended concretes incorporating silica fume (SF), ground granulated blast furnace slag (GBBFS), fly ash (FA), thermally activated alum sludge ash and palm oil fuel ash, spalling occurred in all specimens after exposure to 800 °C at a heating rate of 5 K/min, regardless of the binder composition [196].

Regarding sulfoaluminate cements (CSA), not much research regarding thermal loads and spalling has been carried. Yu et al. [197] have reported no visible spalling or cracking was observed in the magnesium phosphate cement (MPC) pastes with CSA exposed to elevated temperatures, except in the case of the presence of 10 wt.% CSA in the paste at 1100 °C. However, total deterioration of concrete samples based on CSA was observed by Tchekwagep et al. in their research [116]. All samples have shown explosive spalling in temperature range of 400-500 °C. CSA concrete was considered to be not suitable for environments exposed to temperatures above 150 °C due to the fragility of its ettringite phase [18]. However, Sodol et al. [108] conducted a series of tests within this temperature range and observed no spalling.

Table 7 General fire spalling performance of PC, GGBFS, and CSA concretes [116], [177], [179], [185], [188], [196], [197]

Parameter	PC	GGBFS-Blends	CSA
Spalling Risk Level	High	Moderate to high (depends on moisture and density)	Low to moderate (formulation dependent)
Main Spalling Mechanism	Rapid pore pressure buildup due to moisture evaporation and weak thermal resistance	Delayed vapor release due to dense matrix; risk increases with high internal moisture	Fast ettringite dehydration releases moisture quickly, reducing pressure
Impact of Moisture Content	Highly sensitive, high moisture greatly increases spalling risk	Very sensitive; trapped moisture in dense matrix can cause explosive spalling	Moderate sensitivity: rapid phase changes may aid moisture escape

Thermal Cracking	Significant: thermal stress leads to cracking and promotes spalling	Reduced thermal cracking due to better matrix bonding	Cracking behaviour depends on binder, less aggressive than PC
Heating Rate	Very sensitive to rapid heating; promotes explosive spalling	Moderately sensitive, controlled heating reduces risk	Less sensitive, quicker dehydration stabilizes the matrix
Microstructure Impact	Coarse pores allow vapor movement but promote structural breakdown	Refined structure retains strength longer but traps water	Compact matrix may prevent pressure buildup if properly balanced
Temperature Threshold for Spalling	Often begins around 200–300 °C, peaks around 400–500 °C	Begins around 300 °C if moisture trapped, less aggressive than PC	No sufficient data
Spalling Behaviour	Explosive spalling common under fire exposure	Layered or surface flaking more common than explosive spalling	Minimal to no visible spalling in most low-to-mid temperature exposures

Since the current state of the art regarding spalling shows many contradictions and lacks consistent findings, more detailed research is needed to better understand how concrete made with different cements and blends behaves during fire, particularly concerning spalling. As blended cements and alternative binders are being developed and used more frequently and in various forms, it is important to study their behaviour under fire exposure while also considering other factors and components of concrete mixes. A very limited assumption can be made based on the binder type, *Table 7*. It is important to remember that, when it comes to this hazardous phenomenon, the overall context of the concrete element and its surroundings must be considered to mitigate the negative effects.

Chapter 3

3. Materials and methods

3.1. Materials

3.1.1. Portland cements

Three types of Portland cement supplied by Cementa AB and CEMEX Poland were utilized in this study. These included cements classified under EN 197-1 standards: CEM II/B-V 32.5 R – HSR, CEM I 42.5N (Anläggningscement), and CEM I 52.5R (Snabbcement Skövde). The physical and chemical characteristics of each cement, as reported by the manufacturers, are presented in *Table 8*, *Table 9*, and *Table 10*.

Table 8 Properties of CEM II/B-V 32.5 R – HSR

Blaine fineness (m^2/kg)	Setting time (min)	Bulk density (kg/m^3)	LOI (%)	Insoluble (%)	Chloride (%)	Alkali Na_2Oe (%)	SO_3 (%)
352	298	1100	n/a	0-0.2	0.062	1.30	2.64

Table 9 Properties of the CEM I 42.5N

Blaine fineness (m^2/kg)	Setting time (min)	Bulk density (kg/m^3)	LOI (%)	Insoluble (%)	Chloride (%)	Alkali Na_2Oe (%)
330	170	1250	0.5-0.4	0-0.2	0.01-0.03	0.40-0.58

Table 10 Properties of the CEM I 52.5 5R

Blaine fineness (m^2/kg)	Setting time (min)	Bulk density (kg/m^3)	LOI (%)	Insoluble (%)	Chloride (%)	Alkali Na_2Oe (%)	SO_3
362	223	972	2.56	0-0.2	0.01	0.62	<4.0

3.1.2. Calcium sulfoaluminate cement (CSA)

ALI CEM GREEN, based on data provided by the producer, is a blend of sulfoaluminate clinker (ALI PRE GREEN) and finely ground calcium sulfate. It contains 40% pre-consumer recycled material and has CO_2 emissions of 380 kg/t (Core Process, A3 Stage), significantly lower than the 750+ kg/t typical for CEM I cements. The XRF results are shown in *Table 11* , and its properties in *Table 12* .

Table 11 XRF results for ALI CEM GREEN (all in wt.%)

MgO	Al_2O_3	SiO_2	SO_3	Cl	K_2O	CaO	TiO_2
2.31	18.32	5.35	24.06	0.10	0.48	45.49	0.38
Cr_2O_3	MnO	Fe_2O_3	CuO	ZnO	SrO	BaO	LOI
0.06	0.14	1.26	0.24	0.08	0.23	0.08	1.41

Table 12 Properties of ALI CEM GREEN

Blaine fineness (cm^2/g)	Setting time (min)	Bulk density (kg/m^3)
5000 ± 500	≤25	1100

3.1.3. Ground Granulated Blast Furnace Slag (GGBFS)

The used in this research GGBFS type "Merit" was delivered by Swecem. Merit is a material obtained from blast furnace slag, a by-product of iron manufacturing. It goes through wet granulation followed by fine grinding. Due to its favourable chemical composition and latent hydraulic properties, it demonstrates potential as a supplementary cementitious material (SCM) for concrete production. The material conforms to the requirements of SS EN 15167-1, carries CE certification and is available on the Swedish market. The physical properties and chemical composition as provided by the producer are shown in *Table* 13 *13* and *Table 14*, respectively. The XRD diffractogram is shown in *Figure 7.*

Table 13 Physical properties of Merit (GGBFS).

D_{50} (mm)	Blaine fineness (m^2/kg)	Density (g/cm^3)	Bulk density (g/cm^3)	Glass content %
30-34	30-35	2.8-3.0	0.9-1.1	97-99

Table 14 Chemical composition of Merit (GGBFS), wt.%.

CaO	SiO_2	Al_2O_3	MgO	TiO_2	Mn_2O_3	Cl
30-34	30-35	10-13	12-15	1.5-2.5	0.3-0.6	<0.1

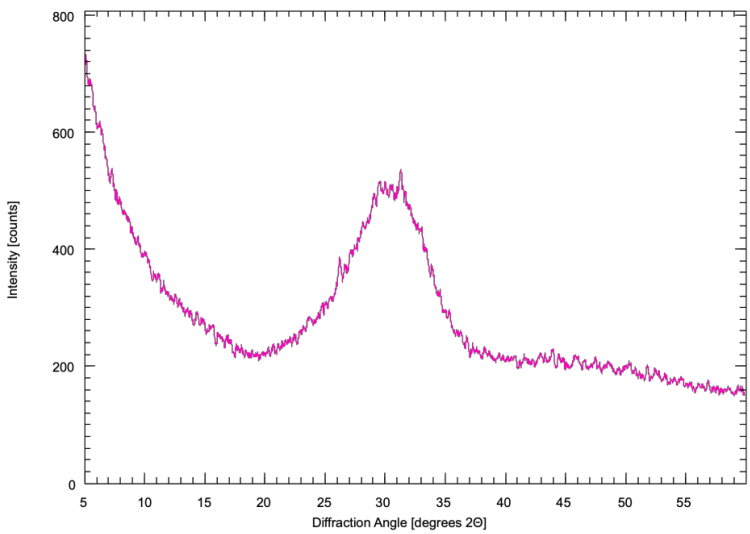

Figure 7 GGBFS "Merit" XRD diffractogram

3.1.4. Powders

- *Quartz powder*

The quartz powder Norquartz 45 was sourced from Sibelco. According to the information provided by the manufacturer, most particles (99.2%) have a size of 45 µm. The chemical properties are shown in *Table 16* and the SEM BSE image in *Figure 8.*

Table 15 Chemical properties of quartz powder Norquartz 45

Component	SIO_2	Al_2O_3	Fe_2O_3	LOI	pH	Density
Average (%)	99.6	0.25	0.02	0.15	6.5	2.65

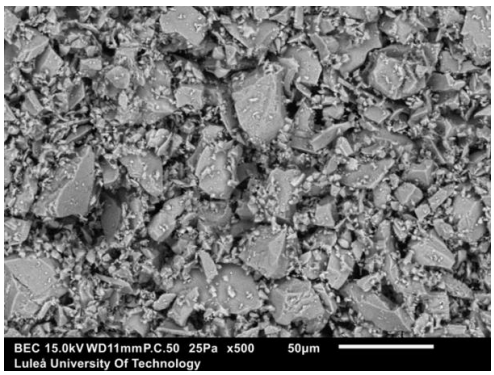

Figure 8 SEM BSE image of quartz powder

- *Limestone powder*

Limestone powder was obtained from a local producer. Its XRF results are presented in *Table 17*, and the SEM BSE image in *Figure 9*.

Table 16 XRF results: Limestone powder (wt.%)

Na_2O	MgO	Al_2O_3	SiO_2	K_2O	CaO	TiO_2	MnO	Fe_2O_3	LOI
0.75	0.95	0.73	3.59	0.23	54.09	0.09	0.21	1.55	37.82

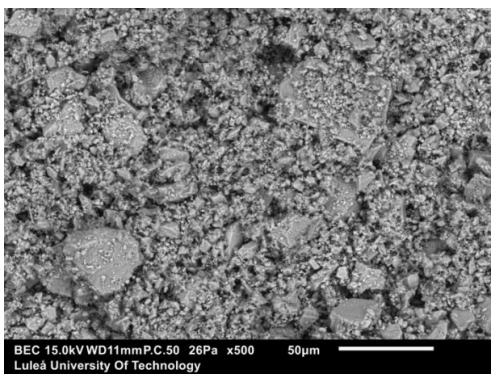

Figure 9 SEM BSE image of limestone powder

- *Eggshell powder*

Eggshells were collected as food waste from hen eggs available in Sweden. The shells were cleaned with tap water, initially mechanically crushed to minimize their volume, and dried in a laboratory oven at 105°C for 24 hours. Afterward, they were ground in a Retsch planetary ball mill PM 100 at a speed of 400 rpm for 30 minutes to achieve a fine powder. XRF results are shown in *Table 18*, and a SEM BSE image in *Figure 10*.

Table 17 XRF results of eggshell powder (wt.%)

MgO	Al_2O_3	SO_3	Cl	K_2O	CaO	SrO	LOI
0.30	0.05	0.30	0.05	0.05	52.38	0.05	46.80

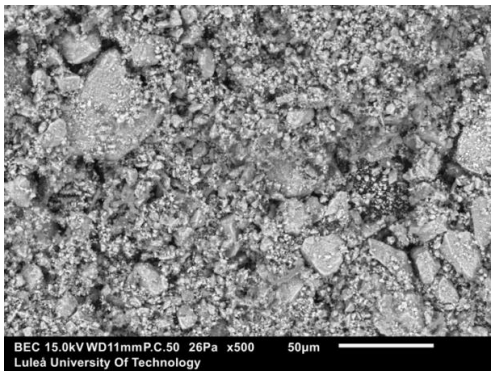

Figure 10 SEM BSE image of eggshell powder

3.1.5. Aggregates

The Jehander Heidelberg cement group supplied crushed granite aggregates with a gradation of 0-4 mm and 4-8 mm. These aggregates are preferred due to their mechanical properties such as high compressive strength, low water absorption, and high resistance to wear and tear and high granite melting point [198]. Its specific gravity is 2.7 t/m^3.

3.1.6. Admixtures

To evaluate the influence of admixtures (SS EN 934) on the thermal properties of concrete under elevated temperatures, three types of admixtures supplied by Master Builders were incorporated into the mixes. Detailed specifications of these admixtures are presented in *Table 11*.

- *Accelerator*

Master X-Seed 100 (Master Builders, ACC) is a suspension containing nanoparticles formulated to enhance the early hydration kinetics of cementitious systems, particularly within the initial 6 to 12 hours after mixing. According to the manufacturer, the mechanism involves promoting the rapid nucleation and growth of calcium silicate hydrate (C-S-H) phases, thereby facilitating earlier strength development and accelerating the hardening process.

- *Air entrainer*

Master Air from Master Builders (AE) is an air-entraining admixture that enhances creation of a system of small, closely spaced air pores.

- *Plasticizer*

Master Glenium ACE 30 from Master Builders (SP) is a superplasticizer formulated using modified polymers, designed to enhance concrete. It is intended to reduce casting time and promote rapid strength development and a faster formwork removal.

Table 18 Admixtures specification

	ACC	SP	AE
Form:	Liquid	Liquid	Liquid
Density:	1.135 ± 0.03	1.064 ± 0.02	1.0 ± 0.01
pH value:	11 ± 1.5	5.5 ± 1	8.4 ± 10.4
Chloride content:	<0.01% (not measurable)	18% ± 1.0%	N/A
Dry content:	18% ± 1.0%		12.5% ± 0.1%
Na_2O equivalent:	1.7	N/A	<1.8%

3.1.7. Fibers

Fibers were used in concrete mixes to study spalling events in larger concrete elements. The two most common types used were PVA and basalt.

- *PVA fibers*

MasterFiber 400 is manufactured by BASF Construction Solutions GMBH. The technical data are presented in *Table 19*, and an SEM BSE image is shown in *Figure 11*.

Table 19 Technical data. PVA fibers.

Polymer Type	Sectional shape	Density	Eq. Diameter	Tensile strength
PVA	Round	1300 kg/m^3	200 µm	750 MPa
Effect on strength	**Colour**	**Longitudinal shape**	**Fiber length**	**Secant modulus**
32.5 kg/m^3	Yellowish	straight	18 mm	7100 MPa

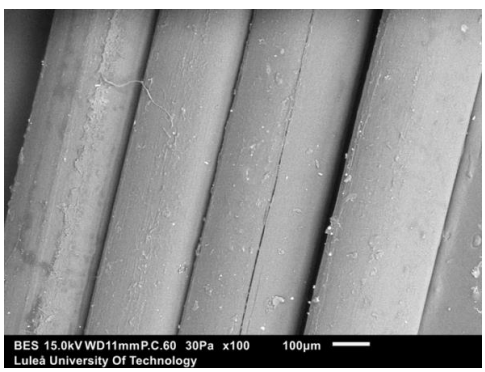

Figure 11 SEM BSE image of PVA fibers

- *Basalt fibres*

MasterFiber 050, basalt microfibers, are manufactured by BASF Construction Chemical Italia SpA. The technical data are presented in *Table 20*, and an SEM image is shown in *Figure 12*.

Table 20 Technical data for basalt fibers.

Polymer Type	Sectional shape	Density	Eq. Diameter
basalt	round	2670 kg/m^3	13 µm
Melting point	**Colour**	**Longitudinal shape**	**Fiber length**
1350°C	greyish	straight	16 mm

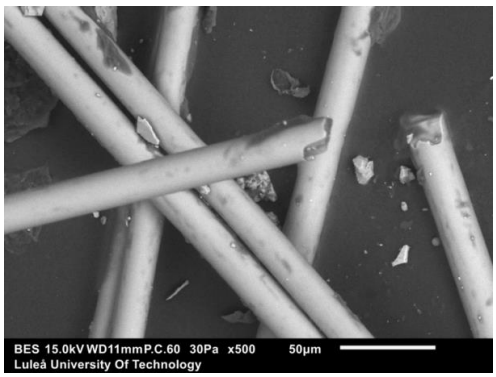

Figure 12 SEM BSE image of basalt fibers

3.2. Methods

3.2.1. Cement paste sample preparation

- *Mix design*

The binder paste was prepared following the guidelines of RILEM TC-238 SCM [199]. A total of 80 grams of solid materials was combined with 32 grams of distilled water. Mixing was performed using a vacuum laboratory mixer operating at 390 rpm for 2 minutes. After mixing, the paste was transferred to a plastic container, sealed, and stored for 28 days at room temperature (20°C) and a relative humidity of 50–60%. The paste mix compositions are presented in *Tables 21* and *22.*

Table 21 Mix composition for PC pastes with GGBFS

	PC Cement [g]	GGBFS [g]	Quartz [g]	Water [g]	W/B
Set 1$_{(REF)}$	40	40	-	32	0.40
Set 2	32	32	16	32	0.50

Table 22 Mix composition for CSA pastes with LS and ESP

Mix	CSA Cement [g]	LSP [g]	ESP [g]	Water [g]	W/B
1 (REF)	80	0	0	32	0.40
2	76	4	0	32	0.42
3	72	8	0	32	0.44
4	76	0	4	32	0.42
5	72	0	8	32	0.44

3.2.2. Concrete sample preparation

- *Mix design and sample preparation.*

The mix design process was carried out through multiple trials to achieve good workability without using any additional plasticizer. The water-to-binder ratio was consistently maintained at 0.50 to ensure data uniformity and to be able to compare and analyse the results. Concrete specimens (100×100×100 mm) were cast in plastic molds using a 20-liter Hobart A200N mixer, *Figure 13*.

Figure 13 Hobart A200N 20l mixer

A standardized mixing process was followed: dry components were mixed for 5 minutes, followed by water addition and another 5 minutes of mixing. Mixing time ranged from 5 to 10 minutes. Molds were coated with form oil to ease demoulding. After 24 hours, the specimens were demoulded, measured, weighed, labelled, and photographed, then air-cured for 28 days at ambient temperature (21 °C) and relative ambient humidity (65%). Post-curing and post-heating, the same documentation was repeated to track changes such as cracks or deformation and evaluate the effects of thermal exposure on samples. The concrete mix compositions are presented in *Table 23 and 24.*

Table 23 Mix design for PC concrete mixes, for 1 m^3

Mix	PC kg/m^3	PC type	GGBFS kg/m^3	Aggregates 4-8 mm kg/m^3	Aggregates 0-4 mm kg/m^3	Sand B15 kg/m^3	Quartz powder kg/m^3	W/B
1A100	400	32.5	0	522	1131	87	87	0.5
1A5050	200	32.5	200	522	1131	87	87	0.5
1B100	400	42.5	0	522	1131	87	87	0.5
1B5050	200	42.5	200	522	1131	87	87	0.5

1C100	400	52.5	0	522	1131	87	87	0.5
1C5050	200	52.5	200	522	1131	87	87	0.5

Table 24 Mix design for CSA concrete mixes, for 1 m^3

Mix	**Cement kg/m^3**	**LSP kg/m^3**	**ESP kg/m^3**	**Aggregates 4-8 mm kg/m^3**	**Aggregates 0-4 mm kg/m^3**	**Aggregates 0-2 mm kg/m^3**	**W/B**
1 (REF)	392.00	0	0	878.5	614.90	273.40	0.5
2	372.59	19.60	0	878.5	614.90	273.40	0.53
3	353.00	39.20	0	878.5	614.90	273.40	0.55
4	372.59	0	19.60	878.5	614.90	273.40	0.53
5	353.00	0	39.20	878.5	614.90	273.40	0.55

4. Testing

4.1. Temperature load

High-temperature exposure tests were carried out using an LAC LH15 furnace, *Figure 14*. The heating elements are installed on the left and right vertical sides of the chamber, with no mechanical ventilation to circulate the hot air. The samples have been always placed on the floor of the chamber without any spacing.

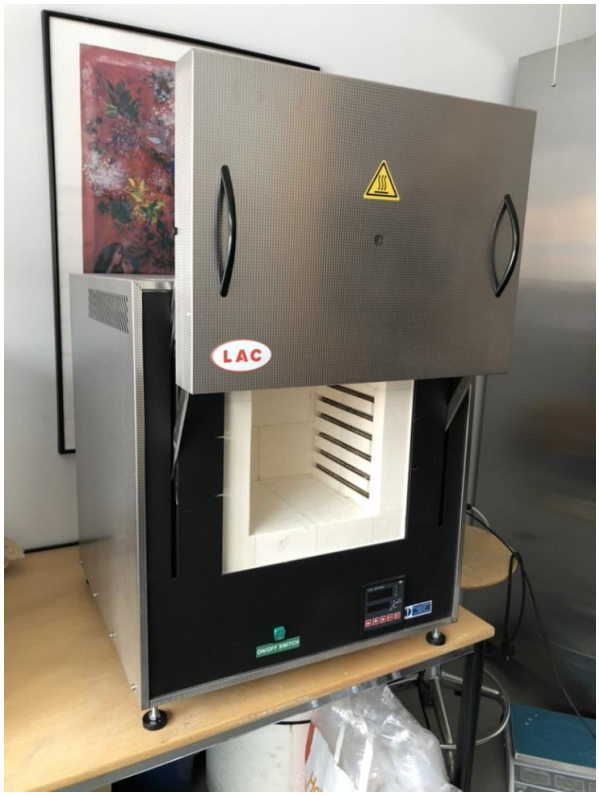

Figure 14 Selected muffle furnace

Two main temperature thresholds were selected: 400°C and 800°C. This choice was based on the feasibility of the experiments, safety considerations, and the typical decomposition behaviour of concrete reported in the literature [81]. At around 400°C, concrete begins to exhibit noticeable physical and chemical changes. Free and some chemically bound water evaporate, and microcracking develops due to differential thermal expansion between the aggregates and the cement matrix. Calcium silicate hydrate (C-S-H), the primary binding phase, starts to dehydrate, gradually weakening the material's structural integrity. At 800°C, concrete experiences severe degradation. Calcium hydroxide (portlandite) decomposes almost completely, and further breakdown of C-S-H significantly compromises the material's strength. Additionally, if quartz-based aggregates are present, they undergo a phase transformation from alpha- to beta-quartz at approximately 573°C [117], [118], [200]. This transformation is accompanied by a sudden volume increase, which introduces internal stresses and can lead to

further cracking and instability within the concrete. At this stage, concrete typically shows extensive cracking, a loss of cohesion, and a significant reduction in mechanical performance, with spalling or explosive failure becoming more likely due to steam pressure and structural instability.

The temperature increased to 400°C within 30 minutes, corresponding to a rate of 13.33°C/min, and reached 800°C in 175 minutes, with a slower rate of 4.57°C/min. Concrete and binder paste specimens were placed directly on the chamber floor without any spacing supports. Once the desired temperature was achieved, it was maintained for one hour. Following the heating phase, the furnace was kept closed to allow the samples to cool down naturally to room temperature for approximately 12 to 24 hours.

4.2. Compressive strength

Compressive strength testing in this study was conducted using a Toni Technik compression machine, *Figure 15*. A constant loading rate of 10 kN/s was applied until specimen failure. The procedure followed the SS EN 12390-3 standard for evaluating the properties of hardened concrete. The maximum load at failure was recorded, and the compressive strength was calculated by dividing this load by the specimen's cross-sectional area.

Figure 15 Compressive strength testing machine

4.3. X-ray diffraction (XRD)

X-ray diffraction (XRD) analysis was performed using a Panalytical Empyrean diffractometer equipped with a θ-θ reflection Bragg-Brentano geometry, a Cu anode (λ = 1.54184 Å), programmable divergence slits, and a Pixcel 3D Medipix2 detector. The X-ray source operated at 45 kV and 40 mA. Measurements were carried out over a 2θ range of 5–75°, with a step size of 0.026° and a counting time of 330.23 seconds per step, resulting in a total scan duration of approximately 1 hour per sample. The irradiated area was circular with a surface of 100 mm². To stop hydration, the samples were immersed in isopropanol for 5 days, followed by storage in a desiccator under vacuum for an additional 5 days. They were then ground using a planetary ball mill until the particle size was reduced to below 63 µm.

4.4. SEM EDX

The paste samples prepared for SEM analysis were first immersed in isopropanol for 7 days to remove water. Subsequently, they were stored in a desiccator for an additional 5 days. impregnation was performed using a low-viscosity epoxy resin. After curing, the samples were polished sequentially with diamond suspensions having particle sizes of 9 µm, 3 µm, and 1 µm.

The scanning electron microscope (SEM) utilized for this analysis was the JSMIT100, that was combined with a Bruker Quantax energy-dispersive spectrometer (EDS), *Figure 16*. Images were acquired in backscattered electron (BSE) mode at magnifications of 500× and 1000×. The operating conditions included an acceleration voltage of 15 kV, an electron beam current of 70 mA, and a chamber vacuum pressure of 30 Pa [201].

Figure 16 SEM instrument

4.5. Microstructural integrity

Two approaches are used to determine the amount of empty voids. This cannot be considered a porosity test, as thermal exposure results not only in the formation of pores, but also in cracks and other empty voids. Internally, this has been referred to as microstructural integrity, aimed at assessing how the arrangement of the matrix is altered under high temperatures, considering all physical changes [191].

The first approach is based on histograms generated from BSE images obtained using a SEM microscope, while the second involves measurements with a gas pycnometer.

4.5.1. SEM BSE histograms

To study how high temperatures affect the concrete's internal structure, histograms from BSE images were analysed. The Microstructural Integrity Index (MII) was introduced to describe the overall quality of the concrete's microstructure. This included features like pores, cracks, and separations in the ITZ, and was used to compare both damaged and undamaged (reference) samples. Thirty images were taken from different spots on the cross-section of the specimens after heating them to 400°C, 800°C, and at room temperature. All images were captured at 400× magnification to clearly show small features like pores, following methods from earlier research [202], [203]. The images were processed using MATLAB 2023b, along with its Image Processing Toolbox. A median filter with a 5-pixel kernel was applied to reduce noise. To detect pores and small cracks, each image was binarized using a method called the “overflow method.” This involved converting the image into black and white every 5 grayscale levels and measuring the white pixel areas. The correct cutoff threshold value was found by identifying where two tangent lines on the graph of pixel area intersected.

Each image was then binarized using this threshold, and the MII was calculated with the formula:

$$MII_i = 1 - \frac{\sum w_i}{a \cdot b} \quad (1)$$

wi: number of pixels showing cracks or pores
a: image length = 5120 pixels
b: image width = 3840 pixels

The MII value ranges from 0 to 1. A value close to 0 means the microstructure is badly damaged, while a value near 1 means it is still in good condition.

4.5.2. Gas pycnometer

The skeletal density of the samples was measured using a helium gas pycnometer (Micromeritics AccuPyc II 1340). All tests were done at room temperature in the lab. To ensure accurate and consistent results, each density value was based on the average of ten repeated measurements. The analysis chamber had a volume of 30 ml, which was suitable for the sample sizes and allowed for precise measurement of the volume displaced by the helium gas.

Chapter 5

5. Results and discussion

5.1. Portland cement blends with GGBFS

Among the tested cement blends incorporating GGBFS, the 50/50 wt.% ratio demonstrated the most promising performance under high-temperature conditions. The following chapter presents a detailed analysis of this blend, examining its thermal behaviour and contributing factors.

5.1.1. Weight change

As a result of elevated temperatures leading to water evaporation, the tested concrete elements showed a weight reduction. *Table 26* presents the average percentage weights loss of individual cubes after exposure to 400 °C and 800 °C for 1 h, allowing for a direct comparison of how different mix designs react to thermal load. The observed mass loss is a key factor, as it directly impacts the concrete's durability and structural integrity under high-temperature conditions [191].

The results show that all mixtures kept 92–95% of their original weight after heating. Among them, the blends containing GGBFS as a 50% replacement for cement performed well. These slag-modified mixtures generally exhibited a smaller reduction in mass compared to those composed only of Portland cement, particularly at 400 °C. This behaviour aligns with findings by Wang [204], who also reported improved thermal resistance in slag-containing mixes.

The reduced weight loss in specimens with GGBFS can be attributed to the denser microstructure and lower porosity typical of well-hydrated slag-blended binders. Such characteristics enhance moisture retention and minimize thermal degradation. This conclusion is supported by Lothenbach et al. [205], who noted that a more compact microstructure decreases permeability and slows the progression of heat-induced damage. The improved thermal stability of slag-modified concretes is closely linked to their internal cohesion and resistance to dehydration.

In contrast, mixes with only Portland cement exhibited slightly higher mass loss after heating to 800 °C. Though the difference is small, it shows that plain Portland cement binders have a limited ability to hold moisture and resist microstructural damage when exposed to heat. The gathered data confirm that incorporating GGBFS into the mix design enhances the thermal resilience of concrete, particularly at intermediate temperatures, by reducing weight loss and preserving internal structure.

Table 25 Weight reduction (average of 4 samples; SD % in parentheses).

Ambient	400°C	800°C
PC 32.5		
100 % (0.16)	92 % (0.02)	92 % (0.02)
PC 32.5 + GGBFS (50/50 %)		
100 % (0.02)	95% (0.04)	92% (0.01)
PC 42.5		
100 % (0.01)	93 % (0.01)	93 % (0.01)
PC 42.5 + GGBFS (50/50 %)		
100 % (0.02)	93 % (0.03)	92 % (0.01)
PC 52.5		
100 % (0.01)	93 % (0)	93 % (0.01)
PC 52.5 + GGBFS (50/50 %)		
100 % (0.01)	95 % (0.01)	92 % (0.01)

5.1.2. Compressive strength

After 28 days of air curing and storage under normal room conditions, the concrete cube samples were exposed to elevated temperatures of 400°C and 800°C for 60 minutes. Once cooled for 24 hours, their compressive strength was tested. The results at ambient temperature serve as a reference point (100%) for evaluating the effect of heat on each mixture regarding change of compressive strength results. The results are presented in *Table 26*.

After heating to 400°C, most samples either retained their original strength or showed noticeable improvements. This trend was especially evident in the mixes containing equal parts of GGBFS and PC, where strength gains were most pronounced. Among these, the mix made with PC 42.5 and slag demonstrated the most significant improvement. Mixes combining slag with either PC 32.5 or PC 52.5 also performed well, suggesting that slag contributes positively to strength development at moderate temperatures. These improvements are likely linked to the enhanced reactivity of slag at elevated temperatures, which promotes the formation of additional binder phases [206]. This contributes to a denser microstructure, improved resistance to internal cracking, and overall better thermal stability. The slower, sustained hydration of slag and the resulting compact gel phases further support structural integrity under thermal stress. In contrast, mixes made without slag exhibited more modest strength increases. While PC 32.5 without slag still showed a notable improvement, the PC 52.5 without slag showed only a marginal gain. A surprising outlier was the PC 42.5 mix without slag, which also showed a higher strength increases after heating. However, at 800°C, all mixes experienced a sharp decline in compressive strength. The mixes containing slag, particularly the one with PC 32.5, were most affected. Meanwhile, the PC 32.5 mix without slag retained the highest proportion of its original strength, indicating superior thermal stability at high temperatures.

These results align with findings by Ponomar et al. [82], who observed that the addition of quartz as a filler could enhance compressive strength under thermal exposure. This improvement was attributed to the formation of iron–silicate phases generated through alkaline interactions between quartz and the existing gel structure. The slag used was iron-rich, which suggests the presence of an iron threshold that contributes to this effect. Further testing is recommended to narrow down the iron content responsible for this event.

Table 26 Changes in compressive strength performance results (average of 4 samples; SD % in parentheses).

Ambient	400°C	800°C
PC 32.5		
100% (3.20)	125% (3.20)	69% (12.0)
PC 32.5 + GGBFS (50/50 %)		
100% (2.0)	128% (7.00)	33% (11.0)
PC 42.5		
100% (2.0)	144% (1.0)	59% (3.0)
PC 42.5 + GGBFS (50/50 %)		
100% (10.0)	167% (6.0)	66% (4.0)
PC 52.5		
100% (7.0)	103% (7.0)	44% (1.0)
PC 52.5 + GGBFS (50/50 %)		
100% (6.0)	135% (4.0)	51% (9.0)

5.1.3. Microstructural integrity

MII values were determined for each concrete specimen exposed to elevated temperatures using SEM images taken at 400× magnification. The average MII ranged from 0.82 to 0.91, reflecting differences in microstructural integrity across the specimens subjected to varying thermal exposures, *Table 27*. A clear downward trend in MII was observed with increasing temperature, which highlights the adverse effects of thermal loading on the concrete microstructure. Notable differences in MII were found among the various concrete mix designs. Specimens containing 42.5 and 52.5-grade cements showed higher MII values compared to those with 32.5-grade cement, indicating a denser matrix and reduced pore connectivity. This was observed despite the visible porosity associated with fly ash particles. The effect of slag on microstructural integrity appeared to be limited under elevated temperature conditions.

The influence of slag became more evident when comparing the behaviour of concrete at 400 and 800 °C. At 400 °C, slag improves thermal resistance and reduces permeability, which helps to minimize the microstructural damage. The thermal exposure at this stage can activate slag reactivity, enhancing its contribution to hydration and extending the slower phase of the hydration process [180]. However, this reaction is constrained by the limited availability of calcium hydroxide, and once saturation is reached, additional slag provides limited benefit and may even slow further hydration. The latent hydraulic activity of slag also strengthens the interfacial transition zone (ITZ), contributing to matrix densification and potentially enhancing durability under moderate heat exposure. At 800 °C, however, the severe thermal environment likely exceeds these protective effects, resulting in significant deterioration of microstructural integrity.

The variation observed in the data is primarily related to the heterogeneous nature of microstructural damage within the concrete visible in *Table 28*. This is influenced by differences in thermal expansion among the constituents, particularly between the aggregates and the binder matrix, along with variability in the shape, size, and volume fraction of aggregates in each analysed image. In this study, it is presumed that MII values were affected by microdamage occurring in the ITZ*, Figure 17*. However, this observation was made through visual inspection and does not provide enough quantitative evidence to determine the exact role of the ITZ.

Table 27 MII values change results

Ambient	400°C	800°C
PC 32.5		
0.83	0.75	0.75
PC 32.5 + GGBFS (50/50 %)		
0.82	0.79	0.74
PC 42.5		
0.86	0.80	0.76
PC 42.5 + GGBFS (50/50 %)		
0.83	0.82	0.80
PC 52.5		
0.91	0.86	0.81
PC 52.5 + GGBFS (50/50 %)		
0.88	0.85	0.86

Further visual inspection has showed that samples stored under ambient conditions displayed an intact matrix with no visible cracks. However, exposure to 400°C caused the evaporation of free, gel, and capillary water, resulting in dehydration [11], which left behind voids and cracks following the contours of the aggregates, which led to prolongation cracks within the matrix. At 800°C, the matrix suffered significant disruption across all samples. This degradation is mainly due to thermal incompatibility. While the C-S-H gel undergoes substantial shrinkage, the aggregates remain dimensionally stable, leading to detachment at the interface. Furthermore, the α-to-β quartz phase transformation at 573°C causes a volumetric expansion [117], [118], thus introducing more stress to the matrix. As the gel water evaporates, the C-S-H gel shrinks notably, increasing the porosity of the concrete. Larger unreacted particles act as physical barriers, limiting shrinkage and restricting the propagation of cracks. Nevertheless, the cracks that do develop are wider and more pronounced, particularly in mixes with higher slag content. Despite these changes, the aggregates remained stable, showing minimal signs of degradation or high-temperature mechanical failure. Although spalling was not observed in any of the samples, the presence of cracks and voids may still contribute to spalling [207], which could ultimately disturb the integrity of the internal structure.

Table 28 Microstructural changes of matrix when exposed to high temperature

Ambient	400°C	800°C
PC 32.5		
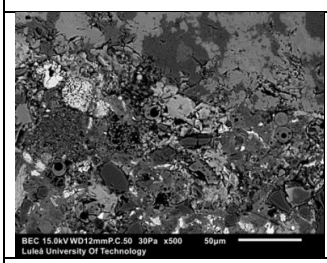	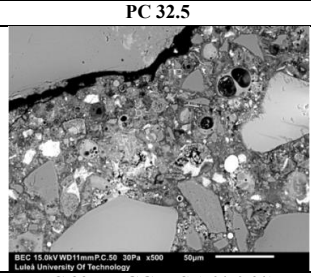	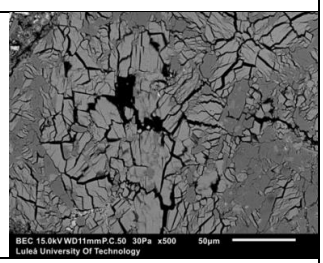
PC 32.5 + GGBFS (50/50 %)		

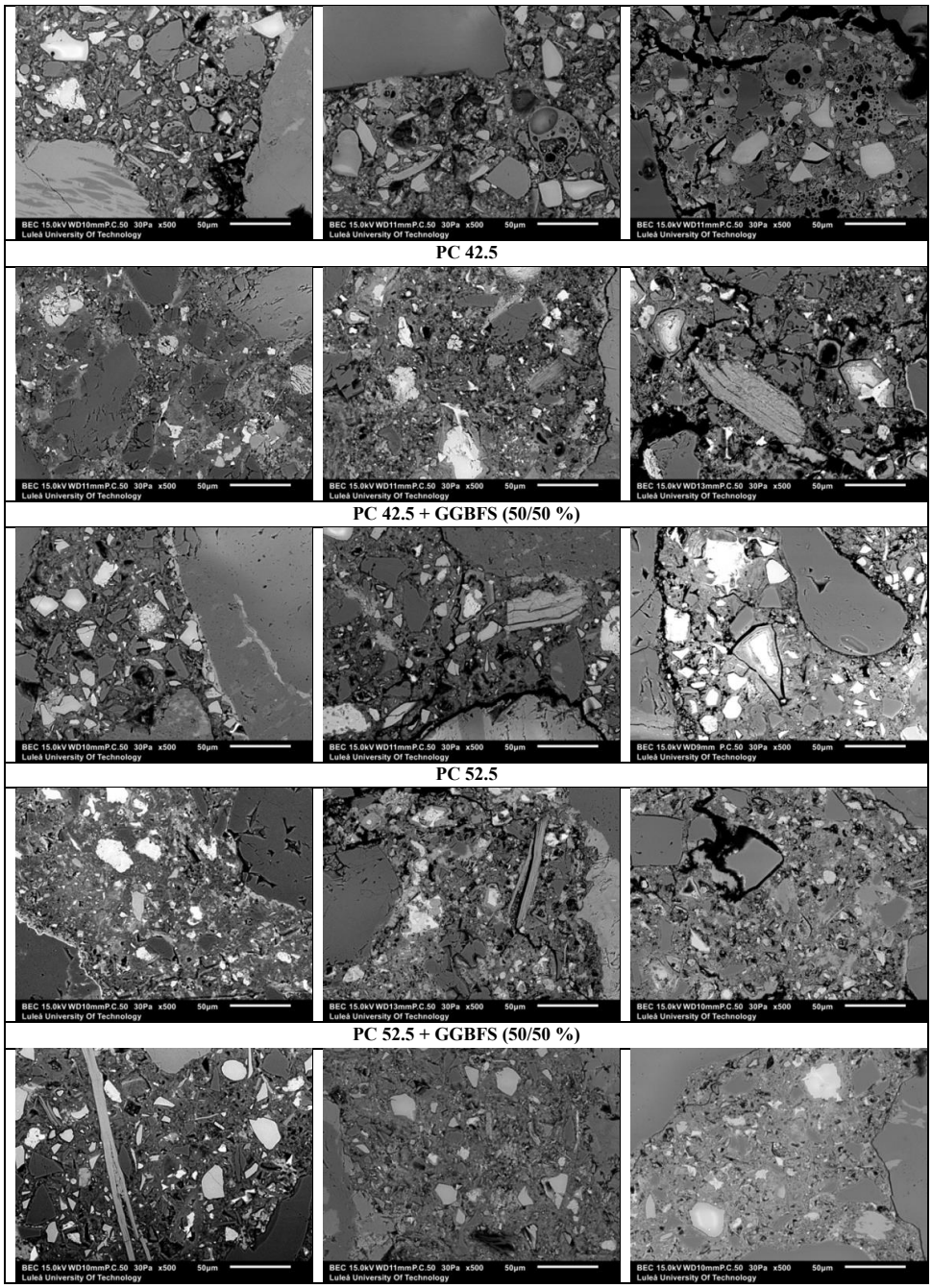
PC 42.5
PC 42.5 + GGBFS (50/50 %)
PC 52.5
PC 52.5 + GGBFS (50/50 %)

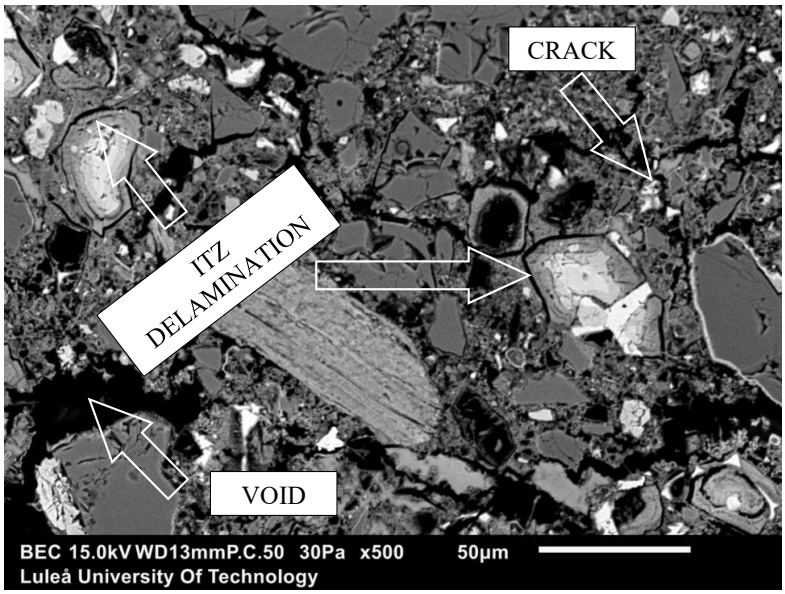

Figure 17 Examples of thermal deterioration of concrete matrix. SEM BSE, Mix PC42.5 + SLAG

5.1.4. Colour alteration

Visual alteration assessment is one of the simplest methods for examining concrete exposed to high temperatures [208], [209], [210], [211]. It involves observing color discoloration, the presence of crazing and cracks, as well as changes in surface texture. Although it does not provide specific data on mechanical performance yet, it can serve as an initial indicator of the condition of a concrete element. Exposure to elevated temperatures led to several visible changes in the concrete samples in this study, *Table 29*. Samples positioned closer to the heat source exhibited more uneven and stained surfaces. However, these visual differences did not appear to correlate directly with variations in compressive strength.

At 400 °C, all specimens became lighter in color developing a noticeable yellow tint due to dehydration. No cracks or spalling were observed.

At 800 °C, the effects were significantly more pronounced. Although none of the samples experienced explosive spalling, clear signs of cracking, surface separation, and distinct color changes were observed. The samples turned various shades of beige, pink, and grey, with varying intensity. Long, reddish surface marks appeared on many specimens, likely due to iron compounds present in the Portland cement, granite aggregate, and the fly ash used in PC 32.5 cement. Samples made with PC 42.5 displayed orange discoloration, while those containing PC 52.5 and GGBFS developed a reddish-brown tone. However, none of the slag-containing samples retained their original green internal hue after exposure to high temperatures (Figure 18).

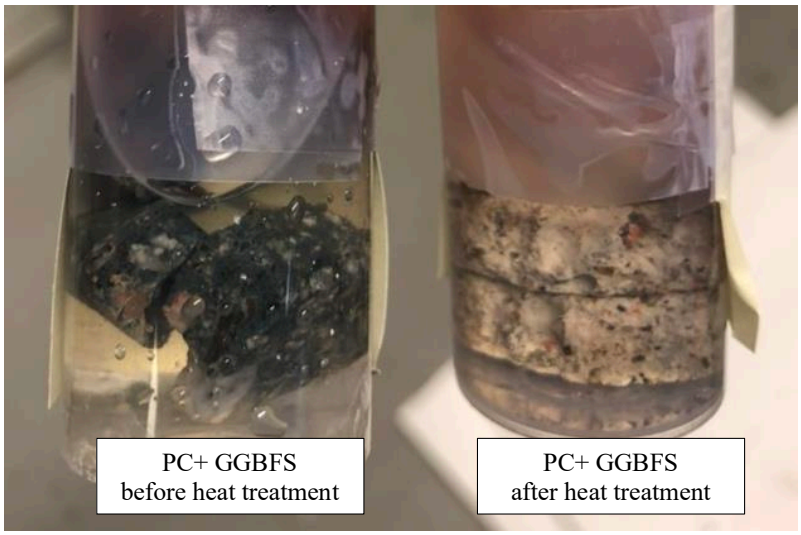

Figure 18 Inner part of samples with GGBFS before and after heat treatment

All specimens after temperature exposure showed signs of surface crazing with cracks, but no consistent crack direction could be identified. At room temperature, the surfaces remained smooth and even. At 400 °C, they became noticeably rougher. By 800 °C, the surface texture had deteriorated becoming rough, sharp, and uneven. All samples showed a tendency to fragment, affecting both their weight and dimensions. This degradation could potentially compromise the accuracy of compressive strength measurements.

Although all specimens lost color intensity as the temperature increased, slag-containing mixes followed a different pattern. Higher slag content resulted in darker, more intense red and brown hues. These mixes also exhibited the most pronounced crazing, extremely rough textures, and the highest degree of surface disintegration. This suggests that slag influences not only the color changes but also the overall physical behavior of concrete under elevated temperature.

Table 29 Visual alteration of samples exposed to high temperature

Ambient	400°C	800°C
PC 32.5		
	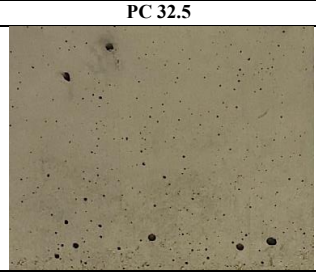	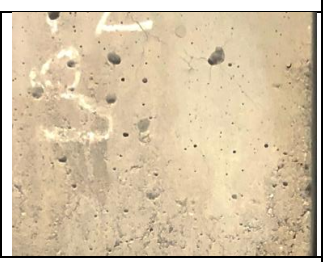
PC 32.5 + GGBFS (50/50 %)		

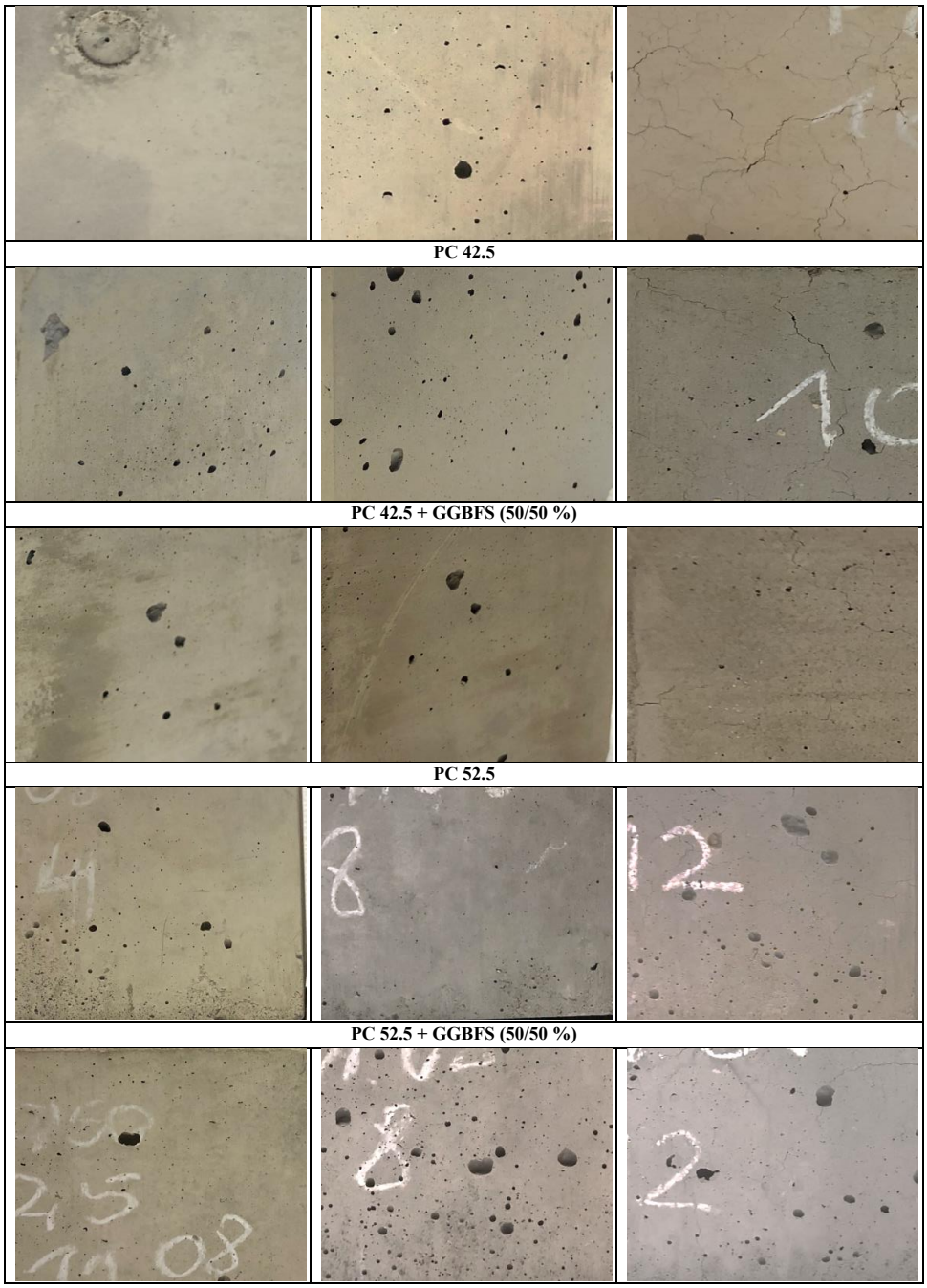

PC 42.5

PC 42.5 + GGBFS (50/50 %)

PC 52.5

PC 52.5 + GGBFS (50/50 %)

5.1.5. New chemical phase: Åkermanite within Melilite.

The decomposition of cement at elevated temperatures has been thoroughly investigated in the literature [81], as well as in Paper C. Once the material reaches the critical temperature at which calcium silicate hydrate (C–S–H) fully decomposes [180], and the high temperature is sustained to penetrate the element, new phases are formed due to melting and cooling (recrystallisation process), [212].

This can be interpreted as a reorganization of chemical structures. The elevated temperatures trigger both chemical and structural changes. If these thresholds are not met, key transformations such as the formation of phases, like åkermanite, merwinite or gehlenite, may not occur.

When blast furnace slag cools slowly, it usually forms a phase called melilite [95]. This phase is a solid solution of gehlenite ($2CaO \cdot Al_2O_3 \cdot SiO_2$) and åkermanite ($2CaO \cdot MgO \cdot 2SiO_2$), made up of the main oxides in the slag: CaO, SiO_2, MgO, and Al_2O_3. The XRD peaks of melilite overlap with typical peaks of gehlenite and åkermanite.

Because the chosen GGBFS has a high magnesium content, åkermanite is more likely to form and become the dominant part of melilite after high-temperature recrystallisation. Its presence is especially important because it shows some resistance to heat and helps the concrete to sustain its strength after being exposed to high temperatures.

Following exposure to 1200 °C [Paper C], the formation of åkermanite ($Ca_2MgSi_2O_7$)-rich melilite in the binder paste (PC + GGBFS) indicates a significant change induced by high temperature, *Figure 19*. This transformation reflects both the original chemical composition of the binder and the complicated reactivity that takes place under extreme thermal conditions [213]. Åkermanite, [214], is a mineral with a melting point above 1450 °C and a density of 2.944 g/cm³ [215]. To date, it has no significant industrial applications. It typically forms through solid-state reactions involving calcium oxide (CaO), magnesium oxide (MgO), and amorphous or reactive silica (SiO_2) around 900 °C [216]. It is more common in systems enriched with supplementary cementitious materials (SCMs) or additives containing Mg and Si, such as slag, fly ash, or certain natural pozzolans [216]. At elevated temperatures, conventional hydration products such as calcium silicate hydrate (C–S–H), portlandite ($Ca(OH)_2$), and ettringite decompose and lose structural integrity [81], making way for recrystallization processes. During the cooling phase, it favours the formation of thermodynamically stable silicates like melilite. The reaction is likely facilitated by the decarbonation of calcite and the dehydroxylation of portlandite, which provide reactive CaO, and by the collapse of the C–S–H structure, which releases SiO_2 [180]. In the presence of MgO, could be GGBFS originated *(Table, 14)*, åkermanite crystallizes according to the general reaction:

$2CaO + MgO + 2SiO_2 \rightarrow Ca_2MgSi_2O_7$ (åkermanite)

From a materials science perspective, the formation of åkermanite at such high temperatures can be advantageous for the residual mechanical performance and microstructural integrity of the material. Åkermanite is a dense, thermally stable phase with relatively low thermal conductivity [217] and good high-temperature resistance. Its crystallization can contribute to partial densification of the matrix, thereby reducing porosity and minimizing microcracking, typically followed by thermal degradation. Due to its refractory nature (high melting point), åkermanite may act as a structural scaffolding in the post-exposure matrix, supporting

dimensional stability and contributing to a longer lifespan. It can be concluded that exposing concrete to higher temperatures is more beneficial for inducing the crystallization of åkermanite, compared to lower temperatures, which may lead to the decomposition of C-S-H. Its presence has diagnostic value and may serve as a marker of high-temperature exposure in slag-modified concrete, contributing to the assessment of the performance of post-fire concrete elements. Another aspect worth investigating is how the recycled content of concrete containing åkermanite might contribute to the performance of new concrete elements exposed to elevated temperatures.

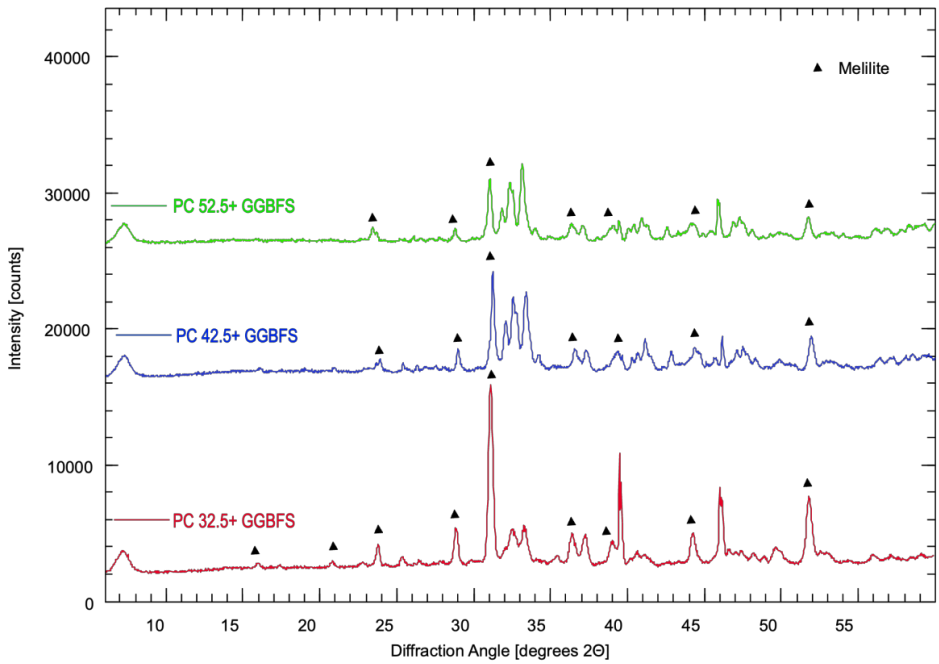

Figure 19 XRD spectra of binder pastes after exposure of 1200°C and cooling down. (Åkermanite cod_9006448)

The XRD analysis reveals a clear trend in the formation of crystalline melilite across the different cement types blended with GGBFS, *Figure 19*. Melilite formation is more pronounced in samples containing lower-grade cement, showing as distinct and sharp diffraction peaks. This can be attributed to the specific composition of the cement and the presence of fly ash and residual clinker that affect hydration behaviour. CEM 32.5 typically contains higher levels of alumina and silica, which favour the development of calcium-aluminate silicate phases. Moreover, the presence of fly ash can enhance this process, *Table* 8. The combined effect of these factors, especially during elevated temperature exposure, could create an environment that promotes the formation of this phase. The PC 42.5 + GGBFS sample also displays peaks in similar regions. However, they are broader and less intense, suggesting a moderate presence of melilite or a higher proportion of amorphous phases. In contrast, the PC 52.5 + GGBFS sample shows poorer peak definition in these key regions, leading to the assumption of a low degree of crystalline melilite.

When pure cement pastes are exposed to 1200 °C for one hour, then cooled and tested using XRD, no peaks corresponding to melilite are observed, *Figure 20*. Such peaks appear only in the mix containing PC 32.5, due to the factory-added fly ash.

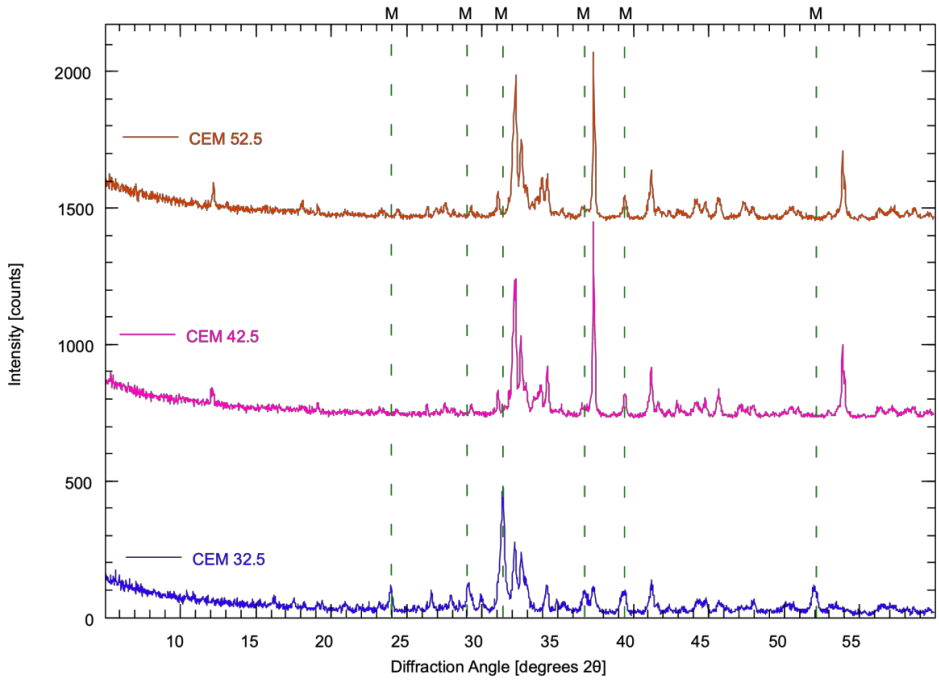

Figure 20 XRD spectra of cement pastes after exposure of 1200°C and cooling down. (Åkermanite cod_9006448)

In summary, the presence of slag and fly ash, interacting with high temperature, induces the formation of new thermally stable phases that enhance the thermal performance of concrete, whereas pure cement does not exhibit this behavior.

5.1.6. Simple Model. The role of GGBFS in åkermanite formation.

Simple models of concrete decomposition exposed to high temperatures are commonly studied and presented in current state-of-the-art research. However, there is relatively limited research on the influence of temperature on the recrystallization and chemical reorganization of a slag-enriched cement-based concrete matrix after cooling following a fire event, and how the newly formed phases contribute. A simplified model is proposed in *Figures 21, 22*. As mentioned before, it is more beneficial for cement-slag blend-based concrete to reach a temperature of approximately 900°C during a fire event and remain at that temperature long enough to enable partial melting of the matrix and promote the formation of åkermanite ($Ca_2MgSi_2O_7$). At this temperature range, the thermal energy is sufficient to destabilize and decompose initial hydration products, such as C–S–H (calcium silicate hydrate), ettringite, and portlandite, leading to the release of reactive CaO, SiO_2, and MgO. These parts can be reorganized under high-temperature conditions and react to form new crystalline phases. Those can contribute to

a denser and more stable microstructure during cooling. At lower temperatures, the energy input is insufficient to induce such chemical transformations, and the matrix remains largely disorganized, retaining a porous, 'unbaked' structure with degraded or amorphous remnants of the original hydration products.

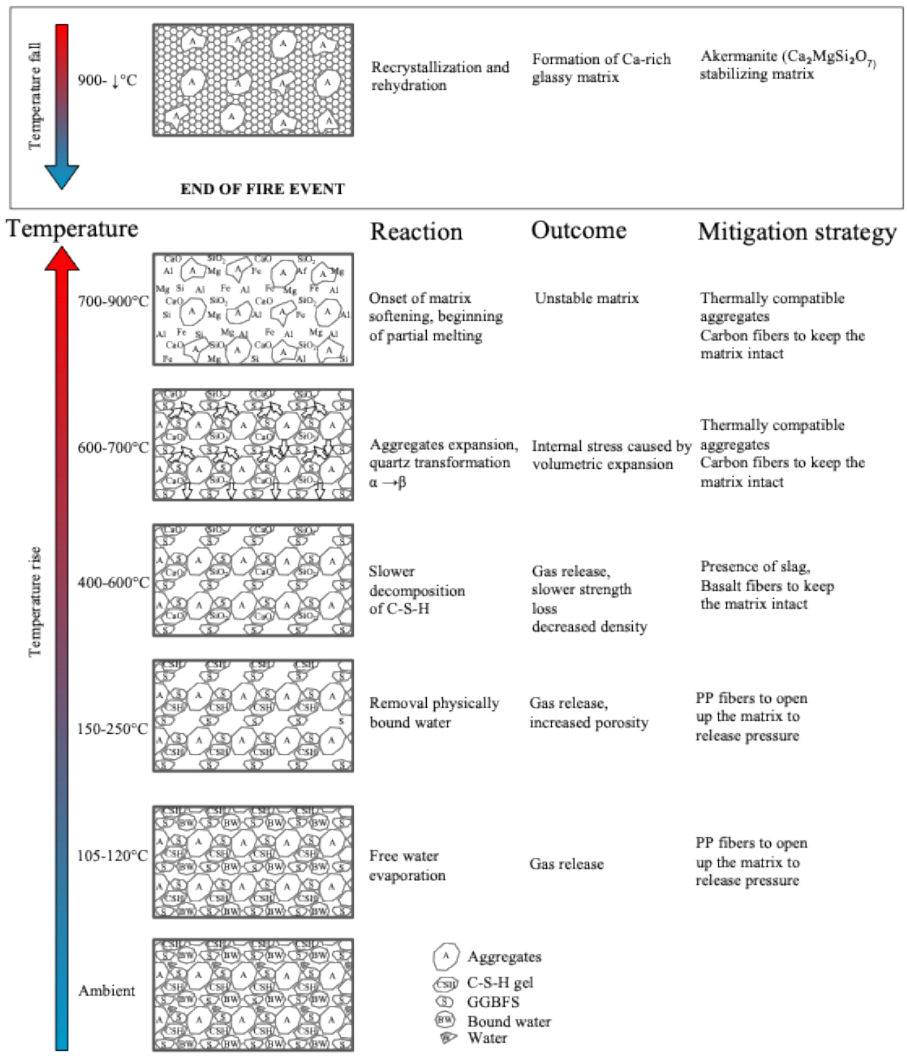

Figure 21 Simple model of alteration of cement-slag matrix during and after exposition to higher temperature, and proposed damage mitigation measures.

Focusing on the role of the chosen ground granulated blast furnace slag (GGBFS Merit), the following simplified model for åkermanite formation within the studied binder system can be proposed:

1. Slag Composition input.

Slag (like selected GGBFS, *Table 4*) contains some elements that are in favour of åkermanite formation, *Table 30*:

Table 30 Components of åkermanite

Component	Function in Reaction
CaO	Calcium source
MgO	Magnesium source
SiO_2	Silicon source
Al_2O_3	Competes with SiO_2 for phase formation

2. Latent hydraulic and pozzolanic reaction

First, slag reacts with water (latent hydraulic) and hydrated cement (pozzolanic reaction) to form C-S-H gel along with small amounts of aluminates or ettringite. Åkermanite does not form at this stage.

3. High-Temperature load (>850–900°C)

As the temperature rises, C-S-H and other hydrates decompose, releasing ions such as Ca^{2+}, SiO_2, and Mg^{2+}. Simultaneously, elements from the original slag become remobilized, contributing to the chemical activity within the system. This process leads to the formation of an oxide-rich matrix, where solid-state reactions begin to take place.

4. Crystallization during cooling

During slow cooling, the following reaction occurs**:**

$$2CaO+MgO+2SiO_2 \rightarrow Ca_2MgSi_2O_7$$

Åkermanite tends to crystallize out of the molten or semi-molten matrix when the Al_2O_3 content is moderate or low. It limits the formation of competing phases such as gehlenite ($Ca_2Al_2SiO_7$), which require a higher concentration of alumina. The formation of åkermanite is favoured due to the presence of Mg^{2+}. It plays a stabilizing role in the crystal structure. Magnesium, with its smaller ionic radius and divalent charge, fits well into the tetrahedral or octahedral sites of the silicate framework and helps create a thermally stable and rigid lattice. This makes the åkermanite structure energetically favourable, particularly at high temperatures. The balanced proportions of CaO, MgO, and SiO_2, often naturally present in slag, are critical because they provide the exact stoichiometric ratio (2:1:2) required for åkermanite formation. This balance ensures the availability of the necessary ions and alignment with the thermodynamic stability field of åkermanite. It is preventing the crystallization of alternative phases like wollastonite, merwinite, or forsterite. To sum up, the chemical environment created by the slag strongly supports the selective crystallization of åkermanite when alumina levels are insufficient to promote gehlenite [218].

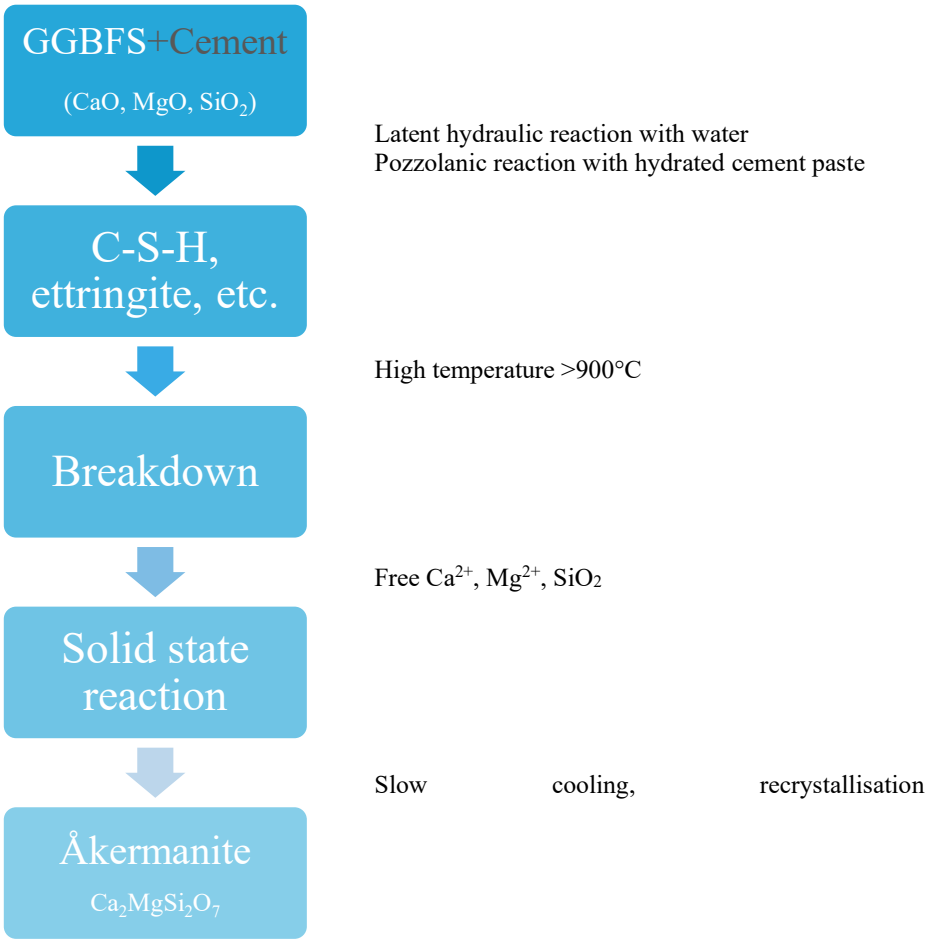

Figure 22 Role of GGBFS in åkermanite formation

Forming åkermanite in concrete can be difficult for several reasons. First, the chemical makeup of ground granulated blast furnace slag (GGBFS) changes depending on how and where it was made. Second, åkermanite only forms at high temperatures, usually between 850 and 950°C, and needs enough time at those temperatures for partial melting and movement of atoms. Also, the way the material cools down matters a lot. Slow and steady cooling helps form åkermanite, while quick cooling can stop it from developing by keeping the structure glassier and more disordered [219]. However, if the slag has the right amounts of calcium, magnesium, and silica, it can support åkermanite formation during fire exposure. Åkermanite is a stable crystal that doesn't react much and fits well with the rest of the binder. It is linked to better resistance to heat, fewer cracks, and a stronger structure after cooling. Due to that, åkermanite can help concrete recover after a fire by protecting its structure, slowing down further damage, and keeping some of its strength.

5.1.7. Elements ratio vs compressive strength performance and temperature in cement-slag blends.

Among the three elemental ratios (Si/Ca, Al/Ca, Al/Si) studied with SEM EDS analysis, the Si/Ca ratio seems to be the most reliable indicator of compressive strength retention at elevated temperatures, *Figure 23 a,b,c*. Among different binder combinations and temperatures, mixes with Si/Ca values in the range of 0.50 to 0.60 showed the most stable or even improved mechanical performance, especially at 400°C. This suggests that a balanced silicate-to-calcium ratio helps form a well-structured, heat-resistant C–S–H gel, which is important for strength in this type of blend. In some cement systems, small increases in the Si/Ca ratio from ambient temperature to 400°C led to noticeable strength improvements. However, when this ratio drops too much at 800°C, strength drops significantly. This is expected, as high heat causes decomposition and calcium loss, weakening the C–S–H gel structure.

The Al/Ca ratio also provides useful information, but its effect depends more on the specific binder chemistry and temperature. Moderate Al/Ca values, typically between 0.16 and 0.27, seem to help strength development, especially at room temperature and 400°C. This could be because aluminium helps form denser, more stable structures or stabilizes certain hydration products. However, when the Al/Ca ratio falls below 0.11, as seen in some samples exposed to 800°C, strength decreases sharply. This suggests that while aluminium may not be the main factor in strength at lower temperatures, its absence under heat can cause the structure to break down faster.

a)

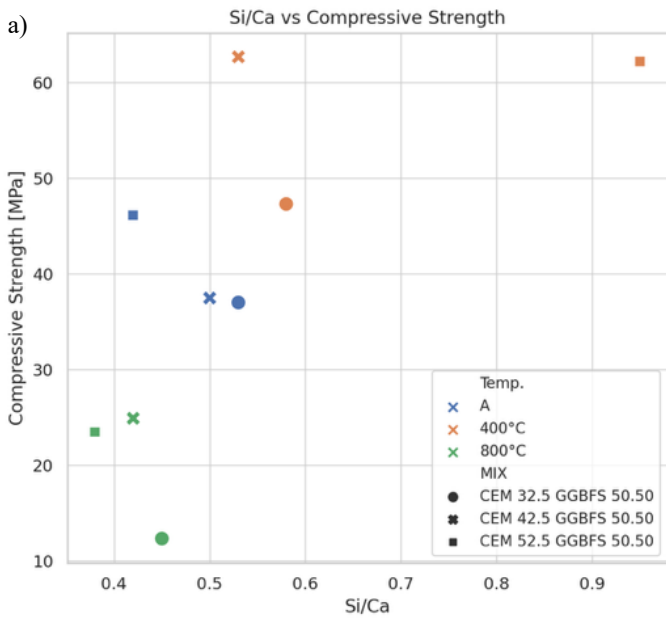

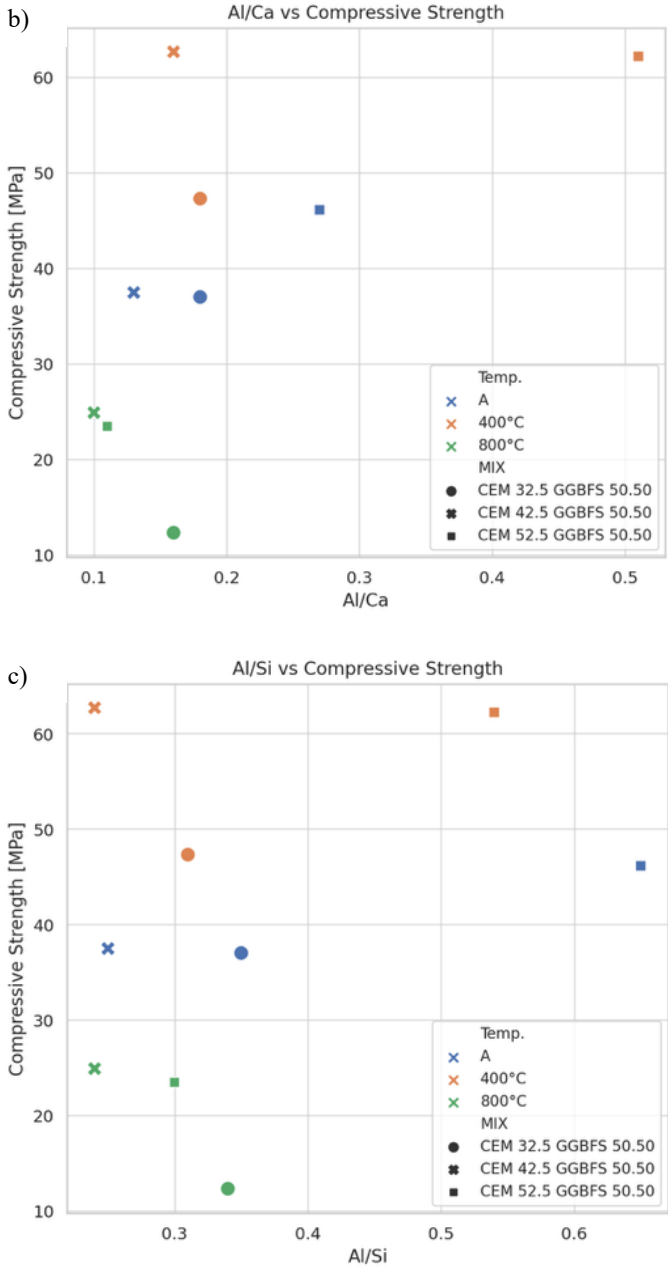

Figure 23 a,b,c Experimental data- correlation charts (Element content ratio, compressive strength, binder and temperature).

The Al/Si ratio appears to be the least reliable for trying to predict the compressive strength result in this case. Although it is often used to understand the complexity of aluminosilicate networks [220], its behaviour in this setup is inconsistent. In some cases, both strong and weak samples, regarding the compressive strength performance, had similar Al/Si ratios, showing that this ratio alone doesn't reflect performance well in this binder system. It may have a secondary role or become relevant only when combined with other microstructural or mineralogical results.

In summary, the Si/Ca and Al/Ca ratios provide the most useful insights for assessing concrete performance at high temperatures. The Si/Ca ratio is especially good for identifying heat-resistant mixtures, while the Al/Ca ratio helps assess the stability of aluminium-containing phases. The Al/Si ratio is less useful in this context. These findings could help in designing concrete mixtures that maintain their strength after high temperature exposure in similar setups.

5.1.8. Summary

Mechanical, chemical, and visual assessments of cement blends containing 50% GGBFS show that they perform almost like conventional Portland cement mixes after exposure to high temperatures. This makes them a viable and sustainable option for structures exposed to fire risk. The strengthening of the concrete matrix observed after heating to 400 °C enhances overall durability and may prolong the service life of affected structures both during and after a fire event.

At higher temperatures, the formation of thermally stable phases such as åkermanite contributes to improved structural cohesion, reducing the risk of rapid material disintegration. Cement-slag blends also tend to exhibit reduced spalling, lower thermal conductivity, and better retention of mass and volume compared to pure PC-based concretes, which can help maintain load-bearing capacity during fire exposure.

There is also potential to reuse fire-affected elements made with cement-slag blends as recycled aggregates in future mixes, supporting resource efficiency and circular construction. If slag sourced from local industries were used to replace 50% of cement, and if this replacement level were accepted by the Swedish construction market, the environmental impact could be significantly reduced. Currently, commercial mixes in Sweden are limited to 30% slag content, suggesting room for improvement in both policy and practice [221].

Since binder performance alone does not fully determine fire resistance, additional research is needed. Testing mixes that combine different materials, such as aggregates, fibers, or additives, will provide a more complete understanding of fire behaviour and structural resilience.

5.2. CSA cements with limestone powder and eggshell powder.

To address the research gap concerning lower-carbon-footprint concretes under high-temperature conditions from a different perspective, this study explores the use of lower temperature clinker firing cement and fillers. Since CSA cements generally do not perform well at elevated temperatures [18], [108], [222], and being inspired by the work of Martin et al. [223] on the contribution of limestone to the hydration of calcium sulfoaluminate cements, high-temperature tests were conducted on concretes based on this type of cement. These concretes were supplemented with additional limestone: powdered limestone and a waste-derived limestone sourced from hen eggshells.

5.2.1. Weight change

Exposure to high temperatures caused mass loss in all tested CSA-based concrete mixtures, primarily due to water evaporation and the decomposition of internal phases during heating. On average, the samples retained between 93% and 97% of their original mass after 1 hour at 400 °C, *Table 31*. The differences between mixtures were relatively small at this temperature threshold, but some variation was observed depending on the type of additive used.

Mixtures containing eggshell powder showed similar trends in mass retention while avoiding spalling. This improvement is likely due to the eggshell powder's ability to facilitate better vapor evacuation and more evenly distribute internal vapor pressure, reducing localized stress and surface damage. It might be attributed to the porous nature of eggshell structure [224]. In contrast, spalling was observed in specimens made only with CSA and in those containing limestone powder (LSP) after exposure to 800 °C, indicating internal pressure buildup and surface instability under heat. These results suggest that the wise choice of supplementary material can influence fire-related performance of this type of cement and the internal structure of matrix, with certain additives improving resistance to thermal damage.

Table 31 Weight change (average of 4 samples; SD % in parentheses; S- spalling).

Ambient	400°C	800°C
CSA		
100 % (0.05)	97 % (0.01)	*S*
CSA + 5% LSP		
100 % (0.02)	93 % (0.01)	*S*
CSA + 10% LSP		
100 % (0.02)	94 % (0.03)	*S*
CSA + 5% ESP		
100 % (0.02)	93 % (0.01)	93% (0.02)
CSA + 10% ESP		
100 % (0.03)	94 % (0.03)	94 % (0.03)

5.2.2. Compressive strength results

The compressive strength results presented in *Table 32* show clear trends regarding the thermal resistance of CSA cement-based concrete modified with LSP and ESP. At ambient conditions, all mixtures exhibited low standard deviations, indicating consistent performance across samples. The sample strength at ambient temperature serves as the 100% reference value. After exposure to 400°C, mixes experienced a sharp reduction in strength to approximately 35–40% of their original values. The mix containing 5% ESP kept the highest relative strength after exposure to this temperature, slightly outperforming the other combination and suggesting improved thermal stability. This strength loss can be explained by the decomposition of

hydration products typical of CSA cement. Ettringite begins to decompose between 80 and 150°C [18], while monosulfate breaks down between 250 and 400°C [108]. These transformations lead to a collapse of the binding structure and the formation of internal voids. In addition, the evaporation of capillary and chemically bound water increases internal vapor pressure, which contributes to microcracking and further strength degradation. At 800°C, only the mixes containing ESP retained their form and measurable residual strengths, whereas all pure CSA and CSA+LSP mixes experienced complete spalling and disintegration. These results show the beneficial role of ESP in improving the mechanical integrity of CSA-based concrete under extreme heat. The effectiveness of ESP can be attributed to its biogenic calcium carbonate (which often has a less crystalline, more porous) composition and fine particle size (easier to grind than geological limestone), which contribute to matrix alteration. This helps regulate the internal release of water vapor, thereby limiting pore pressure build-up. The gradual decomposition of calcium carbonate in ESP involves an endothermic reaction that absorbs heat and reduces thermal stress, lowering the risk of explosive spalling. In high-temperature conditions, ESP may also contribute to the formation of stable mineral phases, which support the residual strength of the concrete after thermal exposure (*Paper D*).

Table 32 Compressive stregth remaining results (average of 4 samples; SD % in parentheses; S- spalling).

Ambient	400°C	800°C
CSA		
100% (3.84)	36.20% (0.75)	*S*
CSA + 5% LSP		
100% (5.86)	35.78% (4.45)	*S*
CSA + 10% LSP		
100% (5.52)	38.11% (1.89)	*S*
CSA + 5% ESP		
100% (3.61)	39.75% (3.59)	18.78% (0.29)
CSA + 10% ESP		
100% (3.05)	36.18% (8.77)	15.01% (1.99)

5.2.3. Visual alteration of concrete samples

The visual examination of CSA-based concrete samples exposed to elevated temperatures did not show notable colour alteration across all mixes. These types of cements contain less F_2O_3 than Portland cements, where this oxide is mainly responsible for colour alteration [97]. The absence of direct visual change makes it difficult to assess the post-fire performance of CSA-based concrete based only on colour analysis.

At 800 °C, the reference CSA mix and both CSA + LSP blends (5% and 10%) experienced explosive spalling, indicating poor thermal stability under high-temperature conditions. Detailed images of the spalled samples are included in Paper E.

In contrast, the CSA + ESP blends (5% and 10%) remained physically intact, though they exhibited visible surface cracking and slight darkening. The samples containing 10% ESP showed greyish discoloration and a network of microcracks. Those with 5% ESP developed a pink-grey hue, reflecting thermal stress and matrix degradation. None of the samples displayed progressive colour change comparable to that observed in concrete based on PC and GGBFS (Table 33).
During the heat treatment of the ESP-containing samples, a distinct smell of burning organics was detected, suggesting the presence of residual organic matter from the eggshells. However,

due to the lack of an olfactometer, no quantitative or qualitative data could be collected regarding the nature or intensity of the odour.

Table 33 Colour alternation of CSA concrete after heating.

Ambient	400°C	800°C
CSA		
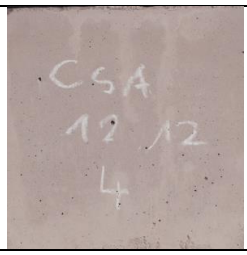	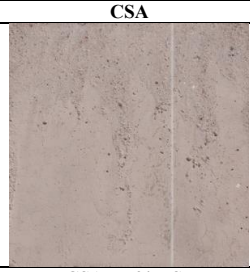	*S*
CSA + 5% LSP		
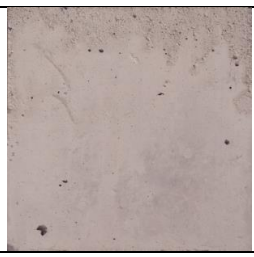	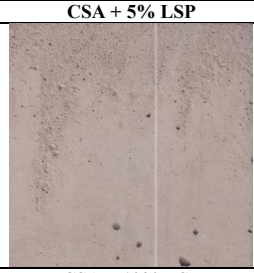	*S*
CSA + 10% LSP		
	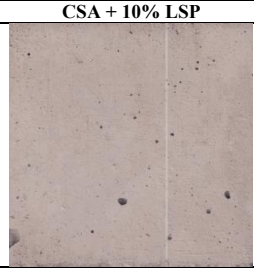	*S*
CSA + 5% ESP		
		
CSA + 10% ESP		

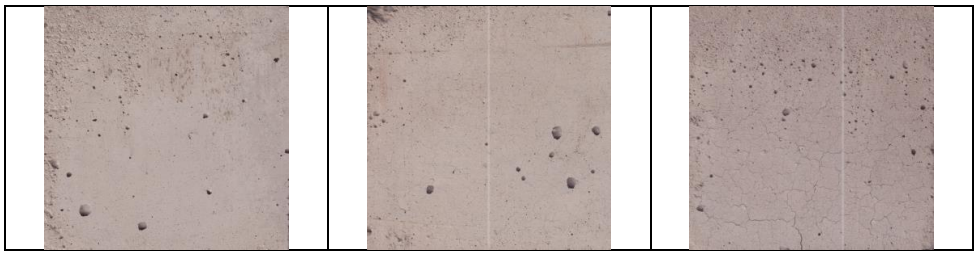

5.2.4. Role of microstructure vs mechanical performance after high temperature exposure

The relationship between concrete density and its performance under high temperatures is closely tied to microstructural characteristics. While higher density often correlates with increased mechanical strength at ambient conditions, it can also lead to reduced permeability and limited pores and their connectivity. Under thermal stress, these dense and impermeable microstructures may trap internal moisture, increasing the risk of spalling. In contrast, slightly more porous systems, despite their lower strength, can offer improved thermal stability and durability by facilitating vapor release and distributing internal stresses more effectively and evenly. This could be the key to maintain the structural integrity of a concrete element during a fire event, potentially allowing for a prolonged period of safe evacuation.

While *Figure 24* indicates that ESP-modified concrete samples exhibit lower compressive strength at elevated temperatures, it is important to note that these samples did not experience spalling. In contrast, some higher-strength mixes with denser matrices did spall under the same conditions. This points to a critical microstructural advantage offered by eggshell powder. It reduces strength to some extent, but it contributes to a matrix that is more thermally stable and better able to tolerate internal stresses.

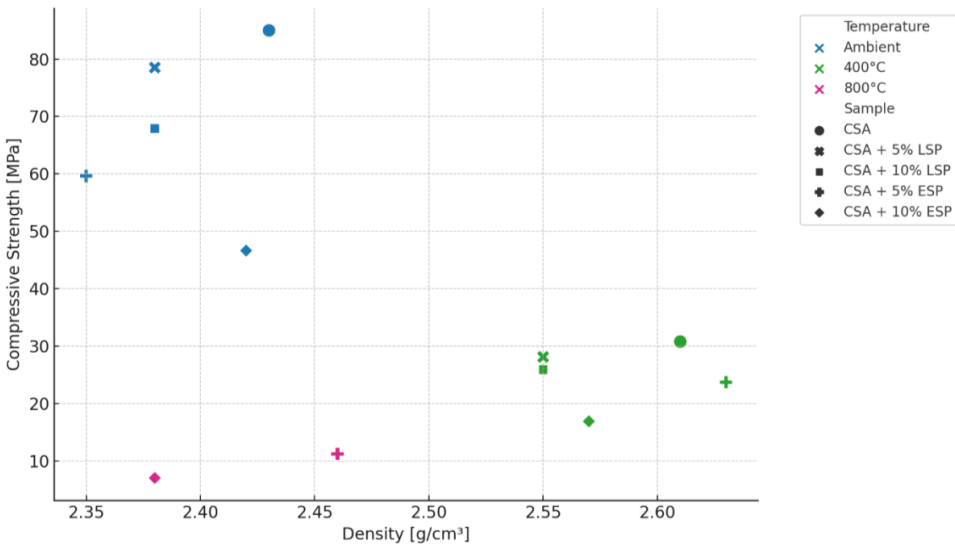

Figure 24 Correlation between compressive strength results and density of samples

At high temperatures, thermal stresses develop due to the differential expansion of binder phases and the buildup of vapor pressure from internal moisture. In dense and impermeable mixes, these stresses often lead to explosive spalling. However, the slight increase in porosity introduced by finely ground and well-dispersed ESP can function as a pressure relief mechanism. The interconnected pore system allows water vapor to escape, which helps reduce internal pressures and significantly lowers the risk of spalling.

In addition, the decomposition of calcium carbonate ($CaCO_3$) in ESP at temperatures above approximately 700°C provides a thermal buffering effect. This endothermic reaction absorbs some of the heat, which moderates the internal temperature rise and delays structural degradation. This process contributes to a reduction in mechanical strength, but it may help preserve the material's mass and overall integrity under fire exposure.

ESP functions not only as a partial cement replacement but also as an additive that enhances fire resistance by altering the matrix. It achieves this through a combination of density, vapor evacuation, and improved thermal stress distribution. While ESP mixes show reduced compressive strength, they remain structurally intact and demonstrate a more resilient, non-explosive failure mode. This characteristic can be a valuable factor for consideration for structures based on other types of binders exposed to high-temperature conditions.

5.2.5. Summary

The results indicate that CSA-based concrete is generally unsuitable for high-temperature exposure, as it experiences a significant drop in compressive strength after heating to 400 °C. At this temperature, it shows no visible changes, making it difficult to perform non-destructive assessment of the material after a fire event.

However, this study shows that partially replacing CSA cement with eggshell powder enhances thermal stability when compared to both limestone-modified and unmodified CSA mixes. While the CSA and CSA–limestone samples failed at 800 °C, the eggshell-modified mixes maintained structural integrity and compressive strength. These findings show the importance of microstructure in sustaining material stability under thermal stress. The improved performance is linked to a more refined pore structure, which facilitates moisture release and reduces internal pressure during heating. Eggshell powder not only contributes to improved high-temperature performance but also supports sustainability through waste valorisation and upcycling. Its use could extend the structural lifespan of elements exposed to fire, providing additional time for evacuation. Future studies should focus on optimizing eggshell dosage and particle size, assessing long-term durability, and characterizing the thermally stable crystalline phases in more detail. Exploring a combination with other bio-based or industrial waste materials may offer further improvements in thermal performance and environmental impact.

6. Spalling events- larger scale testing.

To address the risk of spalling, larger concrete elements (300×300×100 mm) were cast using mixes containing GGBFS and PC and incorporating two different types of fibers, as well as one mix combining both fiber types in a single sample. The volume dosage was addressed by trials on the workability of fresh mix to exclude the usage of plasticiser.
The elements were cast, demoulded the next day, and kept under ambient conditions in the laboratory, tightly wrapped in plastic foil for 28 days. After this period, the samples were photographed, weighed, and transported to the landfill. The outside temperature was 14 °C with no wind. After taking all necessary precautions, the setup was prepared, and testing began using a flame torch fuelled by propane. The hottest point of the torch flame reached a temperature of approximately 1026 °C. [225]. The flame was not touching the concrete element directly. The element was placed on a metal frame 200 mm above the ground, *Figures 25* and *26*. The torch was positioned directly beneath the element. The duration of the test (exposure to high temperature from the flame) for each sample was set to 10 minutes. After the test, the sample was removed from the stand, allowed to cool, and inspected for damage, *Table 35*.

Table 34 Larger scale fire testing. Results.

Case	C 1	C 2	C 3	C 4	C 5
Binder	PC 42.5	PC+GGBFS (50/50)	PC+GGBFS (50/50)	PC+GGBFS (50/50)	PC+GGBFS (50/50)
Fiber type	-	-	Basalt	PVA	Basalt + PVA
Amount [% vol]	-	-	0.13	0.60	0.13+0.60
Initial weight [kg]	19.10	19.12	19.10	19.05	19.00
Final weight [kg]	18.30	18.42	18.29	18.32	18.36
Lost mass [kg]	0.80	0.70	0.81	0.73	0.64
Time to spalling [min]	2:26	0:44	1:59	1:40	1:22
Surface of damage [mm^2]	13350	23950	29039	24741	25574
Max. damage depth [mm]	13	10	12	8	10

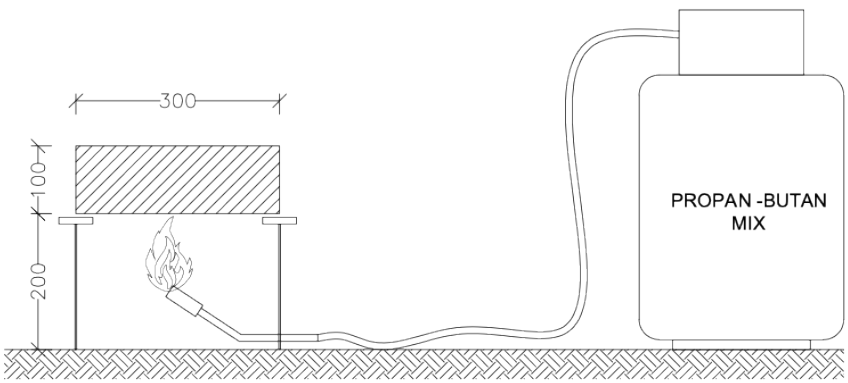

Figure 25 Experimental field setup

Figure 26 Experimental field setup photo

The test did not reveal a clear perfect mix in terms of performance, because all samples showed some degree of spalling, *Table 34*. The reference sample, which used only Portland cement (PC) as a binder, was the last to exhibit visible fire damage and had the smallest surface area affected. However, it suffered the greatest mass loss, indicating more severe internal degradation that, in a real structure, could lead to exposure of reinforcement bars. This suggests that heat spreads faster and deeper in PC concrete, and the matrix bonds are not strong enough to resist this thermal load. It may also indicate that PC concrete has higher thermal conductivity, supporting the findings of Sargam et al. [226]. This is likely due to the lower thermal conductivity of slag pastes compared to cement paste, combined with the reduced dry density of concrete mixes that include higher amounts of supplementary cementitious materials (SCMs).

In contrast, samples containing slag showed larger damaged areas on the surface but shallower damage in depth. This suggests that slag improves the insulating properties of concrete by limiting heat penetration. The degradation of PVA fibres, which occurs at around 239°C [144], was easily reached during the experiment. The voids left by the degraded fibres acted as small chambers that accommodated vapor pressure generated during fire exposure, helping the matrix resist thermal stress. Basalt fibres did not improve the fire resistance of the tested elements. With a melting point of about 1500°C [227], basalt fibres mainly serve as stitching to hold the concrete matrix together. Their primary function is to enhance mechanical properties, especially compressive and flexural strength, rather than reduce spalling. However, Kan et al. [228] emphasized that the effectiveness of basalt fibres depends on using the correct length and dosage within the concrete matrix to achieve the desired performance.

Table 35 External damage of samples after test

Case	Before	After
C1		
C2		
C3		

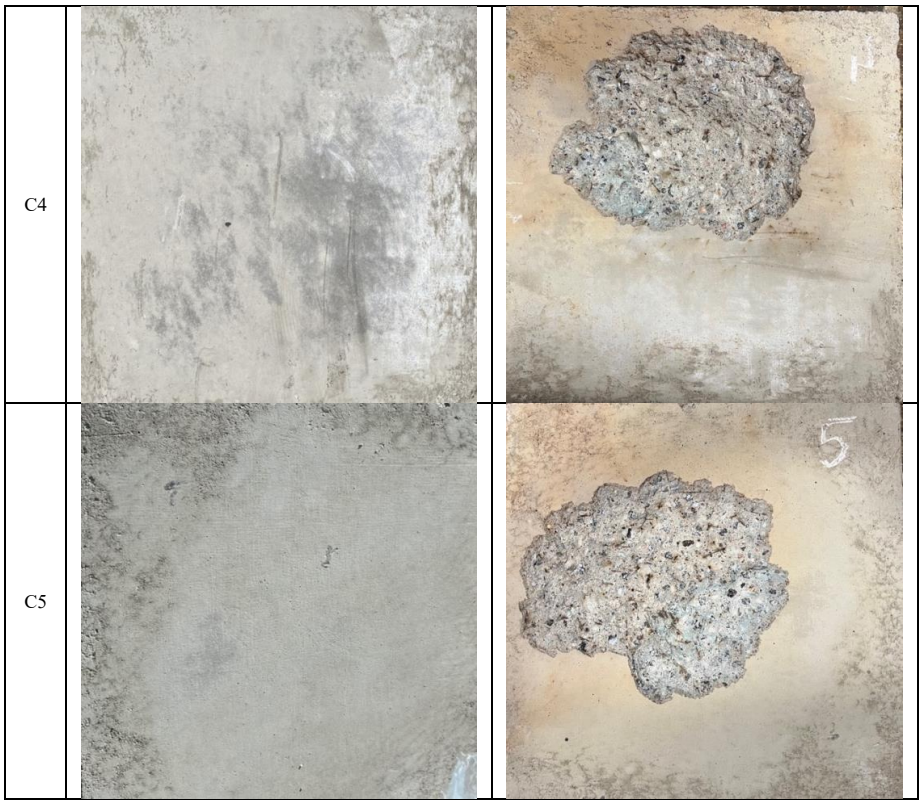

In all samples, water droplets could be seen both during and after the fire exposure, *Figure 27*. The heating generates pressure which forces the remaining pore fluid out of the samples.
Although spalling was observed in all the tested samples, this simple experiment demonstrates that incorporating GGBFS as a partial replacement for cement, combined with the addition of polyvinyl alcohol (PVA) fibers, can improve the fire resistance. The presence of GGBFS contributes to a denser and more stable microstructure, while the PVA fibers help control and accommodate vapour pressure during high-temperature exposure. Together, these effects work to minimize the extent of spalling, which in turn helps to prevent further structural deterioration under fire conditions. By enhancing the durability and resilience of concrete in fire environments, this approach increases the safety of structures but also extends their service life. This also contributes to sustainability by reducing the need for repairs, replacements, and resource consumption over time, making it a potential strategy for more fire-resilient and eco-friendlier construction materials.

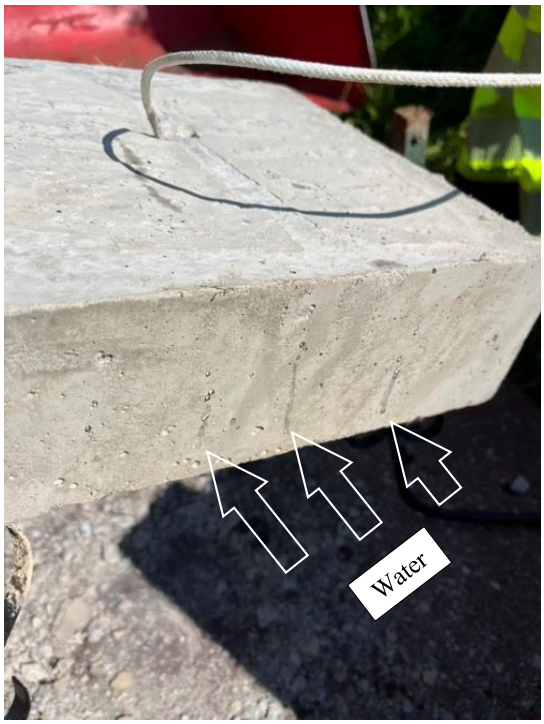

Figure 27 Water droplets

SEM images of samples taken from the spalling areas confirmed the initial assumption regarding fiber behaviour under high-temperature exposure, *Table 36*. The basalt fibers remained intact and well-bonded to the surrounding concrete matrix, indicating their high thermal stability and resistance at elevated temperatures. In contrast, the PVA (polyvinyl alcohol) fibers exhibited signs of thermal decomposition and melting, as evidenced by the presence of voids and empty creases in the matrix where the fibers had originally been embedded. This behaviour is consistent with the relatively low melting point of PVA fibers, which leads to melting during fire exposure. The disappearance of PVA fibers helps to increase porosity and may enhance vapor pressure build-up, which is a known contributing factor to explosive spalling in high-performance concrete.

Table 36 SEM images of samples from spalling areas.

C 1 (PC)	C 2 (PC+GGBFS)
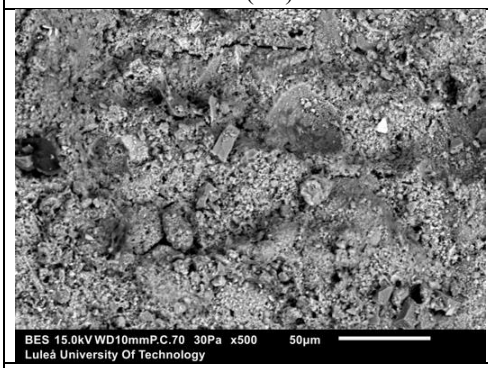	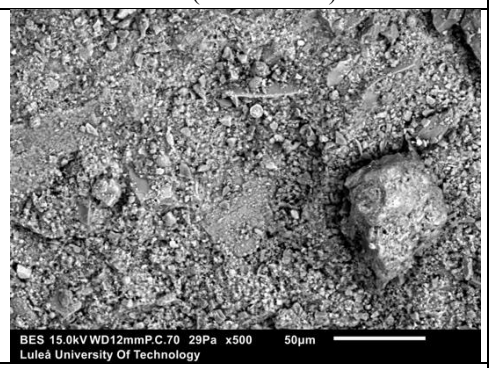
Mix 3 (Basalt fibers)	Mix 4 (PVA fibers)
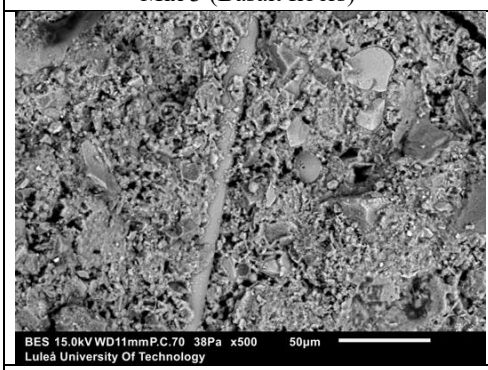	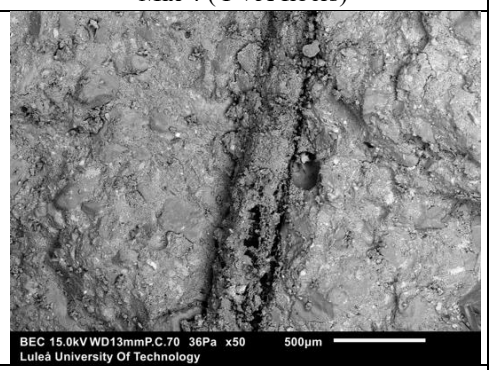
Mix 5 (Basalt + PVA)	Mix 5 (Basalt + PVA)
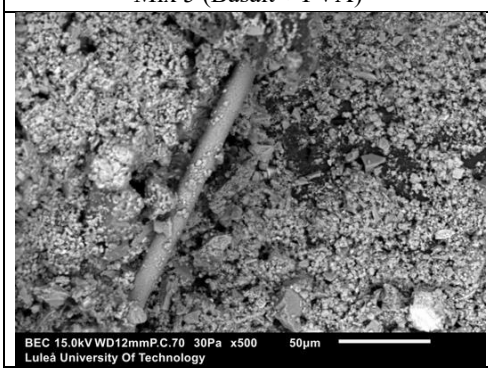	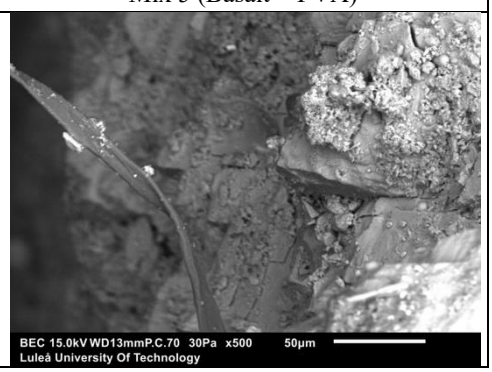

7. Unexpected findings

I have decided to dedicate this last section of my thesis to unexpected events, that occurred during conducting tests, which deserve deeper understanding and comprehension.

Even despite my big urges and scientific cravings, due to time and financial constraints, I couldn't explore and dive deeper.

7.1. Melted concrete

During one experimental setup, a concrete sample composed of a 50/50 blend of CEM 32.5 and GGBFS was exposed to a 1200°C thermal cycle for one hour. An unexpected event occurred when the muffle furnace shut down. The sample had melted *(Figure 28)*, damaging the heating element *(Figure 29)* and triggering the machine's safety switch.

Figure 28 Melted concrete sample

Figure 29 Damage in muffle furnace

The sample was cut to reveal a flat cross-section. A quick visual inspection showed that the aggregates remained intact, while the matrix had liquefied under the thermal load and subsequently crystallised, leaving a glassy, shiny surface with green-yellow shades, *Figure 30 a,b,c*.

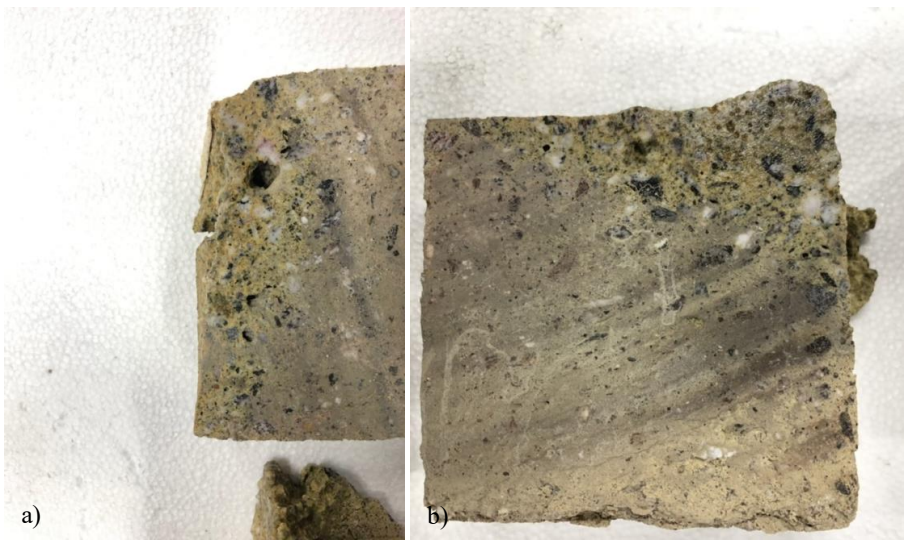

Figure 30 Melted sample- flat section (a,b,c).

The melted part of the sample was cut and prepared for a SEM investigation, using the method described earlier, to quickly check how the material had formed crystals after melting. SEM images showed tree-like, ice-shaped structures in the melted area, *Figure 31 and 32*. This shape usually happens when the material cools and hardens quickly and suggests that a glassy silicate phase turned into crystals [229]. These patterns might be caused by the formation of calcium or iron crystals at high temperatures [82], likely coming from the GGBFS or from cement parts that broke down and then formed crystals again as they cooled.

Similar geometric structures were found in archaeological iron items from the Transitional Byzantine to Ottoman period in Macedonia and Greece [230], suggesting that iron (Fe) plays a key role in forming these patterns. The research conducted by Albertsson et al. [231] with a close collaboration of Luleå University of Technology also found a similar outcome after thermal treatment of slag, identifying those dendritic structures as wüstite, a crystalline form of iron (Fe).

Interestingly, wüstite has been reported to exhibit good conductivity [232], adding another layer of complexity to the reactions occurring in concrete exposed to high temperatures. A deeper understanding of this phenomenon could provide valuable insights into the potential use of concrete elements as conductors, for example, in the increasingly popular concept of an electric road.

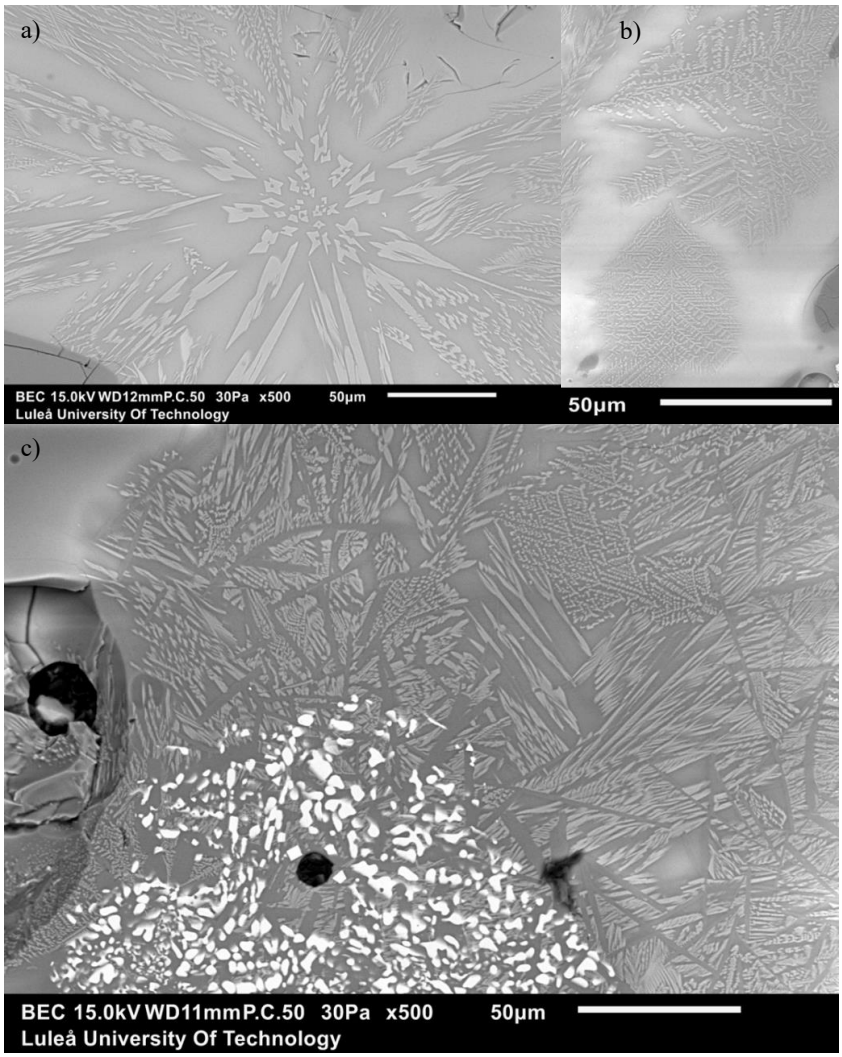

Figure 31 Observed geometrical structures in melted sample (a,b,c)

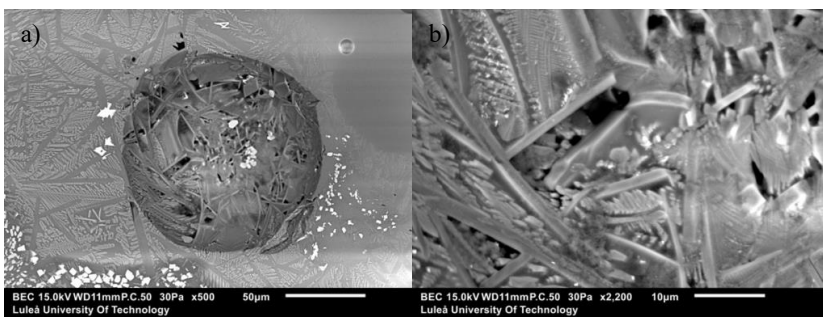

Figure 32 Observed geometrical structures in melted sample (a,b)

7.2. Impact of spalling

In another experiment investigating the impact of concrete admixtures on post-fire temperature performance, the accelerator gave unexpected results. This was due to a dosing error, where 10% of the binder weight was used instead of the recommended maximum of 6%. Samples were prepared following a general mix design with w/b 0.5, and 50/50 cement-slag ratio.

While 100×100×100 mm cubic samples were loaded into the furnace and exposed to 400 °C for one-hour, explosive spalling occurred, causing complete destruction of the samples and significant damage to the furnace chamber. The force of the explosion blew open the chamber door, sending pieces of concrete flying across the laboratory*, Figure 33.*

Figure 33 Testing disturbed concrete with an accelerator

To verify and rule out the possibility of this event being an isolated incident, the test was repeated. The furnace chamber was secured and reinforced with a metal box constructed from 0.5 mm thick sheet metal and square metal profiles for structural support. During the test, it was observed that the samples exploded at 350°C, failing to reach the intended threshold temperature. Opening the chamber, it was revealed how high pressure was created by one sample, causing deflection of the metal plate Figure 34 b,c. It was also reported that the intense gas released occurred, leaving marks on the furnace, *Figure 34a* .

Figure 34 Metal box after explosive spalling event (a,b,c,d).

This event highlights how the influence of high temperature can be both unpredictable and disruptive. Considering that the quality of concrete mixes is sometimes compromised, especially in non-professional production settings, additional preventive measures should be taken. One such measure is to minimize the maximum percentage of accelerators used, to reduce or eliminate potential risks. Overall, the results demonstrate that the choice of admixture is crucial in determining the thermal durability and performance of concrete under elevated temperatures.

Conclusions

This study provides insight into the performance of concrete and paste samples incorporating different types of cement and slag-ground granulated blast furnace slag (GGBFS) when exposed to various temperature thresholds for one hour, followed by evaluation after cooling. The findings indicate that Portland cement (PC) can be successfully replaced by up to 50% GGBFS without compromising post-fire mechanical performance. Moreover, GGBFS promotes the formation of thermally stable phases when samples are exposed to 900 °C and undergo slow cooling. The presence of quartz powder appears to have a synergistic effect, enhancing reactivity in combination with GGBFS.

Discrepancies between laboratory-scale and large-scale spalling tests suggest that spalling remains an unpredictable phenomenon, potentially influenced by non-material-related factors such as structural constraints, moisture gradients, or heating rates.

Tests involving calcium sulfoaluminate (CSA) cements confirm earlier hypotheses that this cement type is not well-suited for high-temperature environments. However, modifying the mix by incorporating eggshell powder (ESP) alters the microstructure in a way that may reduce the risk of spalling.

Answering the research questions

1. How does the partial replacement of Portland cement with GGBFS influence the thermal resistance of concrete in fire exposure? (**Paper B**)

   Partial replacement of Portland cement (50%) with a selected type of GGBFS (specifically, Merit slag) improved the thermal resistance of concrete, particularly after exposure to 400 °C. Under the selected testing regime, the slag-enhanced mixtures exhibited a denser and more stable matrix. This improvement is attributed to both the chemical composition and the physical characteristics of the selected type of slag (MgO), which contributed to enhanced microstructural integrity and the formation of thermally stable phases during and after fire exposure. Other types of slags are recommended to test.

2. What microstructural and chemical changes occur in cement-slag blends during high-temperature exposure? (**Paper C**)

   - Decomposition of hydration products: portlandite ($Ca(OH)_2$) and calcite ($CaCO_3$) begin to decompose, especially above 400–600 °C, releasing CO_2 and leading to increased porosity and potential strength loss.
   - Amorphization and recrystallization: Between 500–900 °C, amorphization occurs (loss of crystalline structure), followed by recrystallization upon cooling. Quartz-containing samples show earlier phase changes and higher porosity.

- Formation of high-temperature phases: At around 900 °C and above, new stable phases such as melilite probably dominated by åkermanite ($Ca_2MgSi_2O_7$) and tricalcium aluminate (C_3A) form. These phases help stabilize the matrix and enhance thermal resistance.
- Quartz effect: Quartz powder accelerates phase transformations and contributes to increased porosity, especially between 400 °C and 800 °C. Its alpha–beta phase transition at 573 °C induces volume changes, which may affect the material's thermal behaviour.
- Elemental shifts: As temperature rises, calcium, silicon, and aluminium content shifts, with Si/Ca and Al/Ca ratios affected by both temperature and quartz presence. These shifts reflect the ongoing decomposition and formation of new mineral phases.
- Porosity evolution: Porosity increases significantly with temperature, particularly in quartz-containing mixes. This can reduce mechanical strength but is partially offset by the formation of thermally stable phases like åkermanite and gehlenite.

3. What are the limiting factors affecting the high-temperature performance of CSA cements compared to PC and slag-based binders? (**Paper D**)

   The high-temperature performance of CSA cements is limited primarily by their mineralogical composition and rapid hydration characteristics. Unlike PC and slag-based binders, CSA cements form hydration products (ettringite and monosulfate) that are less thermally stable and tend to decompose at relatively low temperatures. This leads to microcracking, increased porosity, and loss of mechanical strength. CSA systems typically have a more brittle matrix and less residual strength after exposure to elevated temperatures. Their lower calcium silicate content also reduces the potential for forming high-temperature-resistant phases compared to PC–GGBFS blends. However, adding materials like ESP can improve the microstructure and slightly reduce the risk of spalling, but it does not fully solve the thermal weaknesses of CSA binders.

4. What are the factors influencing the high-temperature performance in concrete systems? (**Paper B, Paper C, Paper D, Paper E**)

   - Type of binder: different binders behave differently under heat. Some form more stable phases, while others decompose quickly.
   - Aggregate type: aggregates with high thermal stability and low thermal expansion reduce cracking and spalling.
   - Water-to-binder ratio: lower w/b ratios generally improve thermal resistance by producing a denser microstructure.
   - Moisture content: high internal moisture can cause spalling due to pore pressure buildup when heated.
   - Presence of supplementary materials: additives such as GGBFS, quartz powder, limestone (LS), eggshell powder (ESP), and fibers can enhance heat resistance by stabilizing the matrix and reducing porosity. Additionally, chemical admixtures can influence the thermal resistance of concrete elements by modifying hydration, setting time, and overall microstructure.

- Exposure temperature and duration: the severity and length of exposure affect which phases decompose and how much damage occurs.
- Cooling regime: slow cooling often helps maintain structural integrity, while rapid cooling increases the risk of cracking.
- Specimen size and testing scale: small-scale tests may not fully capture effects like spalling seen in larger elements.
- Environmental conditions and accompanying events: type of fire, self-degradation of the structure, explosions, fire extinguishing strategies, and weather conditions.

Concluding remarks

This thesis has explored the thermal behaviour of various lower-carbon concrete and paste mixes through a combination of mechanical testing, microstructural analysis, and chemical observations. The aim was to better understand how these sustainable systems perform in simple conditions after exposure to elevated temperatures, and how their composition influences stability, strength, and both visual and internal changes.

The findings confirm that slag-based systems, while promising from a sustainability perspective, undergo significant transformation under heat. When 50 percent of cement was replaced by GGBFS, the blend outperformed pure cement samples after exposure to 400°C.

The appearance of high-temperature phases such as åkermanite opens interesting questions regarding their role in post-fire performance and the potential reuse of heat-exposed materials.

Testing of CSA cement-based mixes highlighted the importance of microstructure. Although CSA is not suited to high-temperature environments, the incorporation of eggshell powder (ESP) altered its microstructure, helping to mitigate spalling and maintain structural integrity.

The origin of the spalling phenomenon remains unresolved. During large-scale testing, spalling occurred in all samples, regardless of mix composition or fibre addition, despite the fact that smaller specimens of the same mixes had never exhibited spalling.

Concrete admixtures, particularly accelerators, significantly disrupted the high-temperature response. The results indicate that these additives cannot be considered thermally neutral. This suggests that thermal behaviour depends not only on binder composition but also on the full chemical profile of the mix.

Reaching the melting point of the matrix allowed for physical and chemical reorganisation. It is worth investigating how extreme temperatures might be used to intentionally toughen the matrix, similar to processes used in the production of toughened glass.

Above all, this thesis is a contribution to the ongoing shift toward more responsible and thoughtful construction practices. It is not a final word, but a small part of a broader conversation. One that connects scientific insight with environmental awareness, and technical skill with curiosity and reflection.

Future work

This project covered a wide range of topics. Due to its complexity of the materials and the difficulties faced during the design of experiments and testing procedures, there is a clear need for further research. In future studies, it would be helpful to narrow the focus and investigate one specific factor or component at a time. This approach would help produce more reliable and detailed results.

It is recommended that future research select a single variable, such as the type of slag, the amount of binder, or the cooling method, and study its effects in depth. By focusing on just one factor, it becomes easier to understand how it influences the behaviour and performance of the concrete, both on a larger scale (mechanical strength) and a smaller scale (changes in microstructure and chemical composition).

In addition to small-scale laboratory experiments, future work should also include large-scale testing. This would help to verify whether the positive results observed in controlled environments can be replicated and reproduced in real construction settings. Large elements (slabs or beams) could be exposed to elevated temperatures and fire-like conditions to observe cracking patterns, spalling behaviour, visual alternation, eventual combustion, and structural failure modes. This type of testing would provide a more complete understanding of how the material behaves when applied in real structures.

Another important aspect for future research is the investigation of recycled post-fire concrete as a secondary raw material. Samples that have developed high-temperature mineral phases (åkermanite) could potentially be reused as recycled aggregate or, if shown to be chemically reactive, as part of the binder system. Studying the reactivity, particle size distribution, and compatibility of this material with fresh binders could open a new chapter, contributing to circular material design and the reduction of construction waste. The thermal history of such recycled material may even enhance certain properties, especially if åkermanite or similar phases contribute to long-term durability or strength development.

Improvements to experimental equipment would also be beneficial. Using a more advanced muffle furnace with programmable heating and cooling profiles, better temperature control, and real-time feedback from multiple thermocouples would allow for more precise thermal exposure. Accurate temperature tracking within each specimen would improve the reliability of the results and the understanding of material behaviour under fire conditions.

It would also be valuable to study how the material performs over time, especially when it is exposed to repeated heating and cooling cycles. This would better reflect real-life fire scenarios and improve the practical relevance of the findings.

Finally, combining laboratory and large-scale experiments with computer-based models and simulations could help predict material behaviour under different stress and temperature conditions. This would support the development of safer, more durable, and environmentally responsible concrete solutions for future construction.

"Not pursuing your dream is a violation against those who cannot even dare to dream"

Joan Thomsen Sekyere

References:

[1] "Nordic Fire Statistics | MSB." Accessed: Jun. 18, 2025. [Online]. Available: https://www.msb.se/en/about-msb/research-and-statistics/nordic-fire-statistics/

[2] P. Friedlingstein *et al.*, "Global Carbon Budget 2023," *Earth System Science Data*, vol. 15, no. 12, pp. 5301–5369, 2023, doi: 10.5194/ESSD-15-5301-2023.

[3] M. Z. Naser, "Observational Analysis of Fire-Induced Spalling of Concrete through Ensemble Machine Learning and Surrogate Modeling," *Journal of Materials in Civil Engineering*, vol. 33, no. 1, Jan. 2021, doi: 10.1061/(ASCE)MT.1943-5533.0003525.

[4] J. G. Quintiere, *Fundamentals of Fire Phenomena*. University of Maryland, USA: John Wiley & Sons, LTD, 2006. Accessed: Jun. 18, 2025. [Online]. Available: www.wiley.com

[5] A. Bwalya, "An overview of design fires for building compartments," *Fire Technol*, vol. 44, no. 2, pp. 167–184, 2008, doi: 10.1007/S10694-007-0031-7/FIGURES/4.

[6] S. Magnusson and S. Thelandersson, "Temperature-time curves of complete process of fire development," 1970, Accessed: Jul. 02, 2025. [Online]. Available: https://portal.research.lu.se/files/5675749/1245424.pdf

[7] B. Jovanović, R. Caspeele, G. Lombaert, E. Reynders, and R. Van Coile, "State-of-the-art review on the post-fire assessment of concrete structures," *Structural Concrete*, vol. 24, no. 4, pp. 5370–5387, 2023, doi: 10.1002/SUCO.202201108.

[8] B. R. Ellingwood, "Load combination requirements for fire-resistant structural design," *Journal of Fire Protection Engineering*, vol. 15, no. 1, pp. 43–61, 2005, doi: 10.1177/1042391505045582.

[9] U. Wickström, "Fire Exposure of Structures According to Standards," *Temperature Calculation in Fire Safety Engineering*, pp. 185–193, 2016, doi: 10.1007/978-3-319-30172-3_12.

[10] S. Chaturvedi, A. Vedrtnam, M. A. Youssef, M. T. Palou, G. Barluenga, and K. Kalauni, "Fire-Resistance Testing Procedures for Construction Elements—A Review," *Fire*, vol. 6, no. 1, 2023, doi: 10.3390/FIRE6010005.

[11] E. Tolentino, F. S. Lameiras, A. M. Gomes, C. A. R. da Silva, and W. L. Vasconcelos, "Effects of High Temperature on the Residual Performance of Portland Cement Concretes," *Materials Research*, vol. 5, no. 3, pp. 301–307, 2002, doi: 10.1590/S1516-14392002000300014.

[12] C. R. Cruz and M. Gillen, "Thermal expansion of Portland cement paste, mortar and concrete at high temperatures," *Fire Mater*, vol. 4, no. 2, pp. 66–70, 1980, doi: 10.1002/FAM.810040203.

[13] S. Luhar, S. Chaudhary, and I. Luhar, "Thermal resistance of fly ash based rubberized geopolymer concrete," *Journal of Building Engineering*, vol. 19, pp. 420–428, 2018, doi: 10.1016/J.JOBE.2018.05.025.

[14] T. Manzoor, J. A. Bhat, and A. H. Shah, "Performance of geopolymer concrete at elevated temperature − A critical review," *Construction and Building Materials*, vol. 420, p. 135578, 2024, doi: 10.1016/J.CONBUILDMAT.2024.135578.

[15] H. Assaedi, F. U. A. Shaikh, and I. M. Low, "Effect of nano-clay on mechanical and thermal properties of geopolymer," *Journal of Asian Ceramic Societies*, vol. 4, no. 1, pp. 19–28, 2016, doi: 10.1016/J.JASCER.2015.10.004.

[16] A. M. Rashad, "An investigation of high-volume fly ash concrete blended with slag subjected to elevated temperatures," *Journal of Cleaner Production*, vol. 93, pp. 47–55, 2015, doi: 10.1016/J.JCLEPRO.2015.01.031.

[17] S. Banerji and V. Kodur, "Effect of temperature on mechanical properties of ultra-high performance concrete," *Fire and Materials*, vol. 46, no. 1, pp. 287–301, 2022, doi: 10.1002/FAM.2979.

[18] J. Kaufmann, F. Winnefeld, and B. Lothenbach, "Stability of ettringite in CSA cement at elevated temperatures," *Advances in Cement Research*, vol. 28, no. 4, pp. 251–261, 2015, doi: 10.1680/JADCR.15.00029.

[19] C. J. Zega and A. A. Di Maio, "Recycled concrete exposed to high temperatures," Magazine of Concrete Research vol. 58, no. 10, pp. 675–682, 2015, doi: 10.1680/MACR.2006.58.10.675.

[20] A. Behnood and H. Ziari, "Effects of silica fume addition and water to cement ratio on the properties of high-strength concrete after exposure to high temperatures," *Cement and Concrete Composites*, vol. 30, no. 2, pp. 106–112, 2008, doi: 10.1016/J.CEMCONCOMP.2007.06.003.

[21] I. Netinger, I. Kesegic, and I. Guljas, "The effect of high temperatures on the mechanical properties of concrete made with different types of aggregates," *Fire Safety Journal*, vol. 46, no. 7, pp. 425–430, 2011, doi: 10.1016/J.FIRESAF.2011.07.002.

[22] J. Bao *et al.*, "A state-of-the-art review on high temperature resistance of lightweight aggregate high-strength concrete," *Journal of Building Engineering*, vol. 69, p. 106267, 2023, doi: 10.1016/J.JOBE.2023.106267.

[23] Y. Xu, Q. Yuan, X. Dai, and G. Xiang, "Improving the freeze-thaw resistance of mortar by a combined use of superabsorbent polymer and air entraining agent," *Journal of Building Engineering*, vol. 52, p. 104471, 2022, doi: 10.1016/J.JOBE.2022.104471.

[24] I. B. Topçu and C. Karakurt, "Properties of Reinforced Concrete Steel Rebars Exposed to High Temperatures," *Advances in Materials Science and Engineering*, vol. 2008, no. 1, p. 814137, 2008, doi: 10.1155/2008/814137.

[25] D. Qin, P. K. Gao, F. Aslam, M. Sufian, and H. Alabduljabbar, "A comprehensive review on fire damage assessment of reinforced concrete structures," *Case Studies in Construction Materials*, vol. 16, p. e00843, 2022, doi: 10.1016/J.CSCM.2021.E00843.

[26] R. Serrano, A. Cobo, M. I. Prieto, and M. de las N. González, "Analysis of fire resistance of concrete with polypropylene or steel fibers," *Construction and Building Materials*, vol. 122, pp. 302–309, 2016, doi: 10.1016/J.CONBUILDMAT.2016.06.055.

[27] J. P. C. Rodrigues, L. Laím, and A. M. Correia, "Behaviour of fiber reinforced concrete columns in fire," *Composite Structures*, vol. 92, no. 5, pp. 1263–1268, 2010, doi: 10.1016/J.COMPSTRUCT.2009.10.029.

[28] J. Novák and A. Kohoutková, "Fire response of Hybrid Fiber Reinforced Concrete to High Temperature," *Procedia Engineering*, vol. 172, pp. 784–790, 2017, doi: 10.1016/J.PROENG.2017.02.123.

[29] S. Shihada, "Effect of polypropylene fibers on concrete fire resistance," *Journal of Civil Engineering and Management*, vol. 17, no. 2, pp. 259–264, 2011, doi: 10.3846/13923730.2011.574454.

[30] J. Dils, G. De Schutter, and V. Boel, "Influence of mixing procedure and mixer type on fresh and hardened properties of concrete: A review," *Materials and Structures/Materiaux et Constructions*, vol. 45, no. 11, pp. 1673–1683, 2012, doi: 10.1617/S11527-012-9864-8/FIGURES/23.

[31] O. Mazanec, D. Lowke, and P. Schiel, "Mixing of high performance concrete: Effect of concrete composition and mixing intensity on mixing time," *Materials and Structures/Materiaux et Constructions*, vol. 43, no. 3, pp. 357–365, 2010, doi: 10.1617/S11527-009-9494-Y.

[32] J. H. Yun and J. S. Jeon, "Fire scenario-based damage assessment of ductile reinforced concrete buildings using computational fluid dynamics models," *Journal of Building Engineering*, vol. 78, p. 107655, 2023, doi: 10.1016/J.JOBE.2023.107655.

[33] M. Cvetkovska, M. Knezevic, Q. Xu, C. Chifliganec, M. Lazarevska, and A. T. Gavriloska, "Fire scenario influence on fire resistance of reinforced concrete frame structure," *Procedia Engineering*, vol. 211, pp. 28–35, 2018, doi: 10.1016/J.PROENG.2017.12.134.

[34] F. Pesavento, M. Pachera, P. Brunello, and B. A. Schrefler, "Concrete Exposed to Fire: From Fire Scenario to Structural Response," *Key Engineering Materials*, vol. 711, pp. 556–563, 2016, doi: 10.4028/WWW.SCIENTIFIC.NET/KEM.711.556.

[35] A. Buchanan and A. Abu, *Structural design for fire safety*. John Wiley & Sons, 2017.

[36] L. Bisby, J. Gales, and C. Maluk, "A contemporary review of large-scale non-standard structural fire testing," *Fire Science Reviews 2013 2:1*, vol. 2, no. 1, pp. 1–27, 013, doi: 10.1186/2193-0414-2-1.

[37] S. Kumar and C. V. S. K. Rao, "Fire Loads in Office Buildings," *Journal of Structural Engineering*, vol. 123, no. 3, pp. 365–368, 1997, doi: 10.1061/(ASCE)0733-9445(1997)123:3(365).

[38] S. Kumar and C. V. S. K. Rao, "Fire load in residential buildings," *Building and Environment*, vol. 30, no. 2, pp. 299–305, Apr. 1995, doi: 10.1016/0360-1323(94)00043-R.

[39] C. Thauvoye, B. Zhao, J. Klein, and M. Fontana, "Fire Load Survey and Statistical Analysis,", Fire Safety Science 9: 991-1002. 2008, doi: 10.3801/IAFSS.FSS.9-991.

[40] U. Dundar and S. Selamet, "Fire load and fire growth characteristics in modern high-rise buildings," *Fire Safety Journal*, vol. 135, p. 103710, 2023, doi: 10.1016/J.FIRESAF.2022.103710.

[41] D.-C. Feng *et al.*, "Climate Change Impacts on the Risk Assessment of Concrete Civil Infrastructures," *ASCE OPEN: Multidisciplinary Journal of Civil Engineering*, vol. 2, no. 1, p. 03124001, 2024, doi: 10.1061/AOMJAH.AOENG-0026.

[42] A. Obododike Ekwuno and C. Author, "A Review of the Consequences of Harsh Environmental Factors on Concrete's Life Span," *International Journal of Advanced Multidisciplinary Research Studies*, vol. 5, no. 1, pp. 910–919, 2025.

[43] J. Alduaij, K. Alshaleh, M. Naseer Haque, and K. Ellaithy, "Lightweight concrete in hot coastal areas," *Cement and Concrete Composites*, vol. 21, no. 5–6, pp. 453–458, 1999, doi: 10.1016/S0958-9465(99)00035-9.

[44] M. A. Bader, "Performance of concrete in a coastal environment," *Cement and Concrete Composites*, vol. 25, no. 4–5, pp. 539–548, 2003, doi: 10.1016/S0958-9465(02)00093-8.

[45] P. F. De, J. Cano-Barrita, B. J. Balcom, T. W. Bremner, M. B. Macmillan, and W. S. Langley, "Moisture distribution in drying ordinary and high performance concrete cured in a simulated hot dry climate," *Materials and Structures*, vol. 37, no. 8, pp. 522–531, 2004, doi: 10.1007/BF02481576.

[46] V. M. Karbhari and I. D. A. Eckel, “Effect of Cold Regions Climate on Composite Jacketed Concrete Columns,” *Journal of Cold Regions Engineering*, vol. 8, no. 3, pp. 73–86, 1994, doi: 10.1061/(ASCE)0887-381X(1994)8:3(73).

[47] Y. Haitao and T. Shizhu, “Preparation and properties of high-strength recycled concrete in cold areas,” *Materiales de Construcción*, vol. 65, no. 318, pp. e050–e0502015, doi: 10.3989/MC.2015.03214.

[48] A. Vasilchenko, O. Danilin, T. Lutsenko, and A. Ruban, “Features of Evaluation of Fire Resistance of Reinforced Concrete Ribbed Slab under Combined Effect ‘Explosion-Fire,’” *Materials Science Forum*, vol. 1038, pp. 492–499, 2021, doi: 10.4028/WWW.SCIENTIFIC.NET/MSF.1038.492.

[49] A. A. Khan, A. Usmani, and J. L. Torero, “Evolution of fire models for estimating structural fire-resistance,” *Fire Safety Journal*, vol. 124, p. 103367, 2021, doi: 10.1016/J.FIRESAF.2021.103367.

[50] K Kawagoe, “Fire behaviour in rooms,” 建築研究報告, pp. 1–70, 1958, Accessed: Jul. 02, 2025. [Online]. Available: https://cir.nii.ac.jp/crid/1572824499073272960

[51] P. Thomas, A. Heselden, and M. Law, “Fully-developed compartment fires: Two kinds of behaviour, vol.18,” 1967. Accessed: Jul. 02, 2025. [Online]. Available: https://firedoc.nist.gov/article/JXcyXYQBWEcjUZEYyMbK

[52] M. Law, *A basis for the design of fire protection of building structures*. 1983. Accessed: Jul. 03, 2025. [Online]. Available: https://pascal-francis.inist.fr/vibad/index.php?action=getRecordDetail&idt=PASCALBTP83X0237899

[53] V. Babrauskas, “A closed-form approximation for post-flashover compartment fire temperatures,” *Fire Safety Journal*, vol. 4, no. 1, pp. 63–73, 1981, doi: 10.1016/0379-7112(81)90005-9.

[54] “EN 1991-1-1: Eurocode 1: Actions on structures - Part 1-1: General actions - Densities, self-weight, imposed loads for buildings,” 2002.

[55] Y. Hasemi, Y. Yokobayashi, and T Wakamatsu, “Modeling of heating mechanism and thermal response of structural components exposed to localized fires: A new application of diffusion flame modeling,” *Proc., 13th Meeting of the UJNR Panel on Fire Research and Safety. Gaithersburg, MD: NIST*, 1997.

[56] A. Jonsdottir and G. Rein, “Out of range,” 2009, Accessed: Jul. 02, 2025. [Online]. Available: https://era.ed.ac.uk/handle/1842/3204

[57] X. Dai *et al.*, “An extended travelling fire method framework for performance-based structural design,” *ire and Materials*, vol. 44, no. 3, pp. 437–457, 2020, doi: 10.1002/FAM.2810.

[58] W. Dai *et al.*, “A Conceptual Framework for a Design Travelling Fire for Large Compartments with Fire Resistant Islands,” 2016, *4th International Fire Science & Engineering Conference (Interflam 2016). Vol. 2 London, UK : Interscience Communications Ltd, 2016. pp. 1039*

[59] J. C. G. Silva, A. Landesmann, and F. L. B. Ribeiro, “Fire-thermomechanical interface model for performance-based analysis of structures exposed to fire,” *Fire Safety Journal*, vol. 83, pp. 66–78, 2016, doi: 10.1016/J.FIRESAF.2016.04.007.

[60] U. Wickström, D. Dat, and K, McGrattan. (2007). “Adiabatic surface temperature for calculating heat transfer to fire exposed structures”. Interflam 2007. 2. 943-953.

[61] K. McGrattan, R. McDermott, J. Floyd, S. Hostikka, G. Forney, and H. Baum, “Computational fluid dynamics modelling of fire,” *International Journal of Computational Fluid Dynamics*, vol. 26, no. 6–8, pp. 349–361, 2012, doi: 10.1080/10618562.2012.659663.

[62] V. Novozhilov, “Computational fluid dynamics modeling of compartment fires,” *Progress in Energy and Combustion Science*, vol. 27, no. 6, pp. 611–666, 2001, doi: 10.1016/S0360-1285(01)00005-3.

[63] R. S. Walls, “A beam finite element for the analysis of structures in fire,” Stellenbosch : Stellenbosch University, 2016. Accessed: Jul. 02, 2025. [Online]. Available: http://hdl.handle.net/10019.1/100331

[64] Z. Liu, J. C. G. Silva, Q. Huang, Y. Hasemi, Y. Huang, and Z. Guo, “Coupled CFD–FEM Simulation Methodology for Fire-Exposed Bridges,” *Journal of Bridge Engineering*, vol. 26, no. 10, p. 04021074, 2021, doi: 10.1061/(ASCE)BE.1943-5592.0001770.

[65] X. Yan and T. Gernay, “Numerical modeling of localized fire exposures on structures using FDS-FEM and simple models,” *Engineering Structures*, vol. 246, p. 112997, 2021, doi: 10.1016/J.ENGSTRUCT.2021.112997.

[66] Y.-J. Kwon, “A Study on the Investigation of Users Guide of One-Way Coupled Analysis for Performance-Based Structural Fire Resistance Design,” *Proceedings of the Korean Institute of Building Construction Conference*, pp. 96–97, 2021.

[67] J. A. Feenstra, H. Hofmeyer, R. A. P. Van Herpen, and M. Mahendran, “Automated two-way coupling of CFD fire simulations to thermomechanical FE analyses at the overall structural level,” *Fire Safety Journal*, vol. 96, pp. 165–175, 2018, doi: 10.1016/J.FIRESAF.2017.11.007.

[68] M. T. Sadrabadi, M. Innocente, E. Gkanas, and I. Papagiannis, “Comparison of the effect of one-way and two-way fire-wind coupling on the modelling of wildland fire propagation dynamics,” *Advances in Forest Fire Research 2022*, pp. 115–121, 2022, doi: 10.14195/978-989-26-2298-9_18.

[69] M. Hurley *et al.*, *SFPE handbook of fire protection engineering*. Springer, 2015. [Online]. Available: https://books.google.com/books?hl=en&lr=&id=xP2zCgAAQBAJ&oi=fnd&pg=PR1&ots=110eCZHGXs&sig=JxrEfbJsw69L31Dh6-k48Sk3c7A

[70] Society for Fire Protection Engineers, *Fire Exposures to Structural Elements*. in The Society of Fire Protection Engineers Series. Cham: Springer Nature Switzerland, 2025. doi: 10.1007/978-3-031-64025-4.

[71] J. K. Richardson, *SFPE engineering standard on calculating fire exposures to structures*. Society of Fire Protection Engineers, 2011.

[72] G. A. Khoury, "Effect of fire on concrete and concrete structures," *Progress in Structural Engineering and Materials*, vol. 2, no. 4, pp. 429–447, 2000, doi: 10.1002/PSE.51.

[73] C. Bailey, "Holistic behaviour of concrete buildings in fire," *Structures and Buildings (ICE Proceedings)* vol. 152, no. 3, pp. 199–212, 2015, doi: 10.1680/STBU.2002.152.3.199.

[74] K. D. Hertz, "Concrete strength for fire safety design," *Magazine of Concrete Research*, vol. 57, no. 8, pp. 445–453, 2015, doi: 10.1680/MACR.2005.57.8.445.

[75] P. Chaunsali and P. Mondal, "Influence of Calcium Sulfoaluminate (CSA) Cement Content on Expansion and Hydration Behavior of Various Ordinary Portland Cement-CSA Blends," *Journal of the American Ceramic Society*, vol. 98, no. 8, pp. 2617–2624, 2015, doi: 10.1111/JACE.13645.

[76] M. A. Tantawy and M. A. Tantawy, "Effect of High Temperatures on the Microstructure of Cement Paste," *Journal of Materials Science and Chemical Engineering*, vol. 5, no. 11, pp. 33–48, 2017, doi: 10.4236/MSCE.2017.511004.

[77] H. Wang, H. Lyu, T. Liu, Y. Li, and K. Hai Tan, "Effect of post-fire curing on compressive strength of ultra-high performance concrete and mortar," *Construction and Building Materials*, vol. 346, p. 128447, Sep. 2022, doi: 10.1016/J.CONBUILDMAT.2022.128447.

[78] K. S. Al-Jabri, M. B. Waris, and A. H. Al-Saidy, "Effect of aggregate and water to cement ratio on concrete properties at elevated temperature," *Fire and Materials*, vol. 40, no. 7, pp. 913–925, 2016, doi: 10.1002/FAM.2351.

[79] J. W. Bullard *et al.*, "Mechanisms of cement hydration," *Cement and Concrete Research*, vol. 41, no. 12, pp. 1208–1223, 2011, doi: 10.1016/J.CEMCONRES.2010.09.011.

[80] E. Menéndez, L. Vega, and C. Andrade, "Use of decomposition of portlandite in concrete fire as indicator of temperature progression into the material: Application to fire-affected builds," *Journal of Thermal Analysis and Calorimetry*, vol. 110, no. 1, pp. 203–209, 2012, doi: 10.1007/S10973-011-2159-4.

[81] C. N. C, "Transition and decomposition temperatures of cement pahses - A collection of thermal analysis data," *Ceramics-Silikáty*, vol. 60, no. 4, pp. 338–343, 2016, doi: 10.13168/cs.2016.0050.

[82] V. Ponomar, E. Adesanya, K. Ohenoja, and M. Illikainen, "High-temperature performance of slag-based Fe-rich alkali-activated materials," *Cement and Concrete Research*, vol. 161, p. 106960, 2022, doi: 10.1016/J.CEMCONRES.2022.106960.

[83] H. M. Yang *et al.*, "High-ferrite Portland cement with slag: Hydration, microstructure, and resistance to sulfate attack at elevated temperature," *Cement and Concrete Composites*, vol. 130, p. 104560, 2022, doi: 10.1016/J.CEMCONCOMP.2022.104560.

[84] A. M. Rashad, "An investigation on very high volume slag pastes subjected to elevated temperatures," *Construction and Building Materials*, vol. 74, pp. 249–258, 2015, doi: 10.1016/J.CONBUILDMAT.2014.10.019.

[85] Q. Li, Z. Li, and G. Yuan, "Effects of elevated temperatures on properties of concrete containing ground granulated blast furnace slag as cementitious material," *Construction and Building Materials*, vol. 35, pp. 687–692, 2012, doi: 10.1016/J.CONBUILDMAT.2012.04.103.

[86] L. Wang, R. Luo, W. Zhang, M. Jin, and S. Tang, "Effects of fineness and content of phosphorus slag on cement hydration, permeability, pore structure and fractal dimension of concrete," *International Journal of Modern Physics B*, vol. 29, no. 2, p. 2140004, 2021, doi: 10.1142/S0218348X21400041.

[87] D. C. Hughes, "Pore structure and permeability of hardened cement paste," *Magazine of Concrete Research*, vol. 37, no. 133, pp. 227–233, 2015, doi: 10.1680/MACR.1985.37.133.227.

[88] Y. Elakneswaran, E. Owaki, S. Miyahara, M. Ogino, T. Maruya, and T. Nawa, "Hydration study of slag-blended cement based on thermodynamic considerations," *Construction and Building Materials*, vol. 124, pp. 615–625, 2016, doi: 10.1016/J.CONBUILDMAT.2016.07.138.

[89] Y. Yao, Y. Wang, Q. Wei, S. Cui, and L. Hao, "Effect of the Formation of Amorphous Networks on the Structure and Hydration Characteristics of Granulated Blast Furnace Slag," *Materials 2020, Vol. 13, Page 1462*, vol. 13, no. 6, p. 1462, 2020, doi: 10.3390/MA13061462.

[90] M. A. Montes-Morán *et al.*, "Linz-Donawitz steel slag for the removal of hydrogen sulfide at room temperature," *Environmental Science & Technology*, vol. 46, no. 16, pp. 8992–8997, 2012, doi: 10.1021/ES301257C

[91] G. De Schutter and L. Taerwe, "Specific heat and thermal diffusivity of hardening concrete," *Magazine of Concrete Research*, vol. 47, no. 172, pp. 203–208, 2015, doi: 10.1680/MACR.1995.47.172.203.

[92] J. A. Naqash, P. N. Reddy, and J. A. Naqash, "Experimental study on TGA, XRD and SEM Analysis of Concrete with Ultra-fine Slag," *International Journal of Engineering (IJE), IJE TRANSACTIONS B: Applications*, vol. 32, no. 5, pp. 679–684, 2019, doi: 10.5829/ije.2019.32.05b.09.

[93] Z. Liu, S. El-Tawil, W. Hansen, and F. Wang, "Effect of slag cement on the properties of ultra-high performance concrete," *onstruction and Building Materials*, vol. 190, pp. 830–837, 2018, doi: 10.1016/J.CONBUILDMAT.2018.09.173.

[94] N. H. Brett, "An X-ray investigation of the thermal decomposition of portlandite," *Mineralogical Magazine*, vol. 37, no. 286, pp. 244–249, 1969, doi: 10.1180/MINMAG.1969.037.286.13.

[95] J. B. Ferreira Neto *et al.*, "Modification of Molten Steelmaking Slag for Cement Application," *Journal of Sustainable Metallurgy*, vol. 2, no. 1, pp. 13–27, 2016, doi: 10.1007/S40831-015-0031-7/TABLES/8.

[96] O. Burciaga-Díaz and J. I. Escalante-García, "Comparative performance of alkali activated slag/metakaolin cement pastes exposed to high temperatures," *Cement and Concrete Composites*, vol. 84, pp. 157–166, 2017, doi: 10.1016/J.CEMCONCOMP.2017.09.007.

[97] J. Lee, K. Choi, and K. Hong, "Color and Material Property Changes in Concrete Exposed to High Temperatures," *Journal of Asian Architecture and Building Engineering*, vol. 8, no. 1, pp. 175–182, 2009, doi: 10.3130/JAABE.8.175.

[98] S. Mengxiao, W. Qiang, and Z. Zhikai, "Comparison of the properties between high-volume fly ash concrete and high-volume steel slag concrete under temperature matching curing condition," *Construction and Building Materials*, vol. 98, pp. 649–655, 2015, doi: 10.1016/J.CONBUILDMAT.2015.08.134.

[99] R. Kumar and B. Bhattacharjee, "Porosity, pore size distribution and in situ strength of concrete," *Cement and Concrete Research*, vol. 33, no. 1, pp. 155–164, 2003, doi: 10.1016/S0008-8846(02)00942-0.

[100] A. S. Cheng, T. Yen, Y. W. Liu, and Y. N. Sheen, "Relation between Porosity and Compressive Strength of Slag Concrete," *Proceedings of the 2008 Structures Congress - Structures Congress 2008: Crossing the Borders*, vol. 314, pp. 1–8, 2008, doi: 10.1061/41016(314)310.

[101] I. Asadi, P. Shafigh, Z. F. Bin Abu Hassan, and N. B. Mahyuddin, "Thermal conductivity of concrete – A review," *Journal of Building Engineering*, vol. 20, pp. 81–93, 2018, doi: 10.1016/J.JOBE.2018.07.002.

[102] P. Shafigh, I. Asadi, and N. B. Mahyuddin, "Concrete as a thermal mass material for building applications - A review," *Journal of Building Engineering*, vol. 19, pp. 14–25, 2018, doi: 10.1016/J.JOBE.2018.04.021.

[103] E. J. Sellevold and Bjøntegaard, "Coefficient of thermal expansion of cement paste and concrete: Mechanisms of moisture interaction," *Materials and Structures/Materiaux et Constructions*, vol. 39, no. 9, pp. 809–815, 2006, doi: 10.1617/S11527-006-9086-Z

[104] A. Hak-Chul Shin and Y. Chung, "Coefficient of Thermal Expansion for Concrete Containing Fly Ash and Slag," in *Proc., 3rd Int. Conf. on Sustainable Construction Materials and Technologies,* Kyoto, Japan, 2013. Accessed: Aug. 18, 2025. [Online]. Available: http://www.claisse.info/Proceedings.htm

[105] J. Dachtar, "Calcium Sulfoaluminate Cement as Binder for Structural Concrete," University of Sheffield, Sheffield, 2004.

[106] M. Ben Haha, F. Winnefeld, and A. Pisch, "Advances in understanding ye'elimite-rich cements," *Cem Cement and Concrete Researc*, vol. 123, p. 105778, 2019, doi: 10.1016/J.CEMCONRES.2019.105778.

[107] S. Liu *et al.*, "Damage resistance of calcium sulfoaluminate cement-based engineered cementitious composite (CSA-ECC) under vehicle-bridge coupling vibration," *Mater Struct*, 2024, doi: 10.1617/s11527-024-02398-8.

[108] K. A. Sodol, Ł. Kaczmarek, and J. Szer, "Fire-Temperature Influence on Portland and Calcium Sulfoaluminate Blend Composites," *Materials*, vol. 13, no. 22, p. 5230, 2020, doi: 10.3390/MA13225230.

[109] J. Bizzozero, C. Gosselin, and K. L. Scrivener, "Expansion mechanisms in calcium aluminate and sulfoaluminate systems with calcium sulfate," *Cement and Concrete Research*, vol. 56, pp. 190–202, Feb. 2014, doi: 10.1016/J.CEMCONRES.2013.11.011.

[110] W. He, R. Li, Y. Yang, Y. Zhang, and D. Nie, "Kinetic and thermodynamic analysis on preparation of belite-calcium sulphoaluminate cement using electrolytic manganese residue and barium slag by TGA," *Environmental Science and Pollution Research*, vol. 30, no. 42, pp. 95901–95916, 2023, doi: 10.1007/S11356-023-29104-5

[111] Z. Zhang *et al.*, "Experimental studies and thermodynamic analysis of calcium sulfoaluminate clinker under carbonation condition," *Construction and Building Materials*, vol. 440, p. 137418, 2024, doi: 10.1016/J.CONBUILDMAT.2024.137418.

[112] B. Lothenbach and F. Winnefeld, "Thermodynamic modelling of cement hydration: Portland cements - blended cements - calcium sulfoaluminate cements," *Cementitious Materials: Composition, Properties, Application*, pp. 103–143, 2017, doi: 10.1515/9783110473728-005

[113] T. Hanein *et al.*, "Alite calcium sulfoaluminate cement: chemistry and thermodynamics," *Advances in Cement Research*, vol. 31, no. 3, pp. 94–105, 2019, doi: 10.1680/JADCR.18.00118.

[114] D. Gao, Y. Meng, L. Yang, J. Tang, and M. Lv, "Effect of ground granulated blast furnace slag on the properties of calcium sulfoaluminate cement," *Construction and Building Materials*, vol. 227, p. 116665, 2019, doi: 10.1016/J.CONBUILDMAT.2019.08.046.

[115] L. H. J. Martin, F. Winnefeld, E. Tschopp, C. J. Müller, and B. Lothenbach, "Influence of fly ash on the hydration of calcium sulfoaluminate cement," *Cement and Concrete Research*, vol. 95, pp. 152–163, 2017, doi: 10.1016/J.CEMCONRES.2017.02.030.

[116] J. J. Kouadjo Tchekwagep, S. Wang, A. K. Mukhopadhyay, S. Huang, and X. Cheng, "Compressive strength of rapid sulfoaluminate cement concrete exposed to elevated temperatures," *Ceramics-Silikáty*, vol. 64, no. 3, pp. 299–309, 2020, doi: 10.13168/cs.2020.0019.

[117] G. Dolino and P. Bastie, "Phase Transitions of Quartz," *Key Engineering Materials*, vol. 101–102, pp. 285–310, 1995, doi: 10.4028/WWW.SCIENTIFIC.NET/KEM.101-102.285.

[118] W. Bragg and R. E. Gibbs, "The structure of α and β quartz," *Proceedings of the Royal Society of London. Series A, Containing Papers of a Mathematical and Physical Character*, vol. 109, no. 751, pp. 405–427, 1925, doi: 10.1098/RSPA.1925.0135.

[119] I. Hager, T. Tracz, J. Śliwiński, and K. Krzemień, "The influence of aggregate type on the physical and mechanical properties of high-performance concrete subjected to high temperature," *Fire and Materials*, vol. 40, no. 5, pp. 668–682, 2016, doi: 10.1002/FAM.2318.

[120] S. Diamond and J. Huang, "The ITZ in concrete – a different view based on image analysis and SEM observations," *Cement and Concrete Composites*, vol. 23, no. 2–3, pp. 179–188, 2001, doi: 10.1016/S0958-9465(00)00065-2.

[121] K. L. Scrivener, A. K. Crumbie, and P. Laugesen, "The interfacial transition zone (ITZ) between cement paste and aggregate in concrete," *Interface Science*, vol. 12, no. 4, pp. 411–421, 2004, doi: 10.1023/B:INTS.0000042339.92990.4C

[122] C. Du, L. Sun, S. Jiang, and Z. Ying, "Numerical Simulation of Aggregate Shapes of Three-Dimensional Concrete and Its Applications," *Journal of Aerospace Engineering*, vol. 26, no. 3, pp. 515–527, 2013, doi: 10.1061/(ASCE)AS.1943-5525.0000181/ASSET/EC281F1B-1FF7-4795-88FB-3818BD257032.

[123] J. H. Yeon, S. Choi, and M. C. Won, "In situ measurement of coefficient of thermal expansion in hardening concrete and its effect on thermal stress development," *Construction and Building Materials*, vol. 38, pp. 306–3152013, doi: 10.1016/J.CONBUILDMAT.2012.07.111.

[124] R. R. Niry, A. L. Beaucour, R. Hebert, A. Noumowé, B. Ledésert, and R. Bodet, "Thermal stability of different siliceous and calcareous aggregates subjected to high temperature," *MATEC Web of Conferences*, vol. 6, p. 07001, 2013, doi: 10.1051/MATECCONF/20130607001.

[125] G. Fiquet, P. Richet, and G. Montagnac, "High-temperature thermal expansion of lime, periclase, corundum and spinel," *Physics and Chemistry of Minerals*, vol. 27, no. 2, pp. 103–111, 1999, doi: 10.1007/S002690050246

[126] Z. Xing, A. L. Beaucour, R. Hebert, A. Noumowe, and B. Ledesert, "Influence of the nature of aggregates on the behaviour of concrete subjected to elevated temperature," *Cement and Concrete Research*, vol. 41, no. 4, pp. 392–402, 2011, doi: 10.1016/J.CEMCONRES.2011.01.005.

[127] S. Roy, T. Miura, H. Nakamura, and Y. Yamamoto, "High temperature influence on concrete produced by spherical shaped EAF slag fine aggregate – Physical and mechanical properties," *Construction and Building Materials*, vol. 231, p. 117153, 2020, doi: 10.1016/J.CONBUILDMAT.2019.117153.

[128] A. Z. Mohd Ali, J. Sanjayan, and M. Guerrieri, "Specimens size, aggregate size, and aggregate type effect on spalling of concrete in fire," *Fire and Materials*, vol. 42, no. 1, pp. 59–68, 2018, doi: 10.1002/FAM.2457.

[129] J. Il Sim, K. H. Yang, and J. K. Jeon, "Influence of aggregate size on the compressive size effect according to different concrete types," *Construction and Building Materials*, vol. 44, pp. 716–725, 2013, doi: 10.1016/J.CONBUILDMAT.2013.03.066.

[130] M. Elices and C. G. Rocco, "Effect of aggregate size on the fracture and mechanical properties of a simple concrete," *Engineering Fracture Mechanics*, vol. 75, no. 13, pp. 3839–3851, 2008, doi: 10.1016/J.ENGFRACMECH.2008.02.011.

[131] M. Aamer Rafique Bhutta, N. Hasanah, N. Farhayu, M. W. Hussin, M. B. M. Tahir, and J. Mirza, "Properties of porous concrete from waste crushed concrete (recycled aggregate)," *Construction and Building Materials*, vol. 47, pp. 1243–1248, 2013, doi: 10.1016/J.CONBUILDMAT.2013.06.022.

[132] C. C. Fan, R. Huang, H. Hwang, and S. J. Chao, "Properties of concrete incorporating fine recycled aggregates from crushed concrete wastes," *Construction and Building Materials*, vol. 112, pp. 708–715, 2016, doi: 10.1016/J.CONBUILDMAT.2016.02.154.

[133] H. Qasrawi, “The use of steel slag aggregate to enhance the mechanical properties of recycled aggregate concrete and retain the environment,” *Construction and Building Materials*, vol. 54, pp. 298–304, 2014, doi: 10.1016/J.CONBUILDMAT.2013.12.063.

[134] E. Anastasiou, K. Georgiadis Filikas, and M. Stefanidou, “Utilization of fine recycled aggregates in concrete with fly ash and steel slag,” *Construction and Building Materials*, vol. 50, pp. 154–161, 2014, doi: 10.1016/J.CONBUILDMAT.2013.09.037.

[135] V. Letelier, E. Tarela, R. Osses, J. P. Cárdenas, and G. Moriconi, “Mechanical properties of concrete with recycled aggregates and waste glass,” *Structural Concrete*, vol. 18, no. 1, pp. 40–53, 2017, doi: 10.1002/SUCO.201500143.

[136] I. Almeshal, B. A. Tayeh, R. Alyousef, H. Alabduljabbar, A. Mustafa Mohamed, and A. Alaskar, “Use of recycled plastic as fine aggregate in cementitious composites: A review,” *Construction and Building Materials*, vol. 253, p. 119146, 2020, doi: 10.1016/J.CONBUILDMAT.2020.119146.

[137] A. Dehghan, M. L. J. Maher, and M. Navarra, “The Effects of Aggregate Properties on Concrete Mix Design and Behaviour,” *Lecture Notes in Civil Engineering*, vol. 248, pp. 457–468, 2023, doi: 10.1007/978-981-19-1004-3_38

[138] V. K. R. Kodur, ; Fu, P. Cheng, T.-C. Wang, and M. A. Sultan, “Effect of Strength and Fiber Reinforcement on Fire Resistance of High-Strength Concrete Columns,” *Journal of Structural Engineering*, vol. 129, no. 2, pp. 253–259, 2003, doi: 10.1061/(ASCE)0733-9445(2003)129:2(253).

[139] C. Maraveas, K. Miamis, and A. A. Vrakas, “Fiber-Reinforced Polymer-Strengthened/Reinforced Concrete Structures Exposed to Fire: A Review,” *Structural Engineering International*, vol. 22, no. 4, pp. 500–513, 2012, doi: 10.2749/101686612X13363929517613.

[140] V. K. R. Kodur, P. P. Bhatt, and M. Z. Naser, “High temperature properties of fiber reinforced polymers and fire insulation for fire resistance modeling of strengthened concrete structures,” *Composites Part B: Engineering*, vol. 175, p. 107104, 2019, doi: 10.1016/J.COMPOSITESB.2019.107104.

[141] J. Šelih, A. C. M. Sousa, and T. W. Bremner, “Moisture and Heat Flow in Concrete Walls Exposed to Fire,” *Journal of Engineering Mechanics*, vol. 120, no. 10, pp. 2028–2043, 1994, doi: 10.1061/(ASCE)0733-9399(1994)120:10(2028).

[142] Y. S. Jenq, S. M. Asce, S. P. Shah, and M. Asce, “Crack Propagation in Fiber-Reinforced Concrete,” *Journal of Structural Engineering*, vol. 112, no. 1, pp. 19–34, 1986, doi: 10.1061/(ASCE)0733-9445(1986)112:1(19).

[143] W. C. Wang, H. Y. Wang, K. H. Chang, and S. Y. Wang, “Effect of high temperature on the strength and thermal conductivity of glass fiber concrete,” *Construction and Building Materials*, vol. 245, p. 118387, 2020, doi: 10.1016/J.CONBUILDMAT.2020.118387.

[144] M. S. Magalhães, R. D. Toledo Filho, and E. M. R. Fairbairn, “Durability under thermal loads of polyvinyl alcohol fibers,” *Matéria (Rio de Janeiro)*, vol. 18, no. 4, pp. 1587–1595, 2013, doi: 10.1590/S1517-70762013000400018.

[145] M. Zeiml, D. Leithner, R. Lackner, and H. A. Mang, “How do polypropylene fibers improve the spalling behavior of in-situ concrete?,” *Cement and Concrete Research*, vol. 36, no. 5, pp. 929–942, 2006, doi: 10.1016/J.CEMCONRES.2005.12.018.

[146] I. Adnan Suhail Abo-Saibaa and N. Abdul-Ameer Alwash, “Rehabilitation of light-weight reinforced concrete ribbed slab exposed to fire using basalt textile reinforced mortar,” *International Journal of Environmental Sciemce*, vol. 11, no. 2s, pp. 271–281, 2025, doi: 10.64252/NE65R092.

[147] D. P. Bentz, “Fibers, Percolation, and Spalling of High Performance Concrete,” *ACI Materials Journal* , vol. 97-M41, 2000.

[148] P. Lura and G. Pietro Terrasi, “Reduction of fire spalling in high-performance concrete by means of superabsorbent polymers and polypropylene fibers: Small scale fire tests of carbon fiber reinforced plastic-prestressed self-compacting concrete,” *Cement and Concrete Composites*, vol. 49, pp. 36–42, 2014, doi: 10.1016/J.CEMCONCOMP.2014.02.001.

[149] F. Liu, B. Wu, and D. Wei, “Failure modes of reinforced concrete beams strengthened with carbon fiber sheet in fire,” *Fire Safety Journal*, vol. 44, no. 7, pp. 941–950, 2009, doi: 10.1016/J.FIRESAF.2009.05.006.

[150] M. Zhou, X. He, H. Wang, C. Wu, J. He, and B. Wei, “Mechanical properties and microstructure of ITZs in steel and polypropylene hybrid fiber-reinforced concrete,” *Construction and Building Materials*, vol. 415, p. 135119, 2024, doi: 10.1016/J.CONBUILDMAT.2024.135119.

[151] H. Guo, X. Long, and Y. Yao, “Fire resistance of concrete filled steel tube columns subjected to non-uniform heating,” Journal of Constructional Steel Research, vol. 128, pp. 542–554, 2017, doi: 10.1016/J.JCSR.2016.09.014.

[152] D. V. Reddy, K. Sobhan, L. Liu, and J. D. Young, “Size effect on fire resistance of structural concrete,” *Engineering Structures*, vol. 99, pp. 468–478, Sep. 2015, doi: 10.1016/J.ENGSTRUCT.2015.05.015.

[153] B. Georgali and P. E. Tsakiridis, "Microstructure of fire-damaged concrete. A case study," *Cement and Concrete Composites*, vol. 27, no. 2, pp. 255–259, 2005, doi: 10.1016/J.CEMCONCOMP.2004.02.022.
[154] C. S. Poon, S. Azhar, M. Anson, and Y. L. Wong, "Strength and durability recovery of fire-damaged concrete after post-fire-curing," *Cement and Concrete Research*, vol. 31, no. 9, pp. 1307–1318, 2001, doi: 10.1016/S0008-8846(01)00582-8.
[155] M. F. Nuruddin, N. M. Azmee, and C. K. Yung, "Effect of fire flame exposure on ductile self-compacting concrete (DSCC) blended with MIRHA and fly ash," *Construction and Building Materials*, vol. 50, pp. 388–393, 2014, doi: 10.1016/J.CONBUILDMAT.2013.09.038.
[156] A. N. Noumowe, R. Siddique, and G. Debicki, "Permeability of high-performance concrete subjected to elevated temperature (600 °C)," *Construction and Building Materials*, vol. 23, no. 5, pp. 1855–1861, 2009, doi: 10.1016/J.CONBUILDMAT.2008.09.023.
[157] F. Kigha, J. A. Sadeeq, and O. S. Abejide, "Effects of Temperature Levels and Concrete Cover Thickness on Residual Strength Characteristics of Fire Exposed Reinforced Concrete Beams," *Nigerian Journal of Technology*, vol. 34, no. 3, pp. 429–437, 2015, doi: 10.4314/NJT.V34I3.1.
[158] D. Wang. *Y.Dong, D.Zhang, W.Wang, X.Lu*, "Monitoring and analysis of reinforced concrete plate-column structure under room temperature and fire based on acoustic emission," *Fracture and Structural Integrity*, vol. 14, no. 53, pp. 236–251, Jul. 2020, doi: 10.3221/IGF-ESIS.53.20.
[159] L. Lim and C. Wade, "Experimental Fire Tests of Two-Way Concrete Slabs. Fire Engineering Research Report 02/12," Christchurch, 2002.
[160] K.-S. Kwon and D.-W. Ryu, "Fire Resistance Performance Test of High Strength Concrete by Type of Mineral Admixture," *Journal of the Korea Institute of Building Construction*, vol. 15, no. 6, pp. 597–605, 2015, doi: 10.5345/JKIBC.2015.15.6.597.
[161] T. Y. Chu, "Radiant heat evaluation of concrete: a study of the erosion of concrete due to surface heating," Albuquerque, NM, and Livermore, CA (United States), 1978. doi: 10.2172/5175759.
[162] I. Almeshal, B. H. Abu Bakar, and B. A. Tayeh, "Behaviour of Reinforced Concrete Walls Under Fire: A Review," *Fire Technology*, vol. 58, no. 5, pp. 2589–2639, 2022, doi: 10.1007/S10694-022-01240-3.
[163] L. E. Lagos, W. Li, M. A. Ebadian, T. L. White, R. G. Grubb, and D. Foster, "Heat transfer within a concrete slab with a finite microwave heating source," *International Journal of Heat and Mass Transfer*, vol. 38, no. 5, pp. 887–897, 1995, doi: 10.1016/0017-9310(94)00200-F.
[164] L. Bodnarova, J. Valek, and P. Novosad, "Testing of Action of Direct Flame on Concrete," *The Scientific World Journal*, vol. 2015, no. 1, p. 371913, 2015, doi: 10.1155/2015/371913.
[165] Z. Huang, "The behaviour of reinforced concrete slabs in fire," *Fire Safety Journal*, vol. 45, no. 5, pp. 271–282, 2010, doi: 10.1016/J.FIRESAF.2010.05.001.
[166] A. Abbasi and P. J. Hogg, "Fire testing of concrete beams with fibre reinforced plastic rebar," *Advanced Polymer Composites for Structural Applications in Construction: ACIC 2004*, pp. 445–456, 2004, doi: 10.1533/9781845690649.5.445.
[167] S. Kim, J. Shim, J. Y. Rhee, D. Jung, and C. Park, "Temperature Distribution Characteristics of Concrete during Fire Occurrence in a Tunnel," *Applied Sciences 2019,* vol. 9, no. 22, p. 4740, 2019, doi: 10.3390/APP9224740.
[168] A. A. A. De Souza, A. L. Moreno JR, "Assessment of the Type of Aggregates and Rehydration on Concrete Submitted to High Temperatures," *IBRACON*, vol. 3, no. 4, pp. 477–493, 2010, https://www.concrete.org/publications/internationalconcreteabstractsportal.aspx?m=details&id=51682515
[169] G. P. Teixeira, J. C. L. Ribeiro, L. G. Pedroti, and G. H. Nalon, "Effects of Post-Fire Rehydration on the Mechanical Properties of Slag-Modified Concrete," *Buildings*, vol. 15, no. 1, p. 136, 2025, doi: 10.3390/BUILDINGS15010136.
[170] G. T. G. Mohamedbhai, "Effect of exposure time and rates of heating and cooling on residual strength of heated concrete," *Magazine of Concrete Research*, vol. 38, no. 136, pp. 151–158, 2015, doi: 10.1680/MACR.1986.38.136.151.
[171] Y. F. Chang, Y. H. Chen, M. S. Sheu, and G. C. Yao, "Residual stress–strain relationship for concrete after exposure to high temperatures," *Cement and Concrete Research*, vol. 36, no. 10, pp. 1999–2005, Oct. 2006, doi: 10.1016/J.CEMCONRES.2006.05.029.
[172] Q. Li, G. Yuan, and Q. Shu, "Effects of heating/cooling on recovery of strength and carbonation resistance of fire-damaged concrete," *Magazine of Concrete Research*, vol. 66, no. 18, pp. 925–936, 2015, doi: 10.1680/MACR.14.00029.
[173] G. Y. Kim *et al.*, "Mechanical Properties of Concrete depending on Cooling Conditions After High Temperature Heating," *Journal of Advanced Concrete Technology*, vol. 12, no. 3, pp. 82–90, 2014, doi: 10.3151/JACT.12.82.

[174] X. Luo, W. Sun, and S. Y. N. Chan, "Effect of heating and cooling regimes on residual strength and microstructure of normal strength and high-performance concrete," *Cement and Concrete Research*, vol. 30, no. 3, pp. 379–383, 2000, doi: 10.1016/S0008-8846(99)00264-1.

[175] J. Bi, P. Liu, and F. Gan, "Effects of the cooling treatment on the dynamic behavior of ordinary concrete exposed to high temperatures," *Construction and Building Materials*, vol. 248, p. 118688, 2020, doi: 10.1016/J.CONBUILDMAT.2020.118688.

[176] F. Gao, W. Tian, and X. Cheng, "Investigation of moisture migration of MWCNTs concrete after different heating-cooling process by LF-NMR," *Construction and Building Materials*, vol. 288, p. 123146, 2021, doi: 10.1016/J.CONBUILDMAT.2021.123146.

[177] R. Jansson, "Fire spalling of concrete-A historical overview," *MATEC Web of Conferences*, vol. 6, p. 1001, 2013, doi: 10.1051/matecconf/20130601001.

[178] K. C. Hover, "The influence of water on the performance of concrete," *Construction and Building Materials*, vol. 25, no. 7, pp. 3003–3013, 2011, doi: 10.1016/J.CONBUILDMAT.2011.01.010.

[179] J. C. Liu, K. H. Tan, and Y. Yao, "A new perspective on nature of fire-induced spalling in concrete," *Construction and Building Materials*, vol. 184, pp. 581–590, 2018, doi: 10.1016/J.CONBUILDMAT.2018.06.204.

[180] Z. Jia, C. Chen, J. Shi, Y. Zhang, Z. Sun, and P. Zhang, "The microstructural change of C-S-H at elevated temperature in Portland cement/GGBFS blended system," *Cement and Concrete Research*, vol. 123, p. 105773, 2019, doi: 10.1016/J.CEMCONRES.2019.05.018.

[181] R. Jansson and L. Boström, "The influence of pressure in the pore system on fire spalling of concrete," *Fire Technology*, vol. 46, no. 1, pp. 217–230, 2010, doi: 10.1007/S10694-009-0093-9.

[182] A. M. Abubaker and C. T. Davie, "Effects of restraint and test configuration on thermo-mechanical stress states in high temperature laboratory tests for spalling in concrete," *Fire Safety Journal*, vol. 141, p. 103990, Dec. 2023, doi: 10.1016/J.FIRESAF.2023.103990.

[183] H. Qin, J. Yang, K. Yan, J. H. Doh, K. Wang, and X. Zhang, "Experimental research on the spalling behaviour of ultra-high performance concrete under fire conditions," *Construction and Building Materials*, vol. 303, p. 124464, 2021, doi: 10.1016/J.CONBUILDMAT.2021.124464.

[184] M. Khaled al-Bashiti and M. Z. Naser, "What can we learn from over 1000 tests on fire-induced spalling of concrete? A statistical investigation of critical factors and unexplored research space," *Construction and Building Materials,* vol. 403, p. 133200, 2023, doi: 10.1016/J.CONBUILDMAT.2023.133200.

[185] K. D. Hertz, "Limits of spalling of fire-exposed concrete," *Fire Safety Journal*, vol. 38, no. 2, pp. 103–116, 2003, doi: 10.1016/S0379-7112(02)00051-6.

[186] Z. Pan, J. G. Sanjayan, and D. L. Y. Kong, "Effect of aggregate size on spalling of geopolymer and Portland cement concretes subjected to elevated temperatures," *Construction and Building Materials*, vol. 36, pp. 365–372, 2012, doi: 10.1016/J.CONBUILDMAT.2012.04.120.

[187] E. Lubloy, "The relationship between conctere composition and structural stability in case of fire," *Construction and Building Materials*, vol. 431, p. 136545, Jun. 2024, doi: 10.1016/J.CONBUILDMAT.2024.136545.

[188] T. Pittrich, F. Weise, and L. Stelzner, "The impact of blended cements on the spalling behavior of concrete at elevated temperatures: a review," *Materials and Structures/Materiaux et Constructions*, vol. 58, no. 5, pp. 1–21, 2025, doi: 10.1617/S11527-025-02713-X/TABLES/6.

[189] E. Burak Pancar, "Reducing High Temperature Effect on Concrete by Changing Concrete Mixture," *International Journal of Structural and Civil Engineering Research*, vol. 6, no. 4, 2017, doi: 10.18178/ijscer.6.4.258-262.

[190] Saurav, A. K. Shukla, and P. Malaviya, "A Comparative Study of Fire Resistance of Concrete Incorporating Ultrafine Slag," pp. 291–304, 2020, doi: 10.1007/978-981-15-6852-7_26.

[191] E. D. Shumuye, J. Zhao, and Z. Wang, "Effect of fire exposure on physico-mechanical and microstructural properties of concrete containing high volume slag cement," *Construction and Building Materials*, vol. 213, pp. 447–4582019, doi: 10.1016/J.CONBUILDMAT.2019.04.079.

[192] E. D. Shumuye, J. Zhao, and Z. Wang, "Effect of the Curing Condition and High-Temperature Exposure on Ground-Granulated Blast-Furnace Slag Cement Concrete," *International Journal of Concrete Structures and Materials*, vol. 15, no. 1, pp. 1–20, 2021, doi: 10.1186/S40069-020-00437-6.

[193] M. Uysal, K. Yilmaz, and M. Ipek, "Properties and behavior of self-compacting concrete produced with GBFS and FA additives subjected to high temperatures," *Construction and Building Materials*, vol. 28, no. 1, pp. 321–326, 2012, doi: 10.1016/J.CONBUILDMAT.2011.08.076.

[194] M. F. Ghazy, M. A. Abd Elaty, and N. M. Zalhaf, "Mechanical Properties of HPC Incorporating Fly Ash and Ground Granulated Blast Furnace Slag After Exposure to High Temperatures," *Periodica Polytechnica Civil Engineering*, vol. 66, no. 3, pp. 761–774, 2022, doi: 10.3311/PPCI.19751.

[195] M. N. Amin and K. Khan, "Mechanical Performance of High-Strength Sustainable Concrete under Fire Incorporating Locally Available Volcanic Ash in Central Harrat Rahat, Saudi Arabia," *Materials 2021, Vol. 14, Page 21*, vol. 14, no. 1, p. 21, 2020, doi: 10.3390/MA14010021.

[196] H. M. Owaid, R. Hamid, M. R. Taha, H. M. Owaid, R. Hamid, and M. R. Taha, "Elevated Temperature Performance of Multiple-Blended Binder Concretes," *High Performance Concrete Technology and Applications*, 2016, doi: 10.5772/64415.

[197] J. Yu *et al.*, "Behavior of magnesium phosphate cement with addition of sulphoaluminate cement at elevated temperatures," *Construction and Building Materials*, vol. 401, p. 132932, 2023, doi: 10.1016/J.CONBUILDMAT.2023.132932.

[198] W. Johannes, "Beginning of melting in the granite system Qz-Or-Ab-An-H2O," *Contributions to Mineralogy and Petrology*, vol. 86, no. 3, pp. 264–273, 1984, doi: 10.1007/BF00373672.

[199] R. O. Snellings Jacek Chwast *et al.*, "RILEM TC-238 SCM recommendation on hydration stoppage by solvent exchange for the study of hydrate assemblages," *Materials and Structures 2018 51:6*, vol. 51, no. 6, pp. 1–4, 2018, doi: 10.1617/S11527-018-1298-5.

[200] I. Van der Molen, "The shift of the α-β transition temperature of quartz associated with the thermal expansion of granite at high pressure," *Tectonophysics*, vol. 73, no. 4, pp. 323–342, 1981, doi: 10.1016/0040-1951(81)90221-3.

[201] J. E. Rossen and K. L. Scrivener, "Optimization of SEM-EDS to determine the C–A–S–H composition in matured cement paste samples," *Materials Characterization*, vol. 123, pp. 294–306, Jan. 2017, doi: 10.1016/J.MATCHAR.2016.11.041.

[202] M. Rajczakowska, M. Szeląg, K. Habermehl-Cwirzen, H. Hedlund, and A. Cwirzen, "Autogenous self-healing of thermally damaged cement paste with carbon nanomaterials subjected to different environmental stimulators," *Journal of Building Engineering*, vol. 72, p. 106619, 2023, doi: 10.1016/J.JOBE.2023.106619.

[203] H. S. Wong, M. K. Head, and N. R. Buenfeld, "Pore segmentation of cement-based materials from backscattered electron images," *Cement and Concrete Research*, vol. 36, no. 6, pp. 1083–1090, 2006, doi: 10.1016/J.CEMCONRES.2005.10.006.

[204] H. Y. Wang, "The effects of elevated temperature on cement paste containing GGBFS," *Cement and Concrete Composites*, vol. 30, no. 10, pp. 992–999, 2008, doi: 10.1016/J.CEMCONCOMP.2007.12.003.

[205] B. Lothenbach, K. Scrivener, and R. D. Hooton, "Supplementary cementitious materials," *Cement and Concrete Research*, vol. 41, no. 12, pp. 1244–1256, 2011, doi: 10.1016/J.CEMCONRES.2010.12.001.

[206] Y. Zhang *et al.*, "Experimental and theoretical study of fire resistance of steel slag powder concrete beams," *Engineering Structures*, vol. 325, p. 119402, 2025, doi: 10.1016/J.ENGSTRUCT.2024.119402.

[207] R. Jansson and L. Boström, "Factors influencing fire spalling of self compacting concrete," *Materials and Structures/Materiaux et Constructions*, vol. 46, no. 10, pp. 1683–1694, 2013, doi: 10.1617/S11527-012-0007-Z.

[208] N. R. Short, J. A. Purkiss, and S. E. Guise, "Assessment of fire damaged concrete using colour image analysis," *Construction and Building Materials*, vol. 15, no. 1, pp. 9–15, 2001, doi: 10.1016/S0950-0618(00)00065-9.

[209] S. E. Guise, "Use of colour image analysis for assessment of fire damaged concrete," Aston University, 1997.

[210] E. Annerel and L. Taerwe, "Methods to quantify the colour development of concrete exposed to fire," *Construction and Building Materials*, vol. 25, no. 10, pp. 3989–3997, 2011, doi: 10.1016/J.CONBUILDMAT.2011.04.033.

[211] J. P. Ingham, "Application of petrographic examination techniques to the assessment of fire-damaged concrete and masonry structures," *Materials Characterization*, vol. 60, no. 7, pp. 700–709, 2009, doi: 10.1016/J.MATCHAR.2008.11.003.

[212] W. Huang, Y. Wang, Y. Zhang, and W. Zheng, "Experimental Study of Alkali-Activated Slag Crushed Aggregate Blocks During and After Exposure to Elevated Temperatures," *Fire Technology*, vol. 60, no. 3, pp. 1993–2018, 2024, doi: 10.1007/S10694-024-01558-0.

[213] S. R. Abdila and M. M. A. B. Abdullah, "In situ DCP to evaluate unconfined compressive strength of soil stabilization using ground-granulated blast slag and fly ash via geopolymer process," *Recent Developments of Geopolymer Materials: Processing and Characterisations*, pp. 201–221, 2024, doi: 10.1016/B978-0-443-24068-3.00010-8.

[214] C. Prasun K. and S. Arup K., "Sensing of Toxic Metals Using Innovative Sorption-Based Technique," *Ion Exchange and Solvent Extraction*, pp. 175–240, 2017, doi: 10.1201/B20021-6.

[215] C. Wu and J. Chang, "Synthesis and apatite-formation ability of akermanite," *Materials Letters*, vol. 58, no. 19, pp. 2415–2417, 2004, doi: 10.1016/J.MATLET.2004.02.039.

[216] W. Huang, Y. Wang, Y. Zhang, and W. Zheng, "Experimental study of high-temperature resistance of alkali-activated slag crushed aggregate mortar," *Journal of Materials Research and Technology*, vol. 23, pp. 3961–3973, 2023, doi: 10.1016/J.JMRT.2023.02.072.

[217] P. Zadehnajar *et al.*, "Recent advances on akermanite calcium-silicate ceramic for biomedical applications," *International Journal of Applied Ceramic Technolog*, vol. 18, no. 6, pp. 1901–1920, 2021, doi: 10.1111/IJAC.13814.

[218] Y. Luo, K. M. Klima, H. J. H. Brouwers, and Q. Yu, "Effects of ladle slag on Class F fly ash geopolymer: Reaction mechanism and high temperature behavior," *Cement and Concrete Composites*, vol. 129, p. 104468, 2022, doi: 10.1016/J.CEMCONCOMP.2022.104468.

[219] W. Xuan, S. Yan, J. Zhang, S. Luo, Q. Wang, and J. Zhang, "A deep insight into the dynamic crystallization of coal slags and the correlation with melt microstructure," *Fuel Processing Technology*, vol. 254, p. 108005, 2024, doi: 10.1016/J.FUPROC.2023.108005.

[220] E. Kapeluszna, Ł. Kotwica, A. Różycka, and Ł. Gołek, "Incorporation of Al in C-A-S-H gels with various Ca/Si and Al/Si ratio: Microstructural and structural characteristics with DTA/TG, XRD, FTIR and TEM analysis," *Construction and Building Materials*, vol. 155, pp. 643–653, 2017, doi: 10.1016/J.CONBUILDMAT.2017.08.091.

[221] M. W. Tait and W. M. Cheung, "A comparative cradle-to-gate life cycle assessment of three concrete mix designs," *International Journal of Life Cycle Assessment*, vol. 21, no. 6, pp. 847–860, 2016, doi: 10.1007/S11367-016-1045-5/TABLES/4.

[222] K. A. Sodol, Ł. Kaczmarek, J. Szer, S. Miszczak, and M. Stegliński, "Impact of Elevated Temperatures on Strength Properties and Microstructure of Calcium Sulfoaluminate Paste," *Materials 2021, Vol. 14, Page 6751*, vol. 14, no. 22, p. 6751, 2021, doi: 10.3390/MA14226751.

[223] L. H. J. Martin, F. Winnefeld, C. J. Müller, and B. Lothenbach, "Contribution of limestone to the hydration of calcium sulfoaluminate cement," *Cement and Concrete Composites*, vol. 62, pp. 204–211, 2015, doi: 10.1016/J.CEMCONCOMP.2015.07.005.

[224] W. T. Tsai, J. M. Yang, H. C. Hsu, C. M. Lin, K. Y. Lin, and C. H. Chiu, "Development and characterization of mesoporosity in eggshell ground by planetary ball milling," *Microporous and Mesoporous Materials*, vol. 111, no. 1–3, pp. 379–386, 2008, doi: 10.1016/J.MICROMESO.2007.08.010.

[225] B. Zhang, Y. Liu, D. Laboureur, and M. S. Mannan, "Experimental Study on Propane Jet Fire Hazards: Thermal Radiation," *Industrial & Engineering Chemistry Research*, vol. 54, no. 37, pp. 9251–9256, 2015, doi: 10.1021/ACS.IECR.5B02064.

[226] Y. Sargam, K. Wang, and J. E. Alleman, "Effects of Modern Concrete Materials on Thermal Conductivity," *Journal of Materials in Civil Engineering*, vol. 32, no. 4, p. 04020058, 2020, doi: 10.1061/(ASCE)MT.1943-5533.0003026

[227] K. Singha, "A Short Review on Basalt Fiber," *International Journal of Textile Science*, vol. 2012, no. 4, pp. 19–28, 2012, doi: 10.5923/j.textile.20120104.02.

[228] M. Khan, M. Cao, X. Chaopeng, and M. Ali, "Experimental and analytical study of hybrid fiber reinforced concrete prepared with basalt fiber under high temperature," *Fire and Materials*, vol. 46, no. 1, pp. 205–226, 2022, doi: 10.1002/FAM.2968.

[229] J. W. Jeffery, "The crystal structure of tricalcium silicate," *Acta Crystallographica*, vol. 5, no. 1, pp. 26–35, Jan. 1952, doi: 10.1107/S0365110X52000083.

[230] N. Nerantzis, "Nerantzis N. (2009) Using Mills to Refine Metals: Iron Smelting Technology of the Transitional Byzantine to Ottoman Period in Macedonia, Greece, In T. L. Kienlin and B. W. Roberts (eds.) Metals and Societies, Studies in Honour of Barbara S. Ottaway, 443-451." Accessed: Jun. 19, 2025. [Online]. Available: https://www.academia.edu/2645314/Nerantzis_N_2009_Using_Mills_to_Refine_Metals_Iron_Smelting_Technology_of_the_Transitional_Byzantine_to_Ottoman_Period_in_Macedonia_Greece_In_T_L_Kienlin_and_B_W_Roberts_eds_Metals_and_Societies_Studies_in_Honour_of_Barbara_S_Ottaway_443_451

[231] G. J. Albertsson, F. Engström, and L. Teng, "Effect of the Heat Treatment on the Chromium Partition in Cr-Containing Industrial and Synthetic Slags," *Steel Research International*, vol. 85, no. 10, pp. 1418–1431, 2014, doi: 10.1002/SRIN.201300231.

[232] J. R. Gavarri and C. Carel, "The complex nonstoichiometry of wüstite Fe1-zO: Review and comments," *Progress in Solid State Chemistry*, vol. 53, pp. 27–49, 2019, doi: 10.1016/J.PROGSOLIDSTCHEM.2018.10.001.

"I let go expectations. And to be clear, I am not talking about having dreams or wanting something to happen. It is important. I am talking about, you know, assuming things will go the way we think they should. For whatever reason. Because you never know what tomorrow will bring and it might be greater than anything you ever expected."

Carrie Bradshaw, And Just Like That (Season 2, Episode 11) [TV series episode].
In M. King (Executive Producer), HBO Max (2023).

And just like that I wrote this PhD thesis.

Marcin Sundin.

Department of Civil, Environmental and Natural Resources Engineering
Division of Structural and Fire Engineering

ISSN 1402-1544
ISBN 978-91-8048-881-5 (print)
ISBN 978-91-8048-882-2 (pdf)

Luleå University of Technology 2025

LULEÅ
UNIVERSITY
OF TECHNOLOGY